# MEASUREMENT, CHARACTERIZATION, AND PREDICTION
# OF STRONG GROUND MOTION

WILLIAM B. JOYNER AND DAVID M. BOORE*

The estimation of ground motion in future earthquakes for engineering purposes is one of the primary motivations for the measurement and processing of strong-motion data. The response spectrum is the best representation of ground motion because it takes account of the natural frequencies of structures. The conventional practice of using peak acceleration to scale standard response spectral shapes is likely to lead to serious error, except at high frequencies, because the shapes of response spectra depend strongly on magnitude and local geologic site conditions. Magnitude, distance, and site conditions are the principal variables used in predicting future ground motions. A number of predictive relationships derived from regression analysis of strong-motion data are available for horizontal peak acceleration, velocity, and response spectral values. Theoretical prediction of ground motion calls for stochastic source models because source heterogeneities control the amplitude of ground motion at most, if not all, frequencies of engineering interest. Stochastic source models have been used for predicting ground motion in regions such as eastern North America where little recorded data are available. Ground motion predictions for large earthquakes have also been made by summation of recordings of smaller earthquakes. This technique does not take proper account of directivity except in very special circumstances. Aside from directivity, it is possible to do the summation in such a way that the low-frequency and high-frequency limits of the spectrum of the predicted motion obey appropriate scaling laws, but the spectrum may be deficient in amplitude at intermediate frequencies.

## INTRODUCTION

There has been great progress in the last ten years in the study of strong earthquake ground motion and its engineering applications. New data and analysis have provided the basis for more reliable empirical estimates of ground motion in future earthquakes. Theoretical methods have been developed for estimation of ground-motion parameters and simulation of ground-motion time series. These methods are particularly helpful for regions such as eastern North America where strong-motion data are sparse. In what follows we survey the field, first reviewing developments in ground-motion measurement and data processing. We then consider the choice of parameters for characterizing strong ground motion and describe the wave-types involved in strong ground motion and the factors affecting ground-motion amplitudes. We conclude by describing methods for predicting ground motion.

Our intent was to make this paper a comprehensive and self-contained manual describing the newer methods of ground-motion prediction. We feel that this goal justifies the added detail and complexity in the paper and the introduction of much material from seismology that many engineers may find unfamiliar.

* U.S. Geological Survey, 345 Middlefield Road MS 977, Menlo Park, CA 94025

## Measurement

Since the time the first strong-motion record was obtained in 1933 most strong-motion data have been recorded on accelerographs with photographic recording. These instruments are triggered by the motion itself, and some part of the initial motion is therefore lost. Numerical calculations with the data require that the photographic film or paper record be digitized. At first this was done manually; later the process was automated. Now, digital recording instruments using force-balance accelerometers are coming into wider use (Anderson *et al.*, 1983). Digital recording eliminates the delays and loss of accuracy associated with digitizing film or paper records and also permits recovery of the initial portion of the signal. Borcherdt *et al.* (1984) give a tabulation and discussion of the characteristics of digital recording systems available in the United States. As more experience is gained with digital recorders their use can be expected to increase further, but conventional recorders are still predominant, and it will be many years before they can be replaced. Of particular interest among new developments in digital instrumentation is the GEOS recording system (Borcherdt *et al.*, 1985), a broad-band system with 16-bit dynamic range that facilitates the simultaneous recording of large and small motions at the same site. GEOS is especially suited for aftershock studies (Borcherdt *et al.*, 1983; Boatwright, 1985).

Special attention has recently been devoted to the collection and analysis of data from spatially distributed arrays and networks of recording instruments. By analyzing data recorded on the El Centro differential array during the 1979 Imperial Valley, California, earthquake Spudich and Cranswick (1984) were able to show that the ground motion consisted of waves radiated from a compact region around the rupture front and that the rupture front progressed more or less coherently from the hypocenter to the limits of the rupture. Data from the SMART 1 digital array in Taiwan have been used to examine the spatial coherence of ground motion (Bolt *et al.*, 1984; Abrahamson, 1985). Because of the earthquake that has been predicted at Parkfield, California, a network of strong-motion instruments has been established there by the California Strong-Motion Instumentation Program (McJunkin and Shakal, 1983), and special strong-motion arrays arrays have been installed there by the Electric Power Research Institute and the California Strong-Motion Instrumentation Program and by the U.S. Geological Survey. At Anza, California, a broad-band, wide-dynamic-range, digital network of short-period seismometers supplemented by accelerographs has been set up to study earthquake source processes in a seismic gap along the San Jacinto fault (Berger *et al.*, 1984).

One of the most important data sets in strong-motion seismology is that recorded in the 1979 Imperial Valley, California, earthquake because it gives good coverage of the near-source region for a shallow earthquake of moment magnitude as large as 6.5. The outstanding need now is for near-source data from shallow earthquakes of larger magnitude. Other significant data sets recently recorded are listed in Table 1. The 1985 earthquakes in Chile and Mexico are of particular importance because they contributed the first and only extensive data sets from the near-source regions of large subduction-zone earthquakes.

## Processing

Early methods of strong-motion data processing consisted of subtracting a best-fitting parabola from the accelerogram before integrating to velocity and displacement (references on early methods are given by Trifunac, 1971). Subtraction of the parabola—called baseline correction—had no physical basis, but served to remove long-period errors that would be grossly magnified by double integration. Modern data-processing methods are derived from proposals by Trifunac (1971, 1972) that a high-pass digital filter be used for the baseline correction and a centered finite-difference approximation be used to correct for the effect of the instrument.

## TABLE 1. RECENT STRONG-MOTION DATA SETS

| Earthquake | Day | Month | Year GMT | Magnitude | References |
|---|---|---|---|---|---|
| Coalinga, California | 2 | 5 | 83 | $M_L$ 6.7 | Shakal and McJunkin, 1983 Maley *et al.*, 1983 |
| Borah Peak, Idaho | 28 | 10 | 83 | $M_S$ 7.3 | Jackson and Boatwright, 1985 |
| Morgan Hill, California | 24 | 4 | 84 | $M_L$ 6.2 | Brady *et al.*, 1984a, b Huang *et al.*, 1985 Shakal *et al.*, 1986a |
| Central Chile | 3 | 3 | 85 | $M_S$ 7.8 | Saragoni, 1985 |
| Michoacan, Mexico | 19 | 9 | 85 | $M_S$ 8.1 | Anderson *et al.*, 1986 |
| Nahanni, Canada | 23 | 12 | 85 | $M_S$ 6.9 | Weichert *et al.*, 1986 |
| Palm Springs, California | 8 | 7 | 86 | $M_L$ 5.9 | Huang *et al.*, 1986 Porcella *et al.*, 1987a |
| Chalfant Valley, California | 21 | 7 | 86 | $M_L$ 6.0 | Maley *et al.*, 1986 |
| San Salvador, El Salvador | 10 | 10 | 86 | $M_S$ 5.4 | Shakal *et al.*, 1986b |
| Whittier Narrows, California | 1 | 10 | 87 | $M_L$ 6.1 | Etheredge and Porcella, 1987 Shakal *et al.*, 1987 |
| Superstition Hills, California | 24 | 11 | 87 | $M_L$ 5.8 $M_L$ 6.0 | Huang *et al.*, 1987 Porcella *et al.*, 1987b |

The processing scheme initially developed from Trifunac's proposals (Trifunac and Lee, 1973) was used successfully on hundreds of seismograms, but there are two problems with it. The finite-difference approximation used for the instrument correction is satisfactory if the sampling rate is high enough, but at 50 samples per second, the rate used for most records processed before 1975, the approximation is poor for frequencies above about 10 Hz (Raugh, 1981; Shyam Sunder and Connor, 1982). Figure 1 compares the response of the finite-difference instrument-correction filter for sample rates of 50 and 200 samples per second with the exact response of the ideal filter for a natural frequency of 25 Hz and damping of 0.6 critical. Most present-day record processing is done at 200 samples per second, a rate at which the finite-difference approximation is adequate as shown in Figure 1. Other methods of instrument correction, however, are preferable. The correction can be applied exactly in the frequency domain, or it can be implemented to arbitrarily high accuracy with a time-domain convolution filter (Raugh, 1981; Shyam Sunder and Connor, 1982).

Shyam Sunder and Connor (1982) pointed out a second problem with the method described by Trifunac and Lee (1973). In the method an acausal high-pass filter is applied and then the result is integrated without including the filter transient that precedes the start time of the unfiltered data. Integrating an acausally filtered record without including the leading filter transient has the effect of shifting the result by a constant amount and can be thought of as reintroducing the low frequencies that were removed by the filter. In the method described by Trifunac and Lee the effects of excluding the leading filter transient were removed later by filtering the velocity and filtering the displacement. For that and other reasons, however, the method was unnecessarily complex. If the filter transients are included, it is possible to use a simple processing scheme consisting only of instrument correction and high- and low-pass filtering of the acceleration, followed by integration to velocity and displacement. The filter transients should also be included in the computation of response spectra; otherwise, spurious long periods will be incorporated into the result. The low-pass filter is necessary if instrument correction is to be performed because the instrument correction strongly amplifies any high-frequency noise present in the record (Figure 1). Because the accelerograph response is flat up to about half of the natural frequency and the natural frequency is typically about 25 Hz for modern instruments, instrument correction is necessary only for the sake
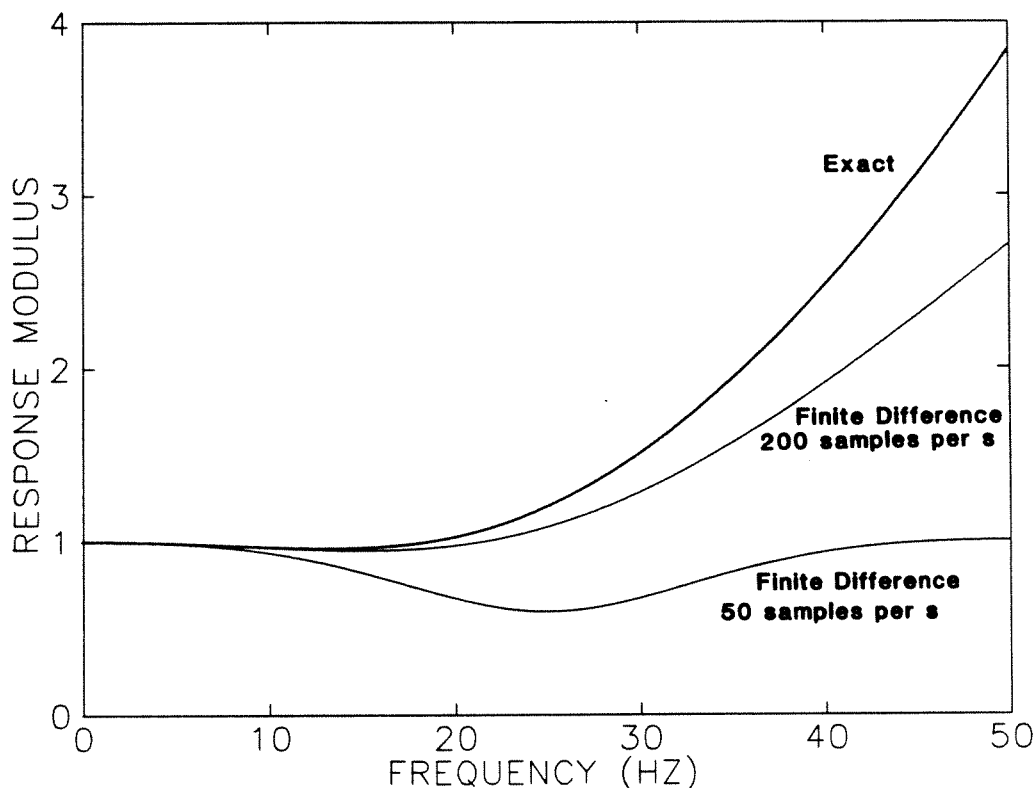
FIGURE 1. The exact response of the ideal instrument-correction filter for a natural frequency of 25 hz and damping of 0.6 critical compared with the response of the finite-difference approximation for 50 and 200 samples per s.

of the high-frequency components of the record. The high-pass filter is generally necessary because any low-frequency noise present in the record is strongly amplified by the double integration to displacement and by the computation of response spectral values at long periods. Direct use of time-domain convolution for the high-pass filter operation requires excessive computer time, much more than recursive filters or frequency-domain filters. Each of the processing stages may be done in a number of different ways. To insure satisfactory results, however, care must be taken with respect to certain key points. If filtering is done in the frequency domain, the record must be padded with enough zeros to avoid wrap-around error. If bidirectional recursive filtering is done, the record must be padded with enough zeros to accomodate the filter transient at the end of the record. If acausal filters are used, as stated previously, subsequent integration and the calculation of response spectra must include the filter transient that precedes the origin time of the original record. It is advisable to avoid using high-pass filters with too sharp a cutoff. Such filters may produce oscillations at frequencies near the cutoff frequencies, as shown by Fletcher et al. (1980).

In the last few years the U.S.Geological Survey has completely revised its standard processing scheme (Raugh, 1981; Converse et al., 1984). Previously the Survey used the methods described by Trifunac and Lee (1973). The revised scheme combines the low-pass filter and instrument correction and offers the option of implementing the combination either in the frequency domain or by time-domain convolution. An advantage of combining the low-pass filter and instrument correction is a substantial reduction in the number of filter weights required for specified accuracy in the time-domain convolution for the instrument correction. For routine operations the high-pass filter is a bidirectional Butterworth recursive filter, although other options are available. The current version contains provision for including the leading filter transient in subsequent computations, but that feature is not described in the latest published manual (Converse, 1984). The California

Joyner and Boore

Strong-Motion Instrumentation Program uses a processing scheme that is a modified version (Shakal and Ragsdale, 1984) of the methods described by Trifunac and Lee (1973). Shyam Sunder and Connor (1982) proposed a scheme in which the instrument correction is performed by time-domain convolution and the low- and high-pass filters are combined and implemented by an elliptical recursive filter. Khemici and Chiang (1984) describe a system in which instrument correction, high- and low-pass filtering, and integration are all combined into one operation in the frequency domain.

Record-processing procedures are available which, if properly applied, are entirely adequate for the ranges of frequency and amplitude that have engineering significance. The most critical problem in applying the record-processing procedures is choosing the cutoff frequency for the high-pass filter. The best recent approach to that problem (Shakal and Ragsdale, 1984; Lee and Trifunac, 1984; Gerald Brady, written communication, 1987; Kenneth Campbell, oral communication, 1987) is to digitize one of the fixed traces which are present on the records from most modern analog strong-motion instruments and use the results to estimate the spectrum of the noise in the processing system. The proper cutoff frequency is chosen on the basis of a comparison between the spectrum of the noise and the spectrum of the accelerograph trace. Whether a filter with a given cutoff frequency removes a significant portion of the signal can be judged with the help of some results from seismology. For earthquakes large enough to be of engineering interest, the Brune (1970, 1971) spectrum of acceleration, which has been shown to be a good description of strong ground motion (Hanks and McGuire, 1981; Boore, 1983; Anderson and Hough, 1984), is approximately flat at intermediate frequencies down to a corner frequency $f_0$ below which the spectrum is proportional to frequency squared. The corner frequency is given by

$$f_0 = 4.9 \times 10^6 \beta (\Delta\sigma/M_0)^{1/3}$$

where the units of $f_0$, $\beta$, $\Delta\sigma$, and $M_0$ are Hz, km/s, bars, and dyne-cm, respectively. For $\beta = 3.2$ km/sec and $\Delta\sigma = 100$ bars (Boore, 1983) the formula simplifies to $f_0 = 10^{-(M-5)/2}$, where M is moment magnitude. Unless the cutoff frequency is significantly less than the corner frequency, application of a high-pass filter should be expected to modify the signal substantially. For example, an earthquake of magnitude 6 has a corner frequency of about 0.3 Hz according to the formula. Unless the cutoff frequency is much smaller than 0.3, we should expect the signal from a magnitude 6 earthquake to be significantly changed by filtering.

Most strong-motion accelerograph data include low-frequency noise sufficient to make high-pass filtering mandatory, and the permanent displacement is thereby lost. If data of sufficient accuracy are obtained, and if the instrument is not subjected to tilt, then it should be possible to forego high-pass filtering and doubly integrate the acceleration to displacement, retaining the permanent displacement. In the case of triggered accelerographs this feat would require determination of the initial velocity. The processing system used by the U.S. Geological Survey (Converse, 1984) contains a procedure for obtaining the initial velocity. The accelerogram is first integrated to velocity without high-pass filtering. The final portion of the velocity trace after the strong motion has subsided is then fit by a least-squares straight line, on the assumption that the velocity must be zero after the strong motion ceases. In fitting the straight line, tapered weights are applied at the beginning and end of the fitted segment to prevent partial cycles of low-level motion from biasing the determination of the line. The tapered weights are cosine half bells. The fitted line is extended to the start time of the record and subtracted, point by point, from the velocity, which is then integrated to give displacement. The slope of the line fitted to velocity is subtracted from the acceleration.

Digital recorders preserve the initial motion, simplifying the task of determining permanent displacement. Iwan et al. (1985) have proposed a scheme for processing digitally recorded data that replaces the high-pass filtering operation by corrections to make the average of both the acceleration and velocity zero over the final portion of the record. The permanent displacement is preserved in this scheme. A constant correction is applied to the portion of the record corresponding to the time of strong shaking, and a different constant correction is applied to the remainder of the record after the end of strong shaking. The values of the two different corrections are chosen so as to achieve the

Joyner and Boore

desired zero values for average velocity and average acceleration over the final portion of the record. Anderson *et al.* (1986) applied this scheme to determine permanent displacement at accelerograph sites in the epicentral region of the 1985 Michoacan, Mexico earthquake, including one site where the resulting vertical displacement of nearly 1 m was confirmed by observations of coastal uplift. The scheme will only work, of course, with data of sufficient relative accuracy.

## CHARACTERIZATION OF STRONG GROUND MOTION

A number of different parameters may be used to characterize strong ground motion for purposes of seismic design. These include peak acceleration, peak velocity, response spectral values, and Fourier spectral values. Peak displacement has also been suggested, but peak displacement is too sensitive to the somewhat arbitrary choice of high-pass filter cutoff used in record processing. The most useful of these parameters are response spectral values. The response spectrum is the basis, either directly or indirectly, of most earthquake-resistant design. It may be used in the dynamic analysis of structures, and it is the basis for the relation, in building codes, between the lateral-design-force coefficient and the period of the building (Structural Engineers Association of California, 1980; Applied Technology Council, 1978). The response spectrum is useful because it represents the response, to a given ground motion, of a set of simple mathematical models of structures. It can be defined as the maximum response, to the given motion, of a set of single-degree-of freedom oscillators (for example, mass-spring systems) having different natural periods and damping. The response spectrum as customarily defined represents the response of a damped elastic system and does not incorporate the nonlinear response to be expected from real structures at high levels of motion. Nonlinear response spectra can be computed, but they would be different for different kinds of structures. As a practical matter, linear response spectra, coupled with response-reduction factors calculated by nonlinear analysis of particular structural types, are more likely to be used than nonlinear response spectra (Cornell and Sewell, 1987).

Although response spectral values may be the most useful of the parameters describing ground motion, the most emphasis in engineering practice, at least in the past, has been placed on peak horizontal acceleration. The conventional method for estimating response spectral values uses peak horizontal acceleration to scale some normalized spectral shape such as the Nuclear Regulatory Commission's Regulatory Guide 1.60 spectrum (U.S. Atomic Energy Commission, 1973). Such a procedure would be generally valid only if the shape of the response spectrum were independent of earthquake magnitude, source distance, and recording site conditions. In fact, a number of independent studies (McGuire, 1974; Mohraz, 1976; Trifunac and Anderson, 1978, Joyner and Boore, 1982) have shown that the shape of the response spectrum is strongly dependent on magnitude and site conditions, and, at frequencies less than about 3 Hz, large errors can result from the practice of scaling fixed spectral shapes by peak acceleration. These errors can be partially avoided by Newmark and Hall's (1969) method, in which the short-period portion of the spectrum is proportional to peak acceleration, the intermediate portion (about 0.3 to 2.0 sec) to peak velocity, and the long-period portion to peak displacement. The proportionality factor between velocity and intermediate period response, however, varies significantly with magnitude and site conditions as indicated by our predictive equations for response and for peak velocity (Joyner and Boore, 1982). Peak displacement, moreover, is, as previously mentioned, a quantity that is highly sensitive to the choice of high-pass filter cutoff. The obvious solution is to predict response values directly (e.g. Joyner and Boore, 1982). Another approach is the use of peak acceleration to scale a normalized spectral shape that varies with magnitude and site conditions (Idriss, 1985, 1987).

The search for a single parameter to characterize ground motion is clearly doomed to failure. Because the shape of the spectrum changes with magnitude and site conditions, a single parameter that represents ground motion well at one frequency must necessarily fail to do so at others.

In general, the study of ground motion has been focused on the horizontal component because of its greater engineering significance, and this review will not deal explicitly with the vertical

component. If needed, estimates of vertical motion can be obtained from procedures similar to those discussed in this paper for estimating the horizontal component of motion.

## PREDICTION OF STRONG GROUND MOTION

### Factors That Affect Strong Ground Motion

**Wave Types Involved in Strong Ground Motion.** Horizontal ground motion is produced by S body waves (shear waves that travel through the earth) and by surface waves (waves that propagate along the surface). Where velocity increases with depth, which is the usual case, fundamental-mode surface waves tend to arrive later than body waves and may be distinguished by their later arrival. Higher-mode surface waves may arrive at more nearly the same time as body waves and may therefore be difficult to distinguish from body waves; in fact the distinction between body waves and higher-mode surface waves is not always meaningful.

The engineering importance of surface waves is sometimes overstated. The strong motion with frequency in the range of about 2–10 Hz seen on horizontal accelerograms recorded within a few tens of km of the source can adequately be described in terms of S body waves, perhaps modified to some degree by scattering and reflection. Surface waves are also recorded by strong-motion instruments (Hanks, 1975). Typically they are recorded at sites on deep sedimentary basins, they have periods in the general range of 3–10 sec, and they arrive later than the S body waves. In some cases, perhaps in most cases, these waves are generated at the margins of the sedimentary basins by conversion from body waves in the high-velocity material bounding the basin (Vidale and Helmberger, 1988). In such basins fundamental-mode surface waves at frequencies of engineering interest are confined to shallow depths, a few hundred meters or so, and sources at seismogenic depths are ineffective in exciting them. They can more readily be excited by body waves incident at basin margins.

Concerning the role of surface waves in strong ground motion, there is a widespread misconception that surface-wave amplitude decays with distance $r$ as $r^{-1/2}$ whereas body waves decay as $r^{-1}$ and surface waves will therefore dominate on distant records. This concept is wrong in at least two different ways. In the first place, while Fourier spectral amplitudes of surface-wave ground motion do in fact decay as $r^{-1/2}$, time-domain amplitudes do not, because of dispersion. Well-dispersed surface waves have a time-domain amplitude decay of $r^{-1}$, and Airy phases, which correspond to stationary points on the group-velocity dispersion curve, have a decay of $r^{-5/6}$ (Ewing *et al.*, 1957, p. 358). Furthermore, fundamental-mode surface waves are confined to the shallower layers, and are therefore subject to greater anelastic attenuation than body waves.

At distances of about 100 km and greater the dominant phase on strong-motion records is the $L_g$ phase, which is a superposition of multiply-reflected S waves trapped in the crust by supercritical reflection (Bouchon, 1982; Kennett, 1985). It is an Airy phase and therefore has a theoretical decay with distance of $r^{-5/6}$. It is dominant over direct body waves at distance probably because direct body waves decay with distance more rapidly than $r^{-1}$ for realistic distributions of velocity with depth. In contrast to the direct body wave whose duration is fixed by the source duration, the $L_g$ phase has a duration that increases with distance—an important point in ground-motion modeling (Herrmann, 1985).

**Magnitude.** Earthquake ground motions depend on the size of the earthquake, the most common measure of which is magnitude. Of the many different kinds of earthquake magnitude that have been defined, the two most commonly cited in earthquake engineering are the Richter local magnitude $M_L$ and the surface-wave magnitude $M_S$. $M_L$ is determined from the trace amplitude on a record made by a particular kind of seismograph, the Wood-Anderson seismograph, located within a few hundred km of the earthquake. $M_S$ is determined from the ground motion associated with surface waves of 20 s period recorded anywhere in the world. For earthquakes in California with $M_L$ less

than about 6.5 the commonly cited magnitude is $M_L$. For earthquakes worldwide with $M_S$ greater than about 6.5 the most commonly cited magnitude is $M_S$.

The recently defined moment magnitude M (Hanks and Kanamori, 1979) has the advantage that it corresponds to a well-defined physical property of the earthquake source. It is defined in terms of the seismic moment $M_0$, which is the product of three factors, the area of the rupture surface, the average slip, and the modulus of rigidity in the source zone. Moment magnitude is thus a measure of the size of an earthquake in a very specific sense. The equation for computing moment magnitude is

$$\text{M} = \frac{2}{3} \log M_0 - 10.7 \tag{1}$$

where the units of $M_0$ are dyne-cm. Use of moment magnitude has the advantage of making it easier to relate earthquake occurrence rates to geologically determined fault slip rates. It is sometimes stated that because $M_L$ is determined from an instrument with a natural period in the period range of greatest engineering interest $M_L$ should be preferred as the measure of earthquake size to use in making ground-motion estimates for engineering purposes. Catalog values of $M_L$ for large earthquakes, however, are commonly poorly determined (Hutton and Boore, 1987; Boore, 1988), and moment magnitude is the better measure for such use. We compiled moment magnitudes for most of the earthquakes in the western North American strong-motion data set prior to 1981 (Joyner and Boore, 1981). Ekström and Dziewonski (1985) gave moments for 35 earthquakes in western North America occuring between 1977 and 1983. Moment determinations are available for most past earthquakes with important strong-motion records and can be expected for most, if not all, such earthquakes in the future.

In developing equations for the empirical estimation of earthquake ground motion we use moment magnitude as the measure of earthquake size (Joyner and Boore, 1981, 1982). Campbell (1981, 1988) and Idriss (1985) used $M_S$ for earthquakes with $M_L$ and $M_S$ greater than or equal to 6.0 and $M_L$ for earthquakes with $M_L$ and $M_S$ less than 6.0. Generally speaking, below a moment magnitude of about 8.0, moment magnitudes are approximately the same as magnitudes assigned by Campbell's rule, which in turn are the commonly cited magnitudes. The 1979 Imperial Valley, California, earthquake, however, was assigned a magnitude of 6.5 by us and 6.9 by Campbell. This discrepancy has a significant effect on the end results because the 1979 Imperial Valley earthquake contributes a large share of the near-source data points to both data sets.

Distance. Because the rupture surface for earthquakes may extend over tens or hundreds of kilometers, there is ambiguity in defining the source distance for a strong-motion record. Various measures of source distance have been used in the development of relationships for estimating ground motion. Some of these are illustrated in Figure 2. The early analyses tended to use epicentral distance because it was readily available. Obvious problems arise with the use of either epicentral or hypocentral distance in the case of earthquakes like the 1966 Parkfield, California, earthquake or the 1979 Imperial Valley, California, earthquake, which have very long rupture zones with the epicenter at one end and recording stations at the other. For some stations the epicenter and hypocenter are many times more distant than the closer portions of the rupture which are in fact the sources of the peak motions. Similar problems arise with the use of distance to the centroid of the rupture. Some stations may be far from the centroid but close to the rupture. In general it must be expected that different parts of the fault rupture will produce the peak motion at different recording stations. It might seem that the distance measure to use is the distance to the part of the rupture producing the peak motion. Where that part of the rupture is located, however, is unknown for many past earthquakes and all future earthquakes. Most recent work has used some variation on the closest distance to the rupture. We used the closest distance to the vertical projecton of the rupture on the surface of the earth (Joyner and Boore, 1981, 1982). Campbell (1981, 1988) used the closest distance to the rupture. In his 1981 paper he interpreted that as the distance to the surface rupture in the case of ruptures that broke the surface. In his 1988 paper he changed the interpretation to the closest distance to the "zone of seismogenic rupture." The top of that zone was identified from
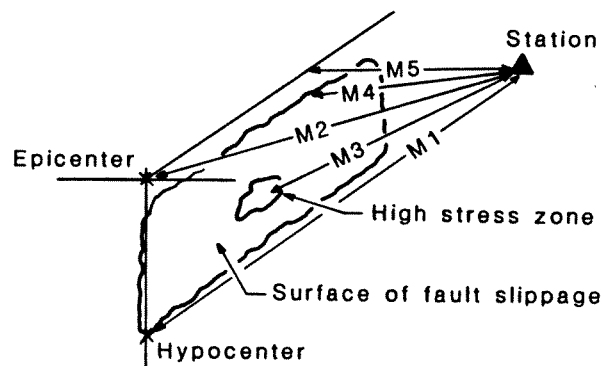
**FIGURE 2.** Diagram illustrating different distance measures used in predictive relationships (from Shakal and Bernreuter, 1981).

the aftershock distribution if possible, otherwise by the intersection of the fault surface with the surface of the basement rock.

For a point source in a uniform medium, geometric spreading of a direct body wave produces a distance dependence of $1/r$ for ground-motion amplitudes, where $r$ is distance. Anelastic attenuation and/or scattering further reduce each frequency component by a factor of $\exp(-\pi f r/Q\beta)$, where $f$ is frequency, $\beta$ is the propagation velocity, and $Q$ is the quality factor, which may depend on frequency ($1/Q$ is equal to twice the fraction of critical damping for the material). In a nonuniform medium geometric spreading may not be well-represented by the $1/r$ factor. In cases where spreading of $1/r$ is assumed, analysis commonly indicates $Q$ increasing with frequency. As Frankel and Wennerberg (1987) point out, however, the apparent frequency dependence of $Q$ may be simply the consequence of underestimating the effect of geometric spreading.

Burger *et al.* (1987) and Barker *et al.* (1988) have shown that, in a layered medium, horizontal ground motion at the shortest ranges is dominated by the upgoing direct S wave, which typically falls off more rapidly than $1/r$. At somewhat greater distances depending on the crustal structure, the motion is dominated by the interaction between the upgoing S wave and the S wave that initially heads downward and is later refracted upward toward the surface. In the vicinity of 100 km the motion is dominated by supercritical reflections from the base of the crust and in some cases from interfaces within the crust. Beyond 100 km the motion is dominated by the $L_g$ phase, which, as noted above, is a superposition of multiple supercritically reflected S waves and has a falloff of $r^{-5/6}$. These complications can be modeled but only if the crustal structure is well-known and only for specific source depths. In most cases simpler methods will be relied upon for estimating ground motion.

There is no clear-cut basis for choosing a simple functional form to represent the dependence of ground-motion amplitudes with distance. We have used $exp(kr)/r$, where $k$ is chosen to fit the data, except for certain long-period response ordinates for which the value of $k$ turned out to be positive. In those cases we used $r^d$, where $d$ is chosen to fit the data (Joyner and Boore, 1981, 1982). Most other workers have used $r^d$ with $d$ generally less than -1.0. It is probably not appropriate to attach much physical significance to the parameter values obtained by fitting these simple functions

Joyner and Boore

to the data.

It is of interest to examine the distance dependence of the Wood-Anderson amplitudes used in assigning Richter local magnitude $M_L$ because many more data are available than in the strong-motion data set. Wood-Anderson amplitudes in northern California were investigated by Bakun and Joyner (1984) and in southern California by Hutton and Boore (1987). There were sufficient data in both data sets to determine both $d$ and $k$ in the function $r^d \exp(kr)$ used to model the distance dependence. The value of $d$ determined for central California was statistically indistinguishable from -1.0, and for southern California it was -1.11. The distance dependence of Wood-Anderson amplitudes found in both studies is very similar to that found for peak horizontal acceleration and velocity from strong-motion data recorded principally in California (Joyner and Boore, 1981, 1982). This similarity indicates that data collected by high-sensitivity seismograph networks can be used in developing locally applicable equations for estimating strong motion in regions where few strong-motion data are available (see Rogers *et al.*, 1988).

A significant issue in estimating future earthquake ground motion is the question of whether or not the shape of the curves relating peak ground-motion amplitudes to distance are dependent on magnitude. This issue is illustrated in Figure 3, which shows the curves for mean peak horizontal acceleration given by Campbell (1981), which have a magnitude-dependent shape, compared with ours, which do not (Joyner and Boore, 1981). Both his equations and ours contain a parameter that takes on the value zero if the shape is magnitude-independent and not otherwise. He finds that the parameter is significantly different from zero in his equations; we do not in ours. The reasons for the conflicting conclusions are not clear. Differences in the definitions of distance may be a factor. Lacking statistical evidence for significance we would include the parameter only if we believed that theoretical considerations called for it. We do give a theoretical argument in the appendix of our paper for a small degree of magnitude-dependence, but too small to justify modifying the equations. We remain unconvinced by other theoretical justifications for magnitude-dependence. As to the finite-source argument, we acknowledge that the whole rupture surface may be large compared to the distance to the recording site, but we would argue that the source of the peak motion is some restricted portion of the whole rupture and may well be small compared to the distance to any recording site on the surface of the earth. As we will show later, the question of magnitude-dependent shape does not make an important difference for predicting peak horizontal acceleration or response spectra at periods near 0.2 s, the difference being small compared to the standard error of an individual prediction. For peak horizontal velocity or response spectra at periods of about 1.0 s or longer, however, the difference is important.

**Site Conditions.** Significant site effects include the effects of topography and local site geology and the effects on the ground motion of structures within which or near which the recording instruments are installed. The effects of topography are the subject of a large literature (*e.g.* Boore, 1972, 1973; Bouchon, 1973; Tucker *et al.*, 1984; Brune *et al.*, 1984; Bard and Tucker, 1985; Geli *et al.*, 1988; Andrews *et al.* 1988), but since the effects are negligible at most sites we will not consider them further here. The effect of local site geology has also been widely discussed (*e.g.* Kanai, 1952; Gutenberg, 1957; Idriss and Seed, 1968; Borcherdt, 1970; Rogers *et al.*, 1984).

In considering local geological effects it is necessary to distinguish between two kinds of site amplification. The more widely recognized but actually less common of the two is the resonant amplification resulting from reinforcing mutiple reflections within low-velocity layers near the surface. This kind of amplification is highly sensitive to frequency. The second kind does not require sharp, reflecting interfaces, is not sensitive to frequency, and results from low velocity, or, more precisely, low impedance near the surface, impedance being the product of density and velocity. If we consider a tube of rays and neglect losses due to reflection, scattering and anelastic attenuation, the energy along a tube of rays is constant. If the effect of changes in the cross-sectional area of the tube can be neglected, which is commonly the case, then amplitude is inversely proportional to the square root of impedance (Aki and Richards, 1980, p. 127).
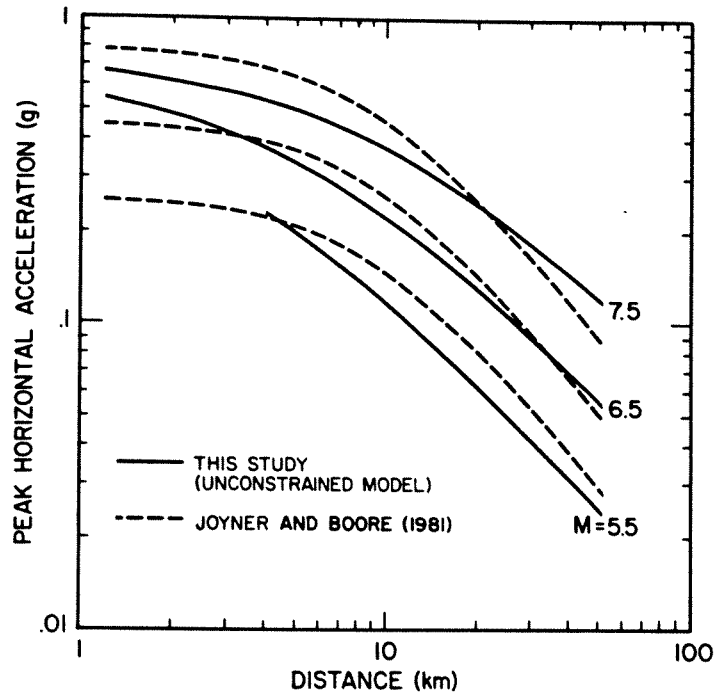
FIGURE 3. Curves of mean peak horizontal acceleration given by Campbell (1981), which have a magnitude-dependent shape, compared with those of Joyner and Boore (1981), which do not. The Joyner and Boore curves for the larger peak of two horizontal components have been reduced by 12 percent so that they may be compared with the mean peak. (Illustration modified from Campbell, 1981.)

Material with low velocity (and thereby low impedance) tends to have low $Q$, so, depending on the frequency of the motion and the thickness of the material, the amplifying effect of low-velocity material may be partly or totally offset by greater attenuation.

Largely because the data on site conditions at strong-motion recording sites are limited, the means used to incorporate site effects into the analysis of strong-motion data sets tend to be rather crude. We divided recording sites into two categories, rock and soil (Joyner and Boore, 1981, 1982). Sites with less than 5 m of soil overlying rock were put into the rock category. We found no statistically significant difference between the rock and soil sites in peak horizontal acceleration or response spectral values at periods less than 0.3 s, suggesting that attenuation in the soils offsets the amplification for high frequencies. Joyner and Fumal (1984) found no correlation at soil sites between peak horizontal acceleration and depth to rock for a range in depth to rock from nearly zero to nearly one km. This suggests that most of the attenuation in soils occurs at shallow depth, perhaps less than something like 100–200 m. For peak horizontal velocity and response at periods longer than about 0.3 s, we found significantly higher values on soil than on rock, higher by a factor of 1.5 for peak horizontal velocity and by a factor of 1.9 for one-second horizontal pseudovelocity response. If the effects of attenuation just offset the effects of amplification for high-frequency measures of ground motion, it would be expected that amplification would dominate for lower-frequency measures, since the limited available data suggest that $Q$ in soils is not dependent on frequency.

Campbell (1981) separated sites with less than 10 m of soil overlying rock into a special category of shallow soil sites. For other sites he, as we, found no significant difference between peak horizontal acceleration on rock and soil. The shallow soil sites, however, had a higher peak acceleration than the other categories by a factor of 1.8 on the average. Though we might argue about the criterion for delimiting the category of shallow soil sites, we do not disagree with the designation of such a

Joyner and Boore

category; our data set simply did not include a sufficient number of shallow soil sites to support a separate category. Results from analysis of Italian strong-motion data (Sabetta and Pugliese, 1987) support higher horizontal accelerations at shallow soil sites. Mohraz (1976) showed that horizontal response spectra at shallow soil sites were preferentially richer in high frequencies than at sites where the soil was more than 60 m thick.

In an attempt to achieve a more physically based method of predicting site effects, Joyner and Fumal (1984) used downhole shear-velocity data at 33 strong-motion sites to develop equations for site effects in terms of the shear velocity averaged from the surface to a depth equal to one-quarter wavelength at the period of interest. Campbell (1988) took a different approach to the site effect on peak horizontal velocity and, like Trifunac and Lee (1979), expressed the site effect in terms of the depth of sediments beneath the recording site. No physical interpretation was given of this representation of the site effect. Unlike Trifunac and Lee, Campbell expressed the site effect in terms of a nonlinear function of sediment depth.

The methods described above do not incorporate the effect of resonance. To do so requires more detailed site information than is often available. For cases where the required information is available, methods of modeling assuming body waves in plane layers can be used. Pioneer work with such methods was done by Idriss and Seed (1968; Schnabel et al., 1972). They used the equivalent-linear method to incorporate nonlinear behavior in the soils, that is, they used a linear analysis with values of the dynamic soil properties chosen by an iterative procedure to correspond with the average strain level determined by the analysis. Joyner and Chen (1975) presented a truly nonlinear method and showed that for motion of short period and high amplitude on thick soil deposits the equivalent-linear method does not give a satisfactory approximation to the nonlinear results. Silva (1976) described a general system for the linear modeling of plane-layered systems based on the Thompson-Haskell method. All these kinds of analyses depend on the assumption of plane layers and, if nonlinearity is presumed, on laboratory data for dynamic soil properties. The adequacy of the plane-layer approximation has been demonstrated at a number of sites (e.g. Joyner et al., 1976; Johnson and Silva, 1981), though there are sites for which it is not appropriate (King and Tucker, 1984). There is some uncertainty, however, over the degree to which laboratory data are representative of the properties of soils in situ and in particular over the level of shaking at which nonlinearity becomes a significant factor for soils in situ.

An extreme example of the effect of site conditions is afforded by the damage in Mexico City from the 1985 Michoacan, Mexico, earthquakes, whose source zones were 300 km or more from the city. More than 300 buildings in Mexico City were destroyed or badly damaged. Nearly all of the buildings that collapsed in the city were located in an old lake bed, characterized by very soft clay soils. Response spectra at 5 percent damping showed amplification of approximately ten times at 2 s period on the lake bed relative to surrounding areas (Anderson et al., 1986; Singh et al., 1988). Materials similar to the soft clays of the old lake bed are found elsewhere in the world, and changes have been made in the upcoming editions of the Recommended Lateral Force Requirements of the Structural Engineers Association of California (1988) and the Uniform Building Code (International Conference of Building Officials, 1988) in an attempt to accomodate situations of this kind.

Many strong-motion records come from instruments located at the ground floor or in the basements of buildings or on the abutments of dams. Such records are affected by the response of the structure in which or near which the instrument is located. Even so-called "free-field" sites may be affected at high frequencies by the response of the instrument shelter (Bycroft, 1978; Crouse et al., 1984), though for the typical shelters used by the U.S. Geological Survey and the California Division of Mines and Geology the effects are at frequencies too high to be of concern (Crouse and Hushmand, 1987). We attempted to minimize the effects of structures by excluding all data recorded on the abutments of dams or in the basements of buildings three or more stories in height (Joyner and Boore, 1981, 1982). Campbell (1981, 1988) included the effect of the building as a parameter to be determined by analysis of the data.

**Fault Type, Depth, and Repeat Time.** Fault type, depth, and repeat time have been suggested as important in determining ground-motion amplitudes because of their presumed relation to the stress state at the source or to stress changes associated with the earthquake. McGarr (1984) argues that ground motion should increase with depth and that ground motion should be greater from reverse faults than from normal faults, with strike-slip faults having intermediate values. Kanamori and Allen (1986) present data showing that faults with longer repeat times have shorter lengths for the same magnitude, indicating a larger average stress drop and, presumably, higher ground motion.

Empirical attempts to correlate fault type, depth, and repeat time with measures of strong ground motion do not support clear-cut conclusions. Campbell (1988) finds that peak horizontal acceleration and velocity in shallow reverse-slip earthquakes are larger on the average by factors of about 1.4 and 1.6, respectively, than in strike-slip earthquakes. Reexamination of data we used in developing our published ground-motion predictive equations indicates values of peak horizontal acceleration higher on the average by a factor of about 1.25 in reverse-slip earthquakes than in strike-slip earthquakes. We cannot tell, however, whether the difference is due to fault type or repeat time. The reverse-slip faults are generally the ones with long repeat times and the strike-slip faults the ones with short repeat times. The conspicuous exception is the 1979 St. Elias, Alaska, earthquake, a reverse-slip event which lies on the boundary between the Pacific and North American plates, and therefore, presumably has a short repeat time. The peak horizontal acceleration values for the St. Elias earthquake on the average fall below the predictions of the equations developed from the whole data set, suggesting that repeat time and not fault type is the controlling variable, but no definite conclusions should be drawn based on a single earthquake.

Data on the amplitude of ground motion from normal-slip earthquakes compared to other types is subject to conflicting interpretations. McGarr (1984; see also McGarr, 1986) found a large difference between normal- and reverse-slip events. For a selected data set with few observations of large events he examined the effect of fault type and focal depth on peak acceleration and peak velocity. To remove the effect of distance he multiplied the peak motions by the hypocentral distance. He assumed that peak acceleration was independent of moment $M_0$, and to remove the effect of $M_0$ on peak velocity he divided by $M_0^{1/3}$. The resulting peak values were approximately proportional to depth. On the average the peak accelerations were about a factor of 3 greater and the peak velocities a factor of 2 greater for reverse- than for normal-slip events. Values for strike-slip events were intermediate. Other studies do not show such large differences. Westaway and Smith (1987) compared peak horizontal acceleration from normal-slip earthquakes with our equations (Joyner and Boore, 1981) and with Campbell's (1981) equations. Both sets of equations are based primarily on data from reverse- and strike-slip events. After considering data from more than 600 records of normal-slip events in the western United States, the Mediterranean region, and New Zealand, Westaway and Smith concluded that there is no significant difference between normal-slip events and others. The data set included some records with source distances greater than 100 km, and the argument could be made that regional differences in attenuation may have obscured differences due to fault type, but the data set also included data, such as the record from the base of the Matahina Dam in New Zealand, at distances short enough so that one would not expect a significant effect due to differences in attenuation (New Zealand Geological Survey, 1987).

The Italian strong-motion data set (Sabetta and Pulgliese, 1987) is particularly pertinent to the comparison between normal- and reverse-slip earthquakes. The data from the Friuli region are all from reverse-slip events and the rest of the data are all from normal-slip events. Sabetta and Pugliese developed predictive equations for peak horizontal acceleration from the whole data set of 95 records and also for the truncated data set of 52 records formed by omitting the records from the Friuli region. The equations developed from the truncated data set gave values only about 10 percent less than the equations developed for the whole data set for a stiff or deep soil site 10 km from a magnitude 6.5 event, indicating that the effect, if any, of fault type was small. Most of the Friuli records were from aftershocks, however, so that this conclusion holds in the general case only if aftershocks can be presumed characteristic of main shocks.

The data discussed up to this point has all come from shallow crustal earthquakes, for which the fault ruptures are confined to a zone within about 20 km of the earth's surface. Another important class of earthquakes is subduction-zone earthquakes such as occur off the Pacific coasts of Japan, Alaska, and Central and South America. Such earthquakes occur over a range of depths of a few hundred kilometers. In an analysis of subduction-zone data from the Northern Honshu zone Crouse et al. (1988) found no significant differences in the horizontal response spectral values from reverse, normal and strike-slip events. Their regression analysis showed a linear dependence of the logarithm of spectral response on focal depth. For periods less than about 1.0 s deeper events gave larger response than shallower events. At 0.1 s period the difference was the largest and corresponded to a factor of 2.5 for an increase of 100 km in depth. At periods greater than about 1.0 s the deeper events gave response that was smaller than shallower events. The difference at 4.0 s was the largest and corresponded to a factor of 1.7 for an increase of 100 km in depth. Crouse et al. suggested that the deeper events might have higher amplitude at short period because of higher stress drop or lower anelastic attenuation. They suggested that the deeper events might have lower amplitude at long period because they are less effective in generating surface waves. They did note, however, that the inclusion of the depth term in the regression did not substantially improve the fit to the data.

**Directivity and Radiation Pattern.** If the angle between the source-to-recording-site vector and the direction of rupture propagation is small, the recorded ground motion may be substantially increased in amplitude. This effect, called directivity (Ben-Menahem, 1961), can be expected to occur for incoherent as well as coherent ruptures (Boore and Joyner, 1978). The work of Boatwright and Boore (1982) shows that strong ground motion can be significantly affected by directivity, but it is not clear how to incorporate directivity into schemes for predicting ground motion in future earthquakes. The variable of importance for directivity is the angle $\theta$ between the rupture direction and the source-to-recording-site vector, and $\theta$ is not known in general for future earthquakes. Furthermore, for sites close to large earthquake ruptures, where reliable prediction is most important, $\theta$ changes during rupture propagation. Araya and Der Kiureghian (1986) have suggested an approach for including directivity in ground-motion predictive equations. Campbell (1988) included directivity as a parameter in his analysis, but he applied it to only 3 recordings out of a total of 134, acknowledging that other recordings in the data set might also be "affected to some degree" by directivity. Most authors of ground-motion predictive equations have not explicitly included a variable representing directivity. To the extent that directivity affects the records in the data set, however, the equations and the estimates of variability will reflect the effect. Near-source recording sites are more likely to be affected by directivity, and the predictive equations will give higher near-source values as a result.

Even without rupture propagation, the ground motion from a point dislocation will depend on the direction the ray leaves the source. This dependence, referred to as radiation pattern, is mentioned here only for the sake of completeness. The radiation pattern, which is relatively simple in a homogeneous medium, is complicated in the real world by scattering and refraction caused by variations in propagation velocity. The fault zone itself probably represents a low-velocity zone, and rays leaving the fault zone at a large angle to the normal may undergo significant refraction. Under these circumstances attempts to incorporate the radiation-pattern effect in ground-motion prediction equations are unlikely to yield much benefit, and no one, to our knowledge, has proposed doing so.

### Empirical Prediction

**The Method of Representative Accelerograms.** Guzman and Jennings (1976) suggested a method, later elaborated by Heaton et al. (1986), for establishing design ground motions. The method begins with the selection of a suite of accelerograms recorded for magnitudes, distances, local site conditions and other factors similar to the postulated design earthquake. Each accelerogram and its response spectrum are multiplied by a constant scaling factor to account for differences in magnitude and source distance between the design earthquake and the accelerogram. The collection

of response spectra is used to portray the range of ground motion to be expected at the site. The method has the advantage of directness and of maintaining a close tie to the basic data. The necessity for deciding which accelerograms represent conditions similar to the design earthquake and which do not, however, introduces an undesirable element of subjectivity. In our view, well-designed regression analyses of the whole data set make more efficient use of the available information than the method of representative accelerograms.

**Development of Predictive Relationships.** A comprehensive review of ground-motion predictive relationships developed before the 1979 Imperial Valley, California, earthquake is given by Idriss (1979). The 1979 Imperial Valley earthquake marked a major change in the strong-motion data base by providing many more near-source data points than had been available previously. More recent reviews have been written by us (Boore and Joyner, 1982) and Campbell (1985). Predictive relationships for ground motion may be expressed in graphical form or as mathematical equations. An example of graphical relationships is provided by the widely-used Schnabel and Seed (1973) curves, which are the basis of the seismic risk maps by Algermissen and Perkins (1976) and Algermissen et al. (1982) as well as the ATC-3 seismic zone maps (Applied Technology Council, 1978). In the case of predictive relationships expressed as mathematical equations, the equations contain parameters that are adjusted in some way so as to fit the available strong-motion data. Brillinger and Preisler (1984, 1985) demonstrated that there is a significant between-earthquake component of variance in ground-motion data in addition to the within-earthquake component. Such being the case, ordinary least squares is not strictly correct as a method for determining the parameters of the predictive equations. Brillinger and Preisler describe maximum-likelihood methods applicable to this case. The need to take account of the between-earthquake variance was recognized by us in our use of a two-stage regression procedure (described below) to develop predictive relationships (Joyner and Boore, 1981). The two-stage procedure gives virtually the same values as the methods of Brillinger and Preisler for each of the two components of the variance, indicating that it is equivalent. Campbell (1981, 1988) uses weighted least squares in a scheme "designed to give each earthquake an equal weight in the analysis in each of nine distance intervals."

In our view it is important to choose a form for the predictive equations based as much as possible on physical grounds. We consider this guideline important because data are sparse or nonexistent for important ranges of the predictive variables. If data were plentiful, it would matter less what form were chosen; either the form would fit the data, or the lack of fit would be obvious. Only those predictive variables should be used whose inclusion can be justified by physical reasoning. Furthermore, the number of adjustable parameters should be kept as small as possible.

A key feature of the data set for shallow earthquakes is the scarcity of data points for distances less than about 20 km and magnitudes greater than 7.0. Confident predictions can simply not be made in that range of magnitude and distance, which is, unfortunately, where predictions are most needed.

Much of the early strong-motion record processing was done on data sampled at 50 samples per second using a finite-difference instrument-correction algorithm. Response values derived from these data may be inaccurate at periods less than about 0.1 s. The peak accelerations obtained from such data may also be in error. Many workers have used uncorrected rather than corrected peak acceleration values to avoid the bias introduced by the early record processing (e.g. Joyner and Boore, 1981, 1982; Campbell, 1981, 1988).

**Examples of Predictive Equations for Shallow Earthquakes.** We now proceed to give examples of a number of predictive equations that have been proposed in the last 10 years. We have attempted to give all the information needed to make predictions of ground motions from the various equations. At the expense of easy visual comparisons of the equations themselves, we have retained the author's form of the equations, units, and preference for natural or common logarithms in order to forestall errors of conversion.

*Joyner and Boore.* Figure 4a shows the distribution in magnitude and distance of the strong-motion data we used in developing predictive equations for peak horizontal acceleration, and Figure 4b shows the distribution we used in developing equations for peak horizontal velocity and pseudovelocity response at 5 percent damping (Joyner and Boore, 1981, 1982). There are more points on Figure 4a than Figure 4b because record processing is necessary to obtain velocity and response spectra, and not all of the records represented on Figure 4a have been processed. The data sets are restricted to earthquakes in western North America with moment magnitude greater than 5.0 and to shallow earthquakes, defined as those for which the fault rupture lies mainly above a depth of 20 km. To minimize the effect of structures we exclude from the data sets all records made at the base of buildings three or more stories in height and on the abutments of dams. We exclude all earthquakes for which the data were in our opinion inadequate for estimating the source distance to an accuracy better than 5 km. Bias may be introduced into a strong-motion data set if low amplitude ground motions are preferentially excluded because they fall below the trigger level of operational instruments or, if recorded, the peak motions are excluded from the data set for any reason having to do with amplitude (*e.g.* a record is not digitized because of its low amplitude). To avoid this bias we exclude, for each earthquake, data recorded at a distance greater than the smallest distance at which an operational instrument did not trigger or at which data were excluded from the data set for a reason related to amplitude.

As previously mentioned, we use a two-stage regression procedure to develop the predictive equations. The precedure is illustrated in Figure 5. In the first stage the equation

$$\log y = A_i + d \log r + kr + s$$
$$r = (r_0^2 + h^2)^{1/2} \tag{2}$$

is fit to the data, where $y$ is the ground-motion parameter to be predicted, $r_0$ is the shortest distance (km) from the recording site to the vertical projection of the earthquake fault rupture on the surface of the earth, and $s$ is the site correction for soil sites (sites with 5 m or more of soil). Initially $d$ is set equal to -1.0. Values of $k$ and $s$ and a value $A_i$ for each earthquake $i$ are determined by linear regression for a trial value of $h$. The final value of $h$ is determined by a simple search procedure to minimize the sum of squares of the residuals, unless the corresponding value of $k$ is positive. In that case $k$ is set to zero and the process repeated this time with variable $d$.

In the second stage a first- or second-order polynomial in magnitude is fit by least squares to the values $A_i$.

$$A_i = a + b(M_i - 6) + c(M_i - 6)^2 \tag{3}$$

where $M_i$ is moment magnitude of earthquake i. In our early papers we used ordinary least squares for the second-stage regression, and, for peak acceleration, excluded all of the earthquakes for which only one recording was available (Joyner and Boore, 1981, 1982). In our 1982 paper, for peak velocity and response spectra, we did not exclude any earthquakes because so few were available. Actually, the correct way to do the second-stage regression is by weighted least squares (Bevington, 1969). The weighting factor, $1/\sigma_i^2$, is the inverse of the variance of $A_i$:

$$\sigma_i^2 = \sigma_a^2/N_i + \sigma_b^2 \tag{4}$$

where $\sigma_a^2$ is the within-earthquake component of the total variance and is given by the variance of data points in the first-stage regression, $N_i$ is the number of records in the data set for earthquake $i$, and $\sigma_b^2$ is the between-earthquake component of the total variance. $\sigma_b^2$ is determined iteratively in the second-stage regression by using zero as a starting value. Use of weighted least squares for the second-stage regression does not produce a large change in the resulting equations.

The final predictive equation is

$$\log y = a + b(M - 6) + c(M - 6)^2 + d \log r + kr + s$$
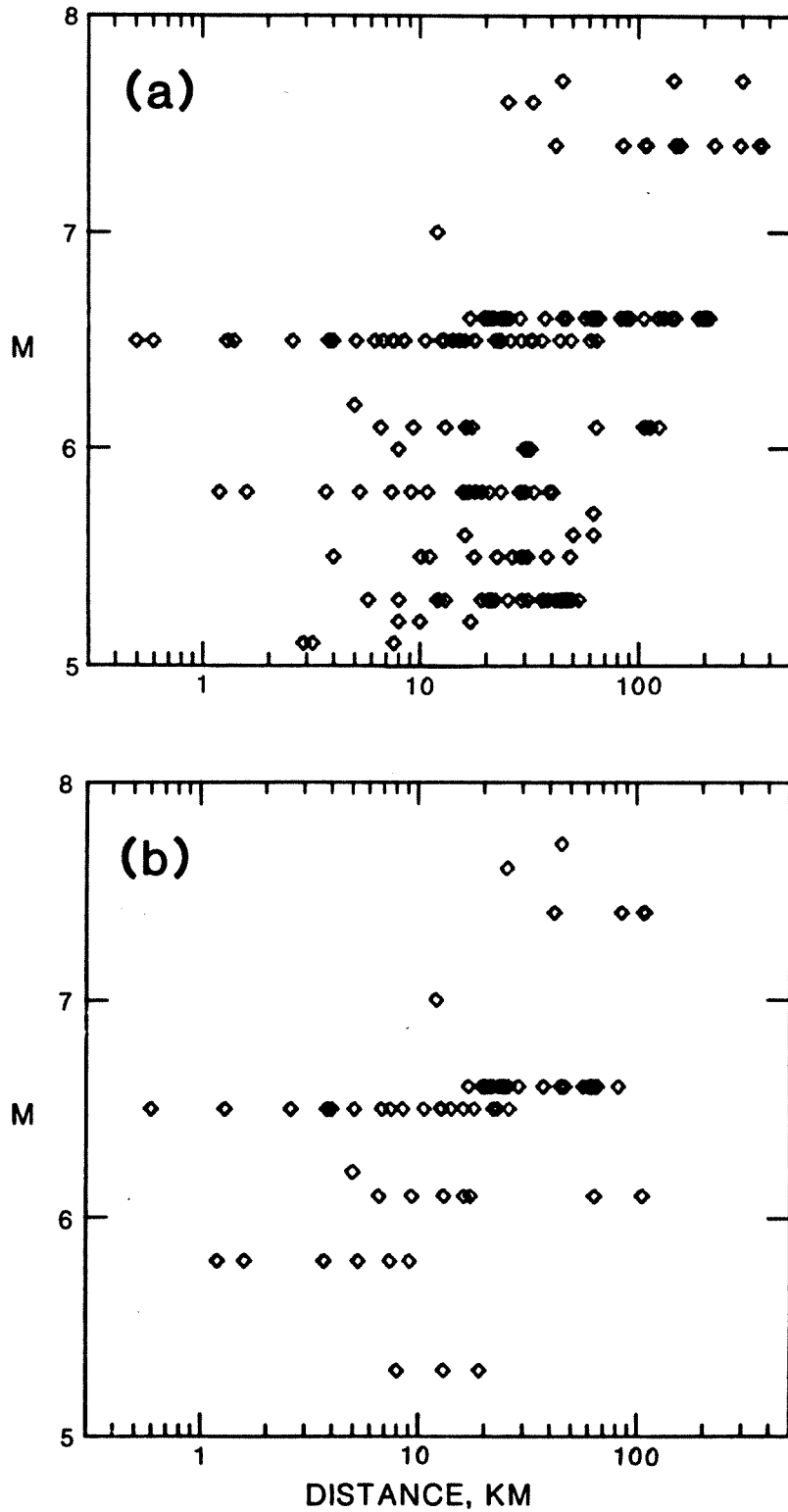$$5.0 \leq M \leq 7.7 \tag{5}$$
$$r = (r_0^2 + h^2)^{1/2}$$

FIGURE 4. Distribution in magnitude and distance of the strong-motion data used by Joyner and Boore (1982) to develop predictive relationships for (a) peak horizontal acceleration and (b) peak horizontal velocity and response spectra.
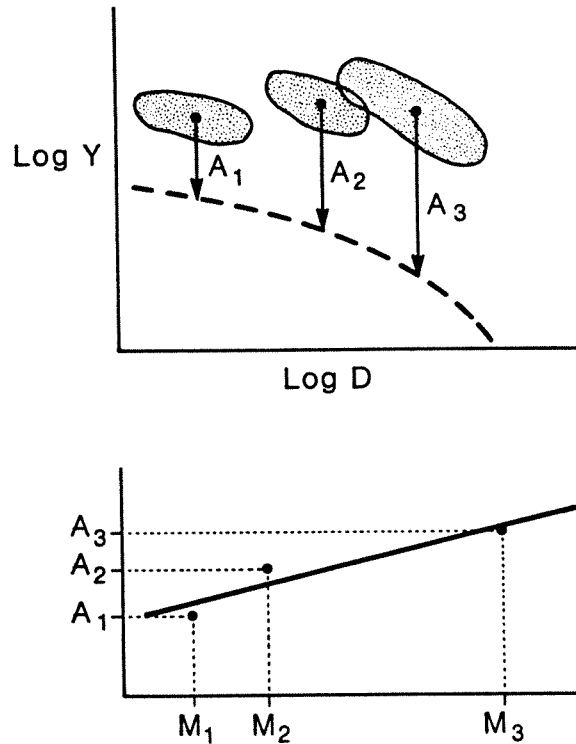
Joyner and Boore

FIGURE 5. Schematic diagram showing the two-stage regression procedure of Joyner and Boore (1981, 1982). The upper part of the figure illustrates the first stage, in which the sum of the squares of the residuals is minimized by varying the shape of the curve representing the dependence on distance (dashed curve) and by shifting all the data points from the $i$th earthquake (contained within a closed curve) by an amount $A_i$. The lower part of the figure illustrates the second stage, in which the offset factors $A_i$ are regressed against magnitude to determine the magnitude dependence.

where values of $a$, $b$, $c$, $d$, $k$, $s$, and $h$ are given in Table 2 for predicting parameters corresponding to the randomly oriented horizontal component and in Table 3 for predicting parameters corresponding to the larger of the two horizontal components. The coefficients for the randomly oriented horizontal component are determined by including in the regression both horizontal components from each site as if they were independent data points. That procedure gives the correct coefficients for the randomly oriented horizontal component, though it would not give correct values for the standard errors of the coefficients, because the two components are not in fact independent. The values given in Table 2 for peak horizontal acceleration and velocity were not determined by regression. They were obtained from the values in Table 3 by changing the constant term $a$ by an amount determined by averaging the difference between the logarithm of the larger peak and the average logarithm of the two peaks over a selected subset of the data. An alternative for the soil effect is

$$s = e \log \left( \frac{V_S}{V_{S0}} \right) \tag{6}$$

where $V_S$ is the site shear velocity averaged to a depth of one-quarter wavelength at the period of interest, and $e$ and $V_{S0}$ are given in Tables 2 and 3 (Joyner and Fumal, 1984).

Equation (5) gives curves of strong-motion amplitude versus distance with a shape independent of magnitude. A magnitude-dependent shape can be obtained by taking

$$h = h_1 \exp[h_2(M - 6)] \tag{7}$$

18                                              Joyner and Boore

TABLE 2. PARAMETERS IN THE PREDICTIVE EQUATIONS OF JOYNER AND BOORE (1982) FOR THE RANDOMLY ORIENTED HORIZONTAL COMPONENT OF PSEUDOVELOCITY RESPONSE (CM/S) AT 5 PERCENT DAMPING AND OF PEAK ACCELERATION ($g$) AND VELOCITY (CM/S)

| Period (s) | $a$ | $b$ | $c$ | $h$ | $d$ | $k$ | $s$ | $V_{S0}$ | $e$ | $\sigma_{\log y}$ |
|---|---|---|---|---|---|---|---|---|---|---|
| Pseudovelocity response | | | | | | | | | | |
| 0.1 | 2.16 | 0.25 | -0.06 | 11.3 | -1.0 | -0.0073 | -0.02 | | | 0.28 |
| 0.15 | 2.40 | .30 | - .08 | 10.8 | -1.0 | - .0067 | - .02 | | | .28 |
| 0.2 | 2.46 | .35 | - .09 | 9.6 | -1.0 | - .0063 | - .01 | | | .28 |
| 0.3 | 2.47 | .42 | - .11 | 6.9 | -1.0 | - .0058 | .04 | 590 | -0.28 | .28 |
| 0.4 | 2.44 | .47 | - .13 | 5.7 | -1.0 | - .0054 | .10 | 830 | - .33 | .31 |
| 0.5 | 2.41 | .52 | - .14 | 5.1 | -1.0 | - .0051 | .14 | 1020 | - .38 | .33 |
| 0.75 | 2.34 | .60 | - .16 | 4.8 | -1.0 | - .0045 | .23 | 1410 | - .46 | .33 |
| 1.0 | 2.28 | .67 | - .17 | 4.7 | -1.0 | - .0039 | .27 | 1580 | - .51 | .33 |
| 1.5 | 2.19 | .74 | - .19 | 4.7 | -1.0 | - .0026 | .31 | 1620 | - .59 | .33 |
| 2.0 | 2.12 | .79 | - .20 | 4.7 | -1.0 | - .0015 | .32 | 1620 | - .64 | .33 |
| 3.0 | 2.02 | .85 | - .22 | 4.7 | -0.98 | .0 | .32 | 1550 | - .72 | .33 |
| 4.0 | 1.96 | 0.88 | -0.24 | 4.7 | -0.95 | 0.0 | 0.29 | 1450 | -0.78 | 0.33 |
| Peak acceleration | | | | | | | | | | |
| | 0.43 | 0.23 | 0.0 | 8.0 | -1.0 | -0.0027 | 0.0 | | | 0.28 |
| Peak velocity | | | | | | | | | | |
| | 2.09 | 0.49 | 0.0 | 4.0 | -1.0 | -0.0026 | 0.17 | 1190 | -0.45 | 0.33 |

where $h_1$ and $h_2$ are chosen to fit the data. As previously mentioned, however, we find that the difference between $h_2$ so chosen and zero is not statistically significant (in particular, see Figure 16 in Boore and Joyner, 1982).

Figure 6 gives the curves for peak acceleration and velocity for the randomly oriented horizontal component, and Figures 7, 8, and 9 give the corresponding pseudovelocity response spectra at 5 percent damping. Figure 7 shows the strong dependence, previously mentioned, of the shape of response spectra on magnitude and site conditions. Figures 8 and 9 show that, between 10 and 40 km at least, there is very little dependence of the shape on distance—in sharp contradiction with conventional wisdom.

Figures 8 and 9 do show that long-period response decreases more than short-period response in going from 0 to 10 km. This reflects the fact that the values of $h$ for short periods are greater than for long periods; the values for peak acceleration are greater than for peak velocity (Tables 2 and 3). It is not completely clear why this should be the case. The larger value of $h$ for peak acceleration and short-period response may represent a limitation in acceleration near the source by the limited strength of near-surface materials.

Tables 2 and 3 give estimates of $\sigma_{\log y}$, the standard deviation of an individual prediction of $\log y$ using the equations. The estimates for peak horizontal acceleration and velocity agree quite well with those of McGuire (1978), who used a data set specially constructed to avoid bias in the estimate of residuals caused by multiple records from a single event or by multiple records from the same site of different events. Some other workers, however, as will be seen, have obtained smaller values for $\sigma_{\log y}$.

*Crouse et al.* The following equation for peak horizontal acceleration and horizontal pseudovelocity

TABLE 3. PARAMETERS IN THE PREDICTIVE EQUATIONS OF JOYNER AND BOORE
(1982) FOR THE LARGER OF TWO HORIZONTAL COMPONENTS
OF PSEUDOVELOCITY RESPONSE (CM/S) AT 5 PERCENT DAMPING
AND OF PEAK ACCELERATION ($g$) AND VELOCITY (CM/SEC)

| Period (s) | $a$ | $b$ | $c$ | $h$ | $d$ | $k$ | $s$ | $V_{S0}$ | $e$ | $\sigma_{\log y}$ |
|---|---|---|---|---|---|---|---|---|---|---|
| Pseudovelocity response | | | | | | | | | | |
| 0.1 | 2.24 | 0.30 | -0.09 | 10.6 | -1.0 | -0.0067 | -0.06 | | | 0.27 |
| 0.15 | 2.46 | .34 | - .10 | 10.3 | -1.0 | - .0063 | - .05 | | | .27 |
| 0.2 | 2.54 | .37 | - .11 | 9.3 | -1.0 | - .0061 | - .03 | | | .27 |
| 0.3 | 2.56 | .43 | - .12 | 7.0 | -1.0 | - .0057 | .04 | 650 | -0.20 | .27 |
| 0.4 | 2.54 | .49 | - .13 | 5.7 | -1.0 | - .0055 | .09 | 870 | - .26 | .30 |
| 0.5 | 2.53 | .53 | - .14 | 5.2 | -1.0 | - .0053 | .12 | 1050 | - .30 | .32 |
| 0.75 | 2.46 | .61 | - .15 | 4.7 | -1.0 | - .0049 | .19 | 1410 | - .39 | .35 |
| 1.0 | 2.41 | .66 | - .16 | 4.6 | -1.0 | - .0044 | .24 | 1580 | - .45 | .35 |
| 1.5 | 2.32 | .71 | - .17 | 4.6 | -1.0 | - .0034 | .30 | 1780 | - .53 | .35 |
| 2.0 | 2.26 | .75 | - .18 | 4.6 | -1.0 | - .0025 | .32 | 1820 | - .59 | .35 |
| 3.0 | 2.17 | .78 | - .19 | 4.6 | -1.0 | .0 | .29 | 1620 | - .67 | .35 |
| 4.0 | 2.10 | 0.80 | -0.20 | 4.6 | -0.98 | 0.0 | 0.24 | 1320 | -0.73 | 0.35 |
| Peak acceleration | | | | | | | | | | |
| | 0.49 | 0.23 | 0.0 | 8.0 | -1.0 | -0.0027 | 0.0 | | | 0.28 |
| Peak velocity | | | | | | | | | | |
| | 2.17 | 0.49 | 0.0 | 4.0 | -1.0 | -0.0026 | 0.17 | 1190 | -0.45 | 0.33 |

response at 5 percent damping was developed from data recorded at deep soil sites (generally greater than 60 m in thickness) during shallow crustal earthquakes in southern California by C. B. Crouse (written communication, 1987; Vyas et al., 1988):

$$\ln y = a + bM_S + cM_S^2 + d\ln(r+1) + kr \tag{8}$$

where $y$ is peak horizontal acceleration (gal) or horizontal pseudovelocity response (cm/s), $M_S$ is surface-wave magnitude, $r$ is closest distance (km) from rupture surface to recording site, and the coefficients $a$, $b$, $c$, $d$, and $k$ are given in Table 4 along with $\sigma_{\ln y}$, the standard deviation of a single prediction of $\ln y$. The values of standard deviation are similar to those in Tables 2 and 3 when the conversion is made from natural to common logarithm (multiply the numbers in Table 4 by 0.43). Both horizontal components were used so that the values of $y$ predicted by equation (8) correspond to the randomly oriented horizontal component.

*Sadigh et al.* Equation (9) for peak horizontal acceleration and horizontal pseudoacceleration response at 5 percent damping was developed using data from the western United States supplemented by significant recordings of earthquakes at depth less than 20 km from other parts of the world (Sadigh, written communication, 1987; Sadigh et al., 1986). Both horizontal components were used.

$$\ln y = a + bM + c_1(8.5 - M)^{c_2} + d\ln[r + h_1 \exp(h_2 M)] \tag{9}$$

where $y$ is peak horizontal acceleration ($g$) or horizontal pseudoacceleration ($g$), M is moment magnitude, $r$ is the closest distance (km) to the rupture surface, and the values of $a$, $b$, $c_i$, $d$, and $h_i$ are given in Table 5 along with expressions for $\sigma_{\ln y}$, the standard deviation of an individual prediction of $\ln y$. Note that $\sigma_{\ln y}$ depends on M and is significantly smaller for M $\geq$ 6.5 than the values in Table 4 and smaller than the values in Tables 2 and 3 if they were converted to natural logarithms. Equation (9) was derived for strike-slip earthquakes; to obtain values corresponding to reverse-slip events, the value of $y$ from equation (9) should be increased by 20 percent.

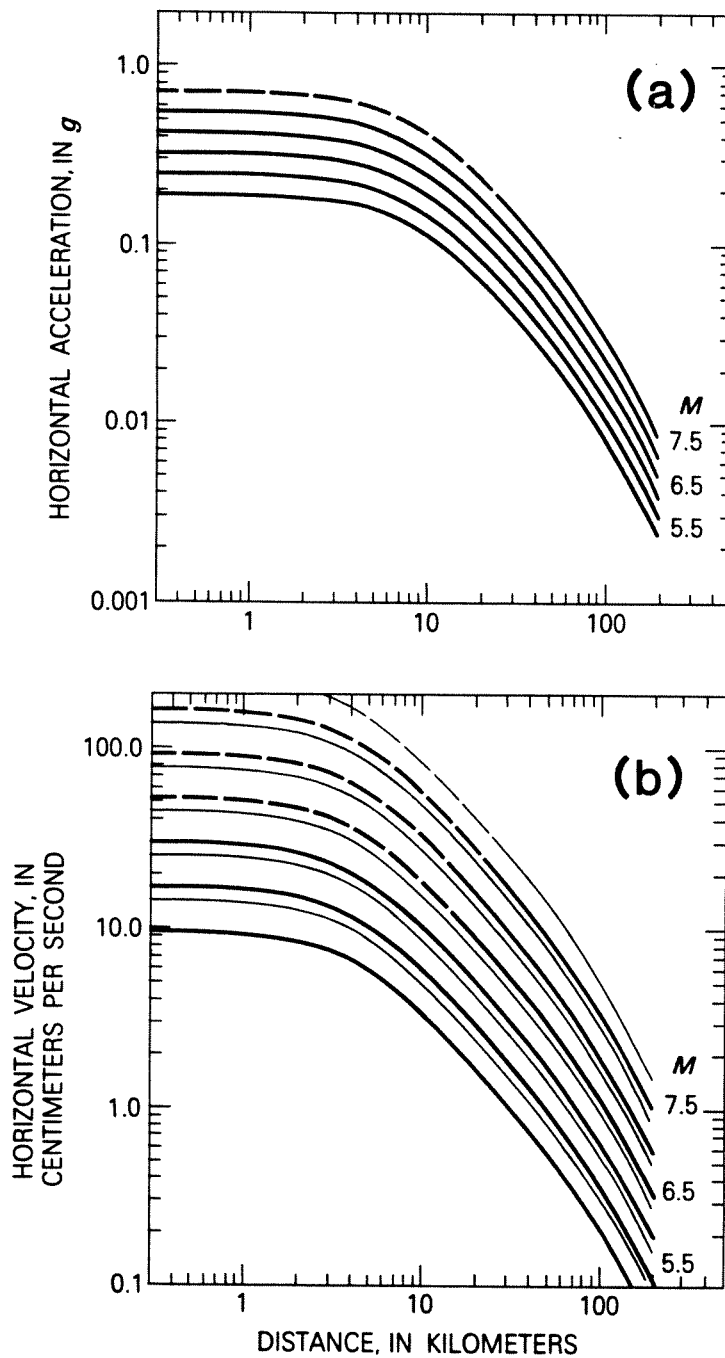20                                                  Joyner and Boore

FIGURE 6. Predictive relationships from Joyner and Boore (1982) for shallow earthquakes giving (a) peak horizontal acceleration, reduced by 13 percent so as to approximate the value for the randomly oriented horizontal component, and (b) peak horizontal velocity at rock sites (heavy lines) and soil sites (light lines), reduced by 17 percent so as to approximate the value for the randomly oriented horizontal component. Curves are dashed where not constrained by data. Distance is the closest distance to the vertical projection of the rupture on the surface of the earth.

*Donovan and Borstein.* Equation (10) was developed for peak horizontal acceleration from data from the western United States (Donovan and Bornstein, 1978). Both horizontal components were
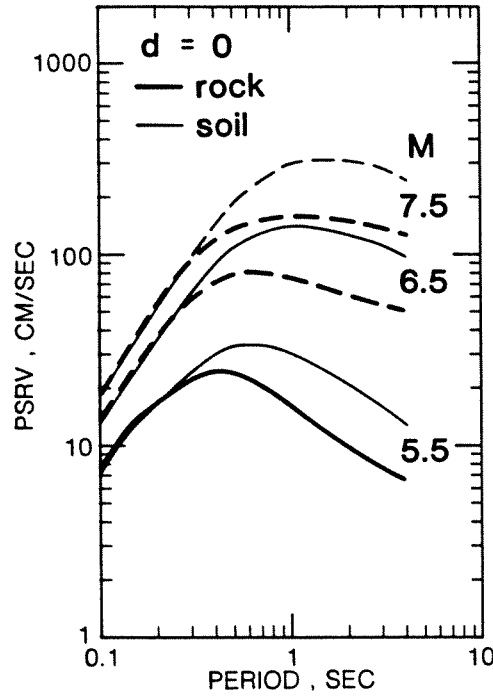
FIGURE 7. Predicted pseudovelocity response spectra of shallow earthquakes for 5 percent damping at rock sites (heavy lines) and soil sites (light lines) for zero distance and the indicated values of moment magnitude (Joyner and Boore, 1982). Spectra correspond to the randomly oriented horizontal component. Curves are dashed where not constrained by data. Distance is as defined for Figure 6.

used.

$$y = a \exp(bM)(r + 25)^d$$

$$a = 2,154,000(r)^{-2.10}$$

$$b = 0.046 + 0.445 \log(r)$$ 　　　　(10)

$$d = -2.515 + 0.486 \log(r)$$

where $y$ is peak horizontal acceleration (gal), $M$ is magnitude, and $r$ is distance (km) to the energy center, presumed to be at a depth of 5 km. Table 6 gives $\sigma_{\ln y}$, the standard deviation of the natural logarithm of an individual prediction of $y$, as it is presumed to vary with $y$.

*Campbell.* Campbell (1988) developed equations for predicting peak horizontal acceleration and velocity from a selected worldwide data set meeting the following criteria: "(1) the largest horizontal component of peak acceleration was at least 0.02 $g$; (2) the accelerograph triggered early enough to record the strongest phase of shaking; (3) the magnitude of the earthquake was 5.0 or larger; (4) the closest distance to seismogenic rupture was less than 30 or 50 km, depending on whether the magnitude of the earthquake was less than or greater than 6.25; (5) the shallowest extent of seismogenic rupture was no deeper than 25 km; and (6) the recording site was located on unconsolidated deposits." Records from instruments on the abutments or toes of dams were excluded. Two equations are given, equation (11) for the unconstrained relationship and equation (12) for the constrained relationship, which includes an anelastic attenuation term to permit extrapolation beyond the near-source region.

$$\ln y = a + bM + d \ln[r + h_1 \exp(h_2 M)] + s$$ 　　　　(11)

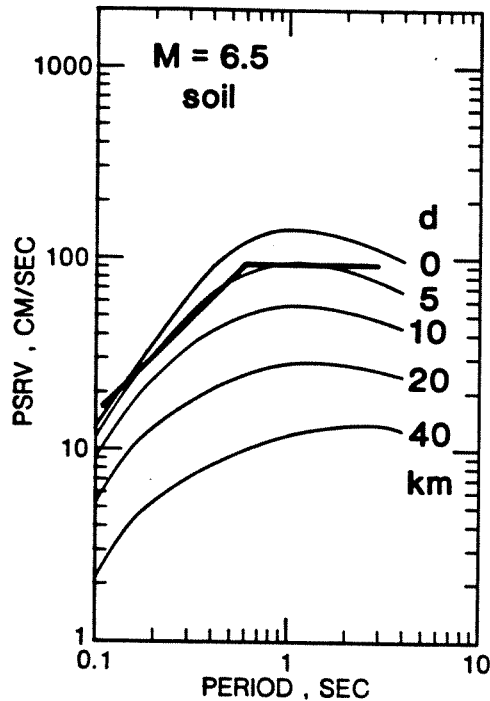$$\ln y = a + bM + d \ln[r + h_1 \exp(h_2 M)] + kr + s$$ 　　　　(12)

FIGURE 8. Predicted pseudovelocity response spectra (light lines) of shallow earthquakes for 5 percent damping at soil sites for a moment magnitude of 6.5 and the indicated distances (Joyner and Boore, 1982) compared to the ATC-3 spectrum (heavy line) for soil type $S_2$ in the highest seismic zone (Applied Technology Council, 1978). Predicted spectra correspond to the randomly oriented horizontal component. Distance is as defined for Figure 6.

where $y$ is the mean of the peak acceleration ($g$) or velocity (cm/s) values for the two horizontal components, $M$ is surface wave magnitude $M_S$ if both local magnitude $M_L$ and $M_S$ are greater than or equal to 6.0 or $M_L$ if both $M_S$ and $M_L$ are less than 6.0, and $r$ is the shortest distance (km) to the zone of seismogenic rupture, identified where possible from the aftershock distribution, otherwise from other data, particularly the intersection of the fault surface with the surface of basement rock (Campbell does not state what magnitude to use if the relative sizes of $M_S$ and $M_L$ do not fall into one of the categories above). A value of -0.0059 was assumed for $k$ for the regression analysis of the data base; in using equation (12) for predicting ground motion, a value appropriate for the region should be chosen. For peak horizontal acceleration

$$s = e_1 K_1 + e_2 K_2 + e_3 K_3 + e_4 K_4 + e_5 K_5 + e_6 (K_4 + K_5) \tanh(e_7 r) \tag{13}$$

and for peak velocity

$$s = e_1 K_1 + e_2 K_2 + e_3 K_3 \tanh(e_4 D) + e_5 (1 - K_3) \tanh(e_6 D) \tag{14}$$

where $s$ incorporates the effects of fault type, directivity, soil type, building size, and building embedment. $D$ is depth (km) to crystalline basement rock. Values of $a$, $b$, $d$, $h_i$, and $e_i$ are given in Table 7 along with values of $\sigma_{\ln y}$, the standard deviation of an individual prediction of $\ln y$. The standard deviations are less than one-half of those in Tables 2 and 3 after conversion from natural to common logarithms. Values of $K_i$ are given in Table 8.

*Idriss.* Equation (15) was developed for the randomly oriented horizontal component of peak horizontal acceleration by Idriss (1985, 1987).

$$\ln y = \ln a + d \ln(r + 20) \tag{15}$$

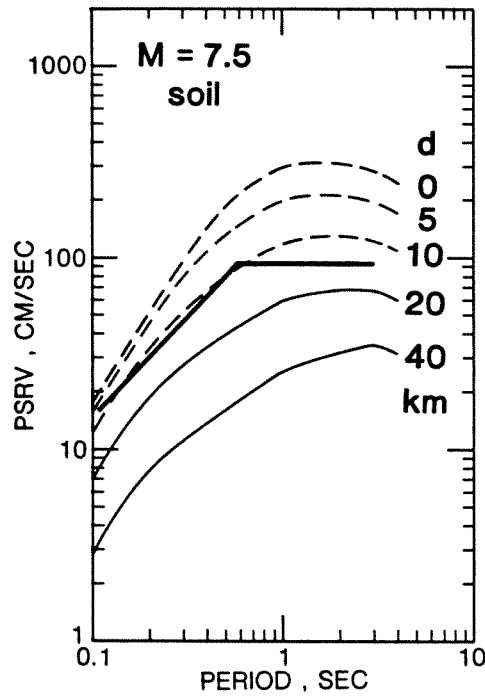23                                            Joyner and Boore

FIGURE 9. Predicted pseudovelocity response spectra (light lines) of shallow earthquakes for 5 percent damping at soil sites for a moment magnitude of 7.5 and the indicated distances (Joyner and Boore, 1982) compared to the ATC-3 spectrum (heavy line) for soil type $S_2$ in the highest seismic zone (Applied Technology Council, 1978). Curves are dashed where not constrained by data. Predicted spectra correspond to the randomly oriented horizontal component. Distance is as defined for Figure 6.

## TABLE 4. PARAMETERS IN THE PREDICTIVE EQUATIONS OF CROUSE (WRITTEN COMMUNICATION, 1987) FOR THE RANDOMLY ORIENTED HORIZONTAL COMPONENT OF PSEUDOVELOCITY RESPONSE (CM/S) AT 5 PERCENT DAMPING AND OF PEAK ACCELERATION (GAL)

| Period (s) | a | b | c | d | k | $\sigma_{\ln y}$ |
|---|---|---|---|---|---|---|
| | | | Pseudovelocity response | | | |
| 0.05 | - 2.44178 | 0.84826 | -0.02579 | -0.52916 | -0.00961 | 0.59914 |
| 0.10 | - 0.61623 | 0.62660 | - .00999 | - .50106 | - .01199 | .68673 |
| 0.20 | - 4.47801 | 2.00876 | - .11673 | - .32102 | - .01423 | .64716 |
| 0.40 | - 1.35559 | 1.17453 | - .04411 | - .47398 | - .00782 | .62089 |
| 0.60 | - 6.02161 | 2.66493 | - .15619 | - .52586 | - .00548 | .62275 |
| 1.00 | - 5.89916 | 2.48235 | - .13036 | - .52261 | - .00405 | .62745 |
| 2.00 | -11.48576 | 4.01914 | - .23152 | - .56791 | - .00280 | .63277 |
| 2.50 | -12.33454 | 4.15828 | - .23359 | - .56280 | - .00320 | .66459 |
| 4.00 | -14.90528 | 4.54962 | - .24999 | - .32351 | - .00738 | .73830 |
| 6.00 | -14.77796 | 4.33959 | -0.23491 | -0.20849 | -0.00791 | 0.79595 |
| | | | Peak acceleration | | | |
| | 2.48456 | 0.73377 | -0.01509 | -0.50558 | -0.00935 | 0.58082 |

Joyner and Boore

## TABLE 5. PARAMETERS IN THE PREDICTIVE EQUATIONS OF SADIGH (WRITTEN COMMUNICATION, 1987) FOR THE RANDOMLY ORIENTED HORIZONTAL COMPONENT OF PSEUDOACCELERATION RESPONSE ($g$) AT 5 PERCENT DAMPING AND OF PEAK ACCELERATION ($g$)

| Period (s) | $a$ | $b$ | $c_1$ | $c_2$ | $d$ | $h_1$ | $M < 6.5$ $h_2$ | $\sigma_{\ln y}$ | $M \geq 6.5$ $h_1$ | $h_2$ | $\sigma_{\ln y}$ |
|---|---|---|---|---|---|---|---|---|---|---|---|
| Pseudoacceleration response at soil sites | | | | | | | | | | | |
| 0.1 | -2.024 | 1.1 | 0.007 | 2.5 | -1.75 | 0.8217 | 0.4814 | $1.332 - 0.148M$ | 0.3157 | 0.6286 | 0.37 |
| 0.2 | -1.696 | 1.1 | .0 | 2.5 | -1.75 | .8217 | .4814 | $1.453 - 0.162M$ | .3157 | .6286 | .40 |
| 0.3 | -1.638 | 1.1 | - .008 | 2.5 | -1.75 | .8217 | .4814 | $1.486 - 0.164M$ | .3157 | .6286 | .42 |
| 0.5 | -1.659 | 1.1 | - .025 | 2.5 | -1.75 | .8217 | .4814 | $1.584 - 0.176M$ | .3157 | .6286 | .44 |
| 1.0 | -1.975 | 1.1 | - .060 | 2.5 | -1.75 | .8217 | .4814 | $1.62 - 0.18M$ | .3157 | .6286 | .45 |
| 2.0 | -2.414 | 1.1 | - .105 | 2.5 | -1.75 | .8217 | .4814 | $1.62 - 0.18M$ | .3157 | .6286 | .45 |
| 4.0 | -3.068 | 1.1 | -0.160 | 2.5 | -1.75 | 0.8217 | 0.4814 | $1.62 - 0.18M$ | 0.3157 | 0.6286 | 0.45 |
| Peak acceleration at soil sites | | | | | | | | | | | |
| | -2.611 | 1.1 | 0.0 | 2.5 | -1.75 | 0.8217 | 0.4814 | $1.26 - 0.14M$ | 0.3157 | 0.6286 | 0.35 |
| Pseudoacceleration response at rock sites | | | | | | | | | | | |
| 0.1 | -0.688 | 1.1 | 0.007 | 2.5 | -2.05 | 1.353 | 0.406 | $1.332 - 0.148M$ | 0.579 | 0.537 | 0.37 |
| 0.2 | -0.479 | 1.1 | - .008 | 2.5 | -2.05 | 1.353 | .406 | $1.453 - 0.162M$ | .579 | .537 | .40 |
| 0.3 | -0.543 | 1.1 | - .018 | 2.5 | -2.05 | 1.353 | .406 | $1.486 - 0.164M$ | .579 | .537 | .42 |
| 0.5 | -0.793 | 1.1 | - .036 | 2.5 | -2.05 | 1.353 | .406 | $1.584 - 0.176M$ | .579 | .537 | .44 |
| 1.0 | -1.376 | 1.1 | - .065 | 2.5 | -2.05 | 1.353 | .406 | $1.62 - 0.18M$ | .579 | .537 | .45 |
| 2.0 | -2.142 | 1.1 | - .100 | 2.5 | -2.05 | 1.353 | .406 | $1.62 - 0.18M$ | .579 | .537 | .45 |
| 4.0 | -3.177 | 1.1 | -0.150 | 2.5 | -2.05 | 1.353 | 0.406 | $1.62 - 0.18M$ | 0.579 | 0.537 | 0.45 |
| Peak acceleration at rock sites | | | | | | | | | | | |
| | -1.406 | 1.1 | 0.0 | 2.5 | -2.05 | 1.353 | 0.406 | $1.26 - 0.14M$ | 0.579 | 0.537 | 0.35 |

## TABLE 6. STANDARD DEVIATION GIVEN BY DONOVAN AND BORNSTEIN (1978) FOR THE NATURAL LOGARITHM OF AN INDIVIDUAL PREDICTION OF PEAK HORIZONTAL ACCELERATION

| Peak acceleration | 0.01 | 0.05 | 0.10 | 0.15 |
|---|---|---|---|---|
| Standard deviation of natural logarithm of peak acceleration | 0.50 | 0.48 | 0.46 | 0.41 |

where $y$ is peak horizontal acceleration ($g$), $M$ is surface-wave magnitude for $M$ greater than or equal to 6 and local magnitude otherwise, and $r$ is the closest distance (km) to the source for $M$ greater than 6 and hypocentral distance otherwise. Values of $a$ and $d$ are given in Table 9 along with $\sigma_{\ln y}$, the standard deviation of an individual prediction of $\ln y$, which is treated as a function of $M$. Idriss proposed that peak acceleration from equation (15) be used to scale the response spectral shapes shown in Figure 10 for different site conditions with magnitude- and period-dependent correction factors shown in Figure 11. Figures 10 and 11 constitute another demonstration of the dependence of the shape of response spectra on magnitude and site conditions.

**Comparisons of Predictive Equations.** To compare the different relationships properly, adjustments must be made for the different definitions of distance. Figure 12a compares peak horizontal acceleration for the randomly oriented horizontal component at magnitude 6.5 as predicted by Donovan and Bornstein (1978), Joyner and Boore (1982), Idriss (1987), and Campbell (1988).

Joyner and Boore

TABLE 7. PARAMETERS IN THE PREDICTIVE EQUATIONS OF CAMPBELL (1988) FOR MEAN PEAK HORIZONTAL ACCELERATION ($g$) AND VELOCITY (CM/S)

| | Acceleration | | Velocity | |
|---|---|---|---|---|
| | Unconstrained | Constrained | Unconstrained | Constrained |
| $a$ | -2.817 | -3.303 | -0.798 | -1.584 |
| $b$ | 0.702 | 0.850 | 1.02 | 1.18 |
| $d$ | -1.20 | -1.25 | -1.26 | -1.24 |
| $h_1$ | 0.0921 | 0.0872 | 0.0150 | 0.00907 |
| $h_2$ | 0.584 | 0.678 | 0.812 | 0.951 |
| $e_1$ | 0.32 | 0.34 | 0.47 | 0.49 |
| $e_2$ | 0.52 | 0.53 | 0.95 | 0.99 |
| $e_3$ | 0.41 | 0.41 | 0.63 | 0.53 |
| $e_4$ | -0.85 | -0.86 | 0.39 | 0.41 |
| $e_5$ | -1.14 | -1.12 | 0.72 | 0.60 |
| $e_6$ | 0.87 | 0.89 | 0.75 | 0.88 |
| $e_7$ | 0.068 | 0.065 | — | — |
| $\sigma_{\ln y}$ | 0.30 | 0.30 | 0.26 | 0.27 |

TABLE 8. PARAMETER $K_i$ IN THE PREDICTIVE EQUATIONS OF CAMPBELL (1988) FOR MEAN PEAK HORIZONTAL ACCELERATION AND VELOCITY

| Peak acceleration | | |
|---|---|---|
| Fault type | $K_1 =$ | 1 reverse<br>0 strike-slip |
| Source directivity | $K_2 =$ | 1 rupture toward site<br>0 other |
| Shallow soil | $K_3 =$ | 1 soils$\leq$10 m deep<br>0 other |
| Embedment | $K_4 =$ | 1 basements of buildings 3–9 stories<br>0 other |
| | $K_5 =$ | 1 basements of buildings 10 or more stories<br>0 other |
| Peak velocity | | |
| Fault type | $K_1 =$ | 1 reverse<br>0 strike-slip |
| Source directivity | $K_2 =$ | 1 rupture toward site<br>0 other |
| Building size | $K_3 =$ | 1 shelters and buildings less than 5 stories<br>0 other |

The definition of distance used in Figure 12a is the closest distance to the vertical projection of the rupture on the surface of the earth. The curves of Donovan and Bornstein and Campbell were adjusted assuming a source depth of 5 km. The curve shown for Idriss is that for deep soil sites. The curve shown for Campbell is that for strike-slip earthquakes recorded at free-field sites with more than 10 m of soil, and no allowance is made for directivity. In this and subsequent comparisons there is no indication of where the curves are not constrained by data as there is in Figures 6, 7, and 9. At short distance, where it matters the most, the different relationships agree to within a fraction of the uncertainty of an individual prediction as given by any of the authors. This suggests that the short-distance predictions at magnitude 6.5 are controlled by the data. The differences at

Joyner and Boore

TABLE 9. PARAMETERS IN THE PREDICTIVE EQUATIONS OF IDRISS (1987) FOR THE RANDOMLY-ORIENTED HORIZONTAL COMPONENT OF PEAK ACCELERATION

| M | Rock and stiff soil sites | | Deep soil sites | | |
| | a | d | a | d | $\sigma_{\ln y}$ |
|---|---|---|---|---|---|
| 4.5 | 606 | -2.57 | 189 | -2.22 | 0.70 |
| 5.0 | 617 | -2.46 | 195 | -2.13 | .58 |
| 5.5 | 452 | -2.28 | 147 | -1.97 | .48 |
| 6.0 | 282 | -2.07 | 98 | -1.79 | .42 |
| 6.5 | 164 | -1.85 | 61.6 | -1.60 | .38 |
| 7.0 | 91.7 | -1.63 | 37.2 | -1.41 | .35 |
| 7.5 | 49.8 | -1.41 | 22 | -1.22 | .35 |
| 8.0 | 28.5 | -1.21 | 13.7 | -1.05 | .35 |
| 8.5 | 15.9 | -1.01 | 8.4 | -0.88 | 0.35 |

large distance are not of much practical importance; they are due, at least in part, to the inclusion of different records in the different data sets. Figure 12b gives the same comparison for magnitude 7.5. The agreement at short distance is not as good as at magnitude 6.5, reflecting the scarcity of data points, but it is within the uncertainty of an individual prediction.

Figure 13a compares 0.2 s pseudovelocity response at 5 percent damping for the randomly oriented horizontal component as predicted for magnitude 6.5 by Crouse (written communication, 1987; Vyas *et al.*, 1988), Idriss (1987), Sadigh (written communication, 1987; Sadigh *et al.*, 1986) and us (Joyner and Boore, 1982). The definition of distance is the same as in Figure 12. The curves shown for Crouse and Idriss are those for deep soil sites; the other two are for soil sites. Figure 13b gives the same comparison for magnitude 7.5. The differences shown for 0.2 s response are somewhat larger than for peak horizontal acceleration but smaller than for longer-period measures of ground motion, shown in Figures 14a and 14b, which give the same comparisons for 1.0 s pseudovelocity response. The maximum differences for motions large enough to be of engineering concern are a little larger than a factor of two; they occur for magnitude 7.5 at distances less than 10 km, a magnitude and distance range for which very few data are available.

For the 1.0 s response at magnitude 7.5 shown on Figure 14b, all four curves at short distances are higher, by factors of 1.5 to 3, than the highest values of the ATC-3 spectrum for firm ground. Ninety cm/s is the highest value of the ATC-3 pseudovelocity response spectrum at 1 hz for 5 percent damping on soil type $S_2$ with a response modification factor of 1 (see Figure 9). Concern that response values near the source may greatly exceed the values implicit in building codes is the reason for the proposal that a zone 5 should be added to the four zones of existing building codes. Zone 5 would lie within 8 km (5 miles) of a fault considered capable of producing a magnitude 7.5 earthquake.

**Predictive Equations Developed from Italian Data.** The predictive equations for shallow earthquakes described and compared in previous sections are based primarily on data from the western United States. There is a large set of strong-motion data recorded from shallow earthquakes in Italy. Predictive relationships for peak horizontal acceleration and velocity based on this data set have been developed by Sabetta and Pugliese (1987). They included only data believed to represent free-field conditions and only data where the triggering earthquake was reliably identified, had a magnitude greater than 4.5, was recorded by at least two stations, had an epicenter determined to an accuracy of 5 km or less, and had a magnitude accurate to 0.3. They used three site categories, stiff, shallow soil (5–20 m thick) and deep soil (more than 20 m thick). The equation fitted to the data is

$$\log y = a + bM - \log(r_0^2 + h^2)^{1/2} + s \tag{16}$$

where $y$ is the larger value from the two horizontal components for either peak acceleration ($g$) or
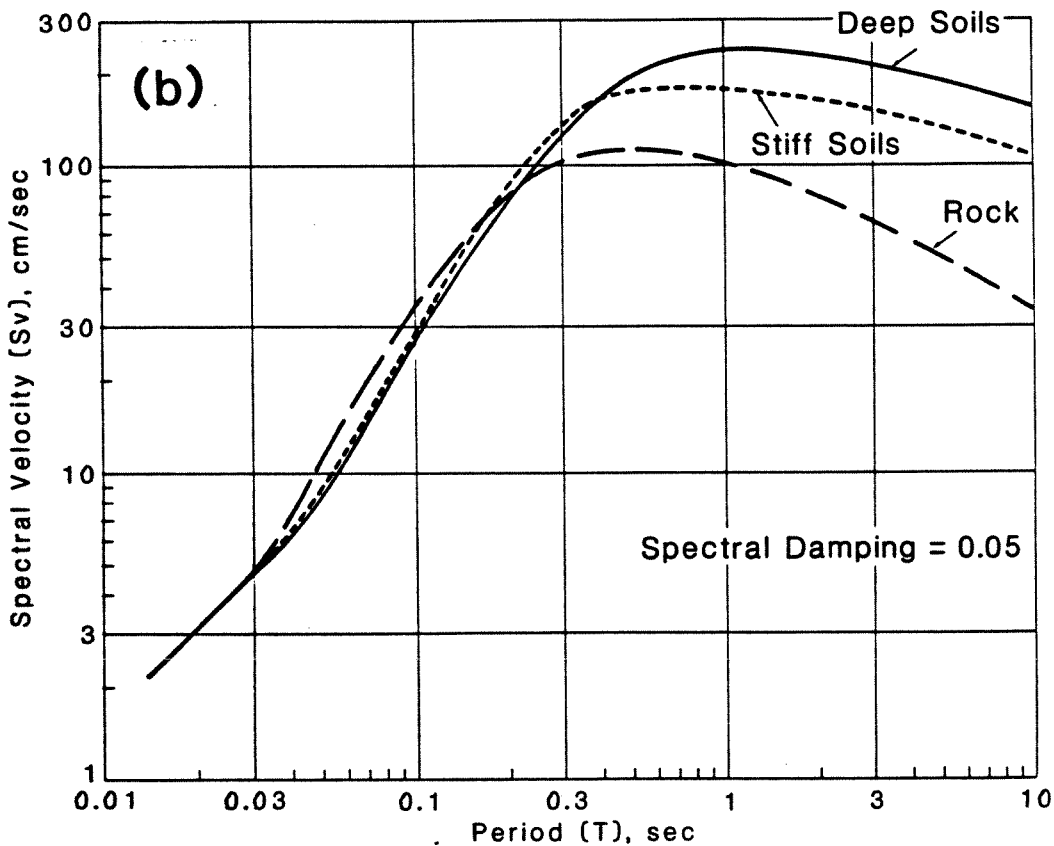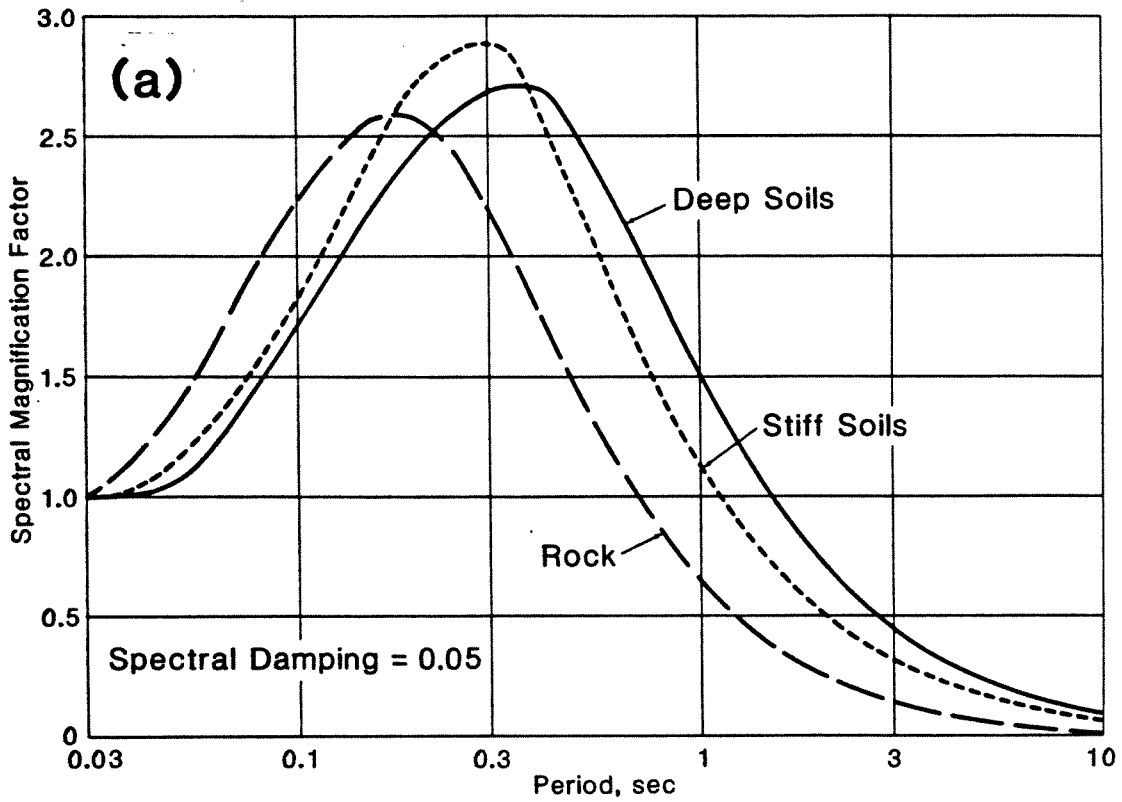
Joyner and Boore

FIGURE 10. (a) Normalized spectral shapes for 5 percent damping for three different soil conditions and magnitudes in the range between 6.5 and 7.0 and (b) the same shape replotted in terms of pseudovelocity response for a zero-period acceleration of 1 $g$ (adapted from Idriss, 1985).
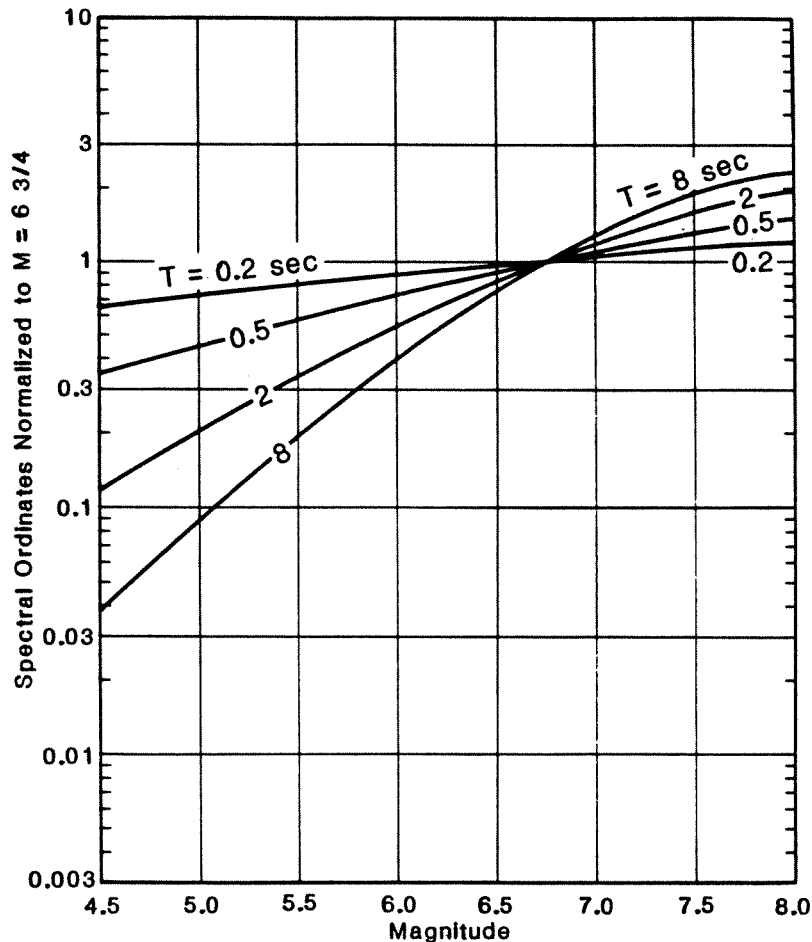
FIGURE 11. Approximate dependence of spectral ordinates on magnitude, normalized to a magnitude of 6.75 (from Idriss, 1987).

velocity (cm/s). $M$ is given by surface-wave magnitude $M_S$ when both $M_S$ and local magnitude $M_L$ are greater than or equal to 5.5, and $M_L$ otherwise. $r_0$ is the closest distance (km) to the vertical projection of the rupture on the surface of the earth. Values of $a$, $b$, $h$, and $s$ are given in Table 10 along with $\sigma_{\log y}$, the standard deviation of an individual prediction of $\log y$. Sabetta and Pugliese tried a magnitude-dependent $h$ but did not find a statistically significant improvement in fit.

Equation (16) is similar in form to ours (Joyner and Boore, 1982), which facilitates comparison. Figures 15a and 15b give the comparison for peak horizontal acceleration and velocity, respectively. For distances less than 100 km the agreement is within a fraction of the standard deviation of an individual prediction for either study. In their paper Sabetta and Pugliese made the comparison using an earlier version of our curves (Joyner and Boore, 1981). Our earlier curve for peak horizontal velocity, which was based on fewer data than our 1982 equations, does not agree as well as the curve shown in Figure 15b. The differences at large distance between the two sets of curves in Figures 15a and 15b have little practical importance. They are probably due to our exclusion, for each earthquake, of data recorded at distances greater than the distance to the closest operational instrument that did not trigger.

**Predictive Equations for Subduction-Zone Earthquakes.** Data from subduction-zone earthquakes is generally treated separately because of presumed differences in source and/or propagation conditions. Jacob and Mori (1984) suggest that "the high variability of stress drops
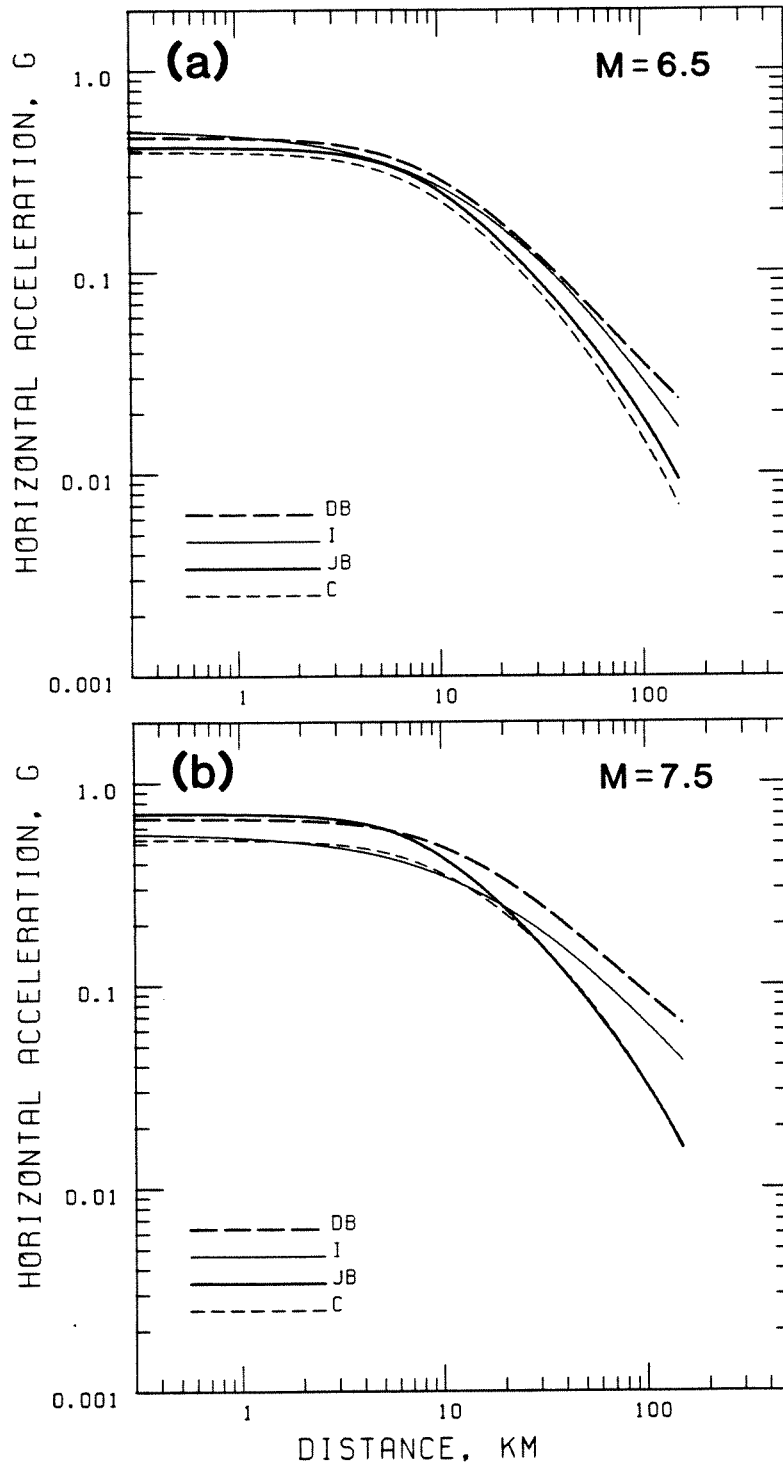
Joyner and Boore

FIGURE 12. Comparison of different relationships for peak horizontal acceleration at magnitude 6.5 (a) and 7.5 (b). DB, from Donovan and Bornstein (1978); I, from Idriss (1987) for deep soil sites; JB, from Joyner and Boore (1982), reduced by 13 percent so as to approximate the value for the randomly oriented horizontal component; C, the constrained relationship of Campbell (1988) for a strike-slip earthquake recorded at a free-field site with soil more than 10 m deep and no allowance made for directivity. The distance plotted is the closest distance to the vertical projection of the rupture on the surface of the earth. The curves of Donovan and Bornstein and those of Campbell are adjusted assuming a source depth of 5 km.
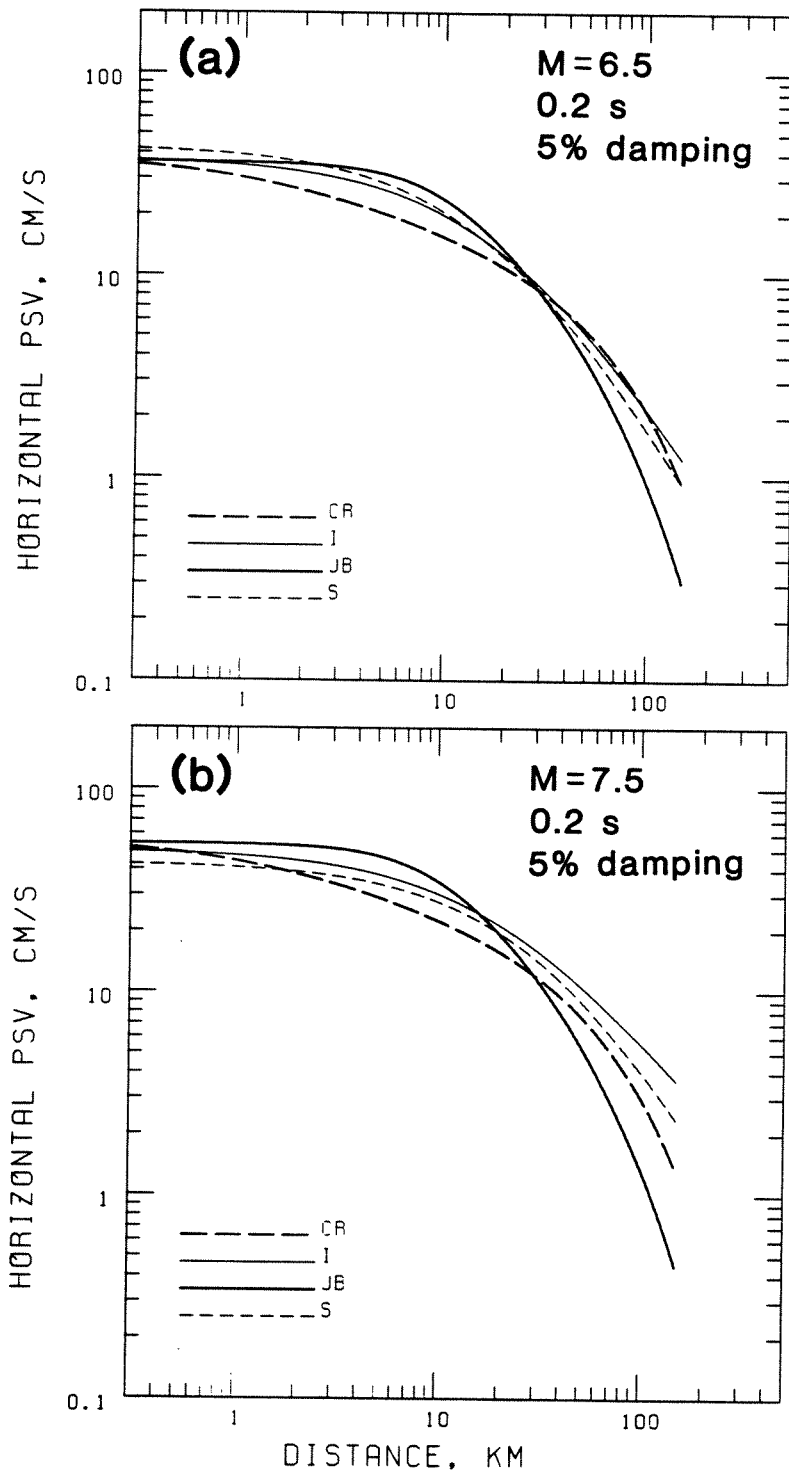
Joyner and Boore

FIGURE 13. Comparison of different relationships for 0.2 s horizontal pseudovelocity response at 5 percent damping for magnitude 6.5 (a) and 7.5 (b). CR, from Crouse (written communication, 1987; Vyas *et al.*, 1988) for deep soil sites; I, from Idriss (1987) for deep soil sites; JB, from Joyner and Boore (1982) for soil sites; S, from Sadigh (written communication, 1987; Sadigh *et al.*, 1986) for soil sites. Distance is as defined for Figure 12.
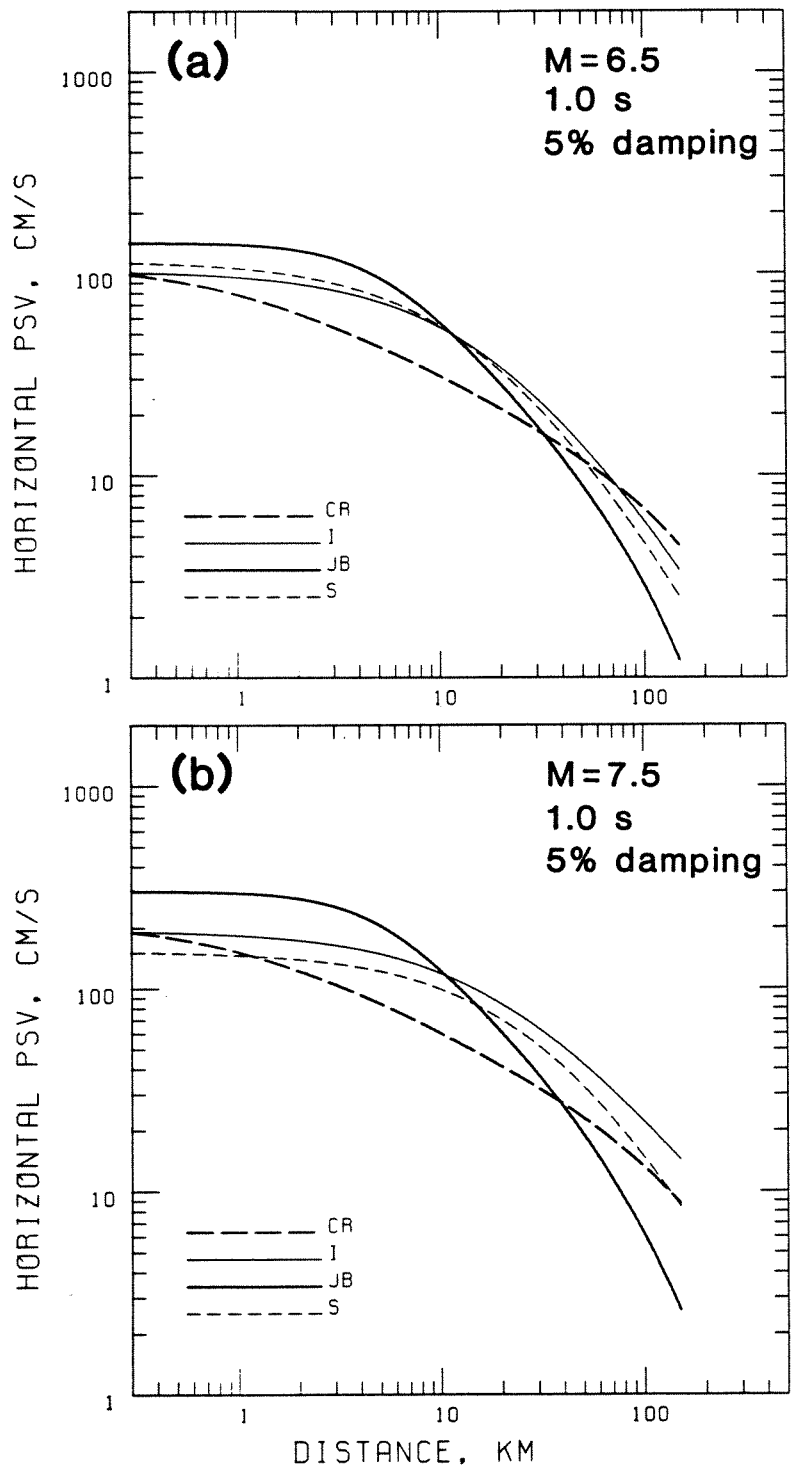
Joyner and Boore

FIGURE 14. Comparison of different relationships for 1.0 s horizontal pseudovelocity response at 5 percent damping for magnitude 6.5 (a) and 7.5 (b). Curves are as defined for Figure 13, and distance is as defined for Figure 12.

typical for some subduction zones" is responsible for the apparently larger scatter in peak horizontal acceleration from Alaskan data compared with data from shallow earthquakes in the rest of the western United States. Boore (1986), however, was successful in simulating teleseismic P waves

Joyner and Boore

## TABLE 10. PARAMETERS IN THE PREDICTIVE EQUATIONS OF SABETTA AND PUGLIESE (1987) FOR THE LARGER PEAK ACCELERATION ($g$) AND VELOCITY (CM/S) OF TWO HORIZONTAL COMPONENTS

|  | $a$ | $b$ | $h$ | $s$ Stiff | $s$ Shallow soil | $s$ Deep soil | $\sigma_{\log y}$ |
|---|---|---|---|---|---|---|---|
| Peak acceleration | -1.562 | 0.306 | 5.8 | 0.0 | 0.169 | 0.0 | 0.173 |
| Peak velocity | -0.710 | 0.455 | 3.6 | 0.0 | 0.133 | 0.133 | 0.215 |

from subduction zone earthquakes with moment magnitudes up to 9.5, using the same stochastic source model with the same stress parameter as he used for simulating strong-motion data from shallow earthquakes in the western United States. This suggests a general similarity between the source processes of subduction-zone earthquakes and shallow crustal earthquakes. There are significant differences in geometry and propagation path between the two kinds of earthquake data. Of particular importance may be less anelastic attenuation along the deeper paths characteristic of data from subduction-zone earthquakes.

The $M_S$ 7.8 Central Chile earthquake and the $M_S$ 8.1 Michoacan, Mexico, earthquake, both in 1985, provided the first extensive sets of data from the epicentral regions of large subduction-zone earthquakes. Figure 16, taken from Anderson *et al.* (1986), shows peak accelerations from these data sets. The values for the Chilean earthquake are substantially higher at distances less than 100 km.

*Crouse et al.* Equation (17) was developed from pseudovelocity response data at soil sites from subduction earthquakes in the Northern Honshu zone (Crouse *et al.*, 1988). Both horizontal components were used.

$$\ln y = a + b\mathrm{M} + d\ln r + qh \tag{17}$$

where $y$ is the pseudovelocity response value (cm/s) at 5 percent damping for the randomly oriented horizontal component, M is moment magnitude, $r$ is distance (km) to the center of energy release, and h is focal depth (km). Values of $a$, $b$, $d$, and $q$ are given in Table 11 along with $\sigma_{\ln y}$, the standard deviation of an individual prediction. The distance to the center of energy release was taken as the hypocentral distance for all earthquakes with M less than 7.5. For most of the larger events the distance was taken as the distance to the centroid of the fault plane defined by the aftershocks. If studies were available identifying the location of the greatest energy release, the distance to that point was used. Crouse *et al.* showed that equation (17) also fits data from stiff-soil sites in the Kurile, Nankai, Alaskan, and Mexican subduction zones but appears not to fit data from stiff-soil sites in the Peru/North Chile and the New Britain/Bougainville zones.

*Kawashima.* Equation (18) for peak horizontal acceleration (gal), velocity (cm/s), and displacement (cm) and horizontal acceleration response (gal) for 5 percent damping was developed from data recorded in Japanese earthquakes with focal depth less than 60 km (Kawashima *et al.*, 1984). Presumably most of the earthquakes are subduction-zone events. Data recorded on structures (including first floor and basement) were excluded.

$$y = a10^{bM}(\Delta + 30)^d \tag{18}$$

where $y$ represents the peak motion or the acceleration response which is the maximum over all possible azimuths of the horizontal component, $M$ is JMA (Japanese Meteorological Agency) magnitude, and $\Delta$ is epicentral distance (km). Values of $a$, $b$, and $d$ are given in Table 12 along with values of $\sigma_{\log y}$, the standard deviation of the common logarithm of an individual prediction of $y$. Different values of $a$, $b$, and $\sigma_{\log y}$ are given for three different site conditions defined in Table 13.
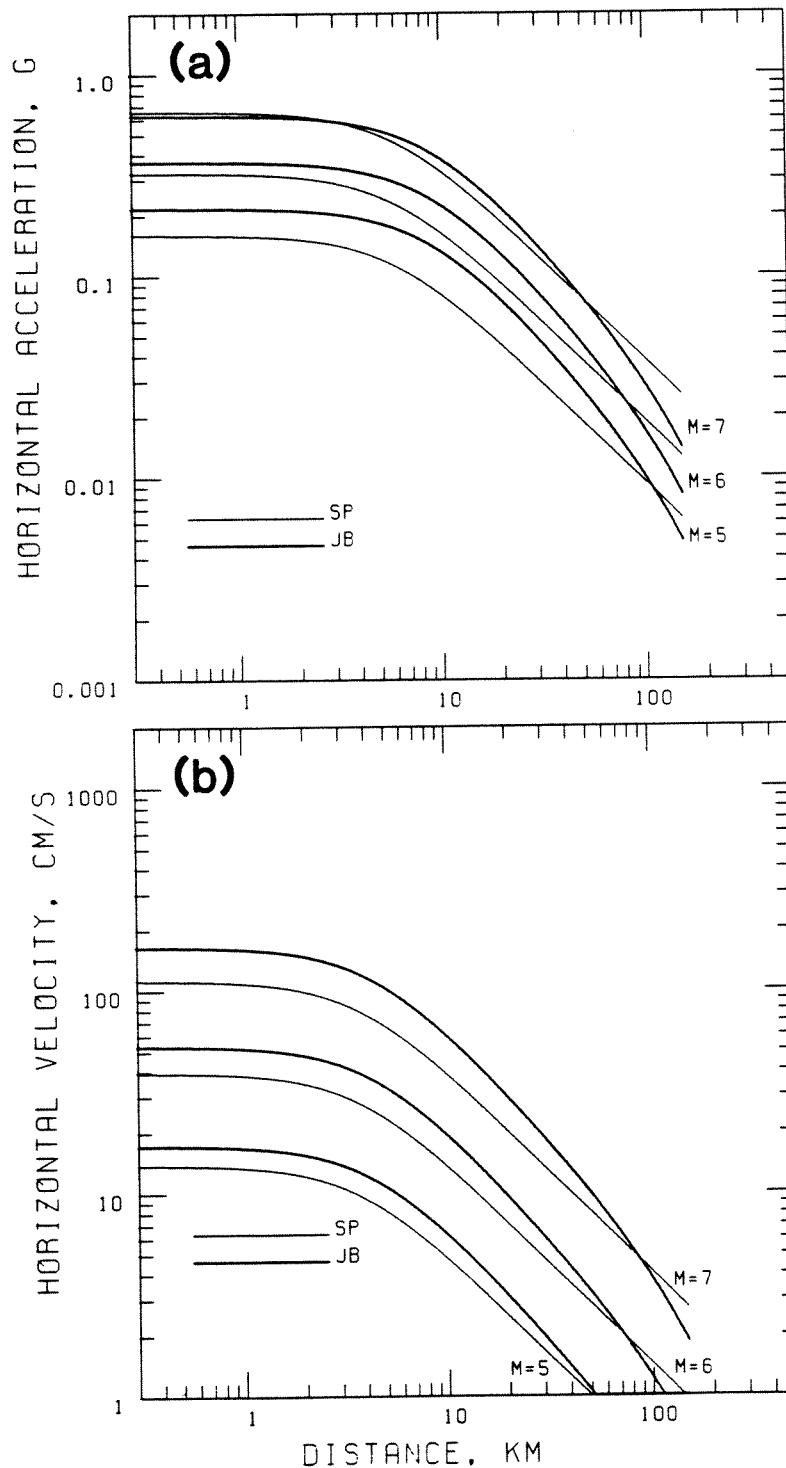
Joyner and Boore

FIGURE 15. (a) Comparison of different relationships for the larger value of peak acceleration from the two horizontal components. SP, from Sabetta and Pugliese (1987) for Italian data at stiff and deep soil sites; JB, from Joyner and Boore (1982) for western North American data. (b) Comparison of different relationships for the larger value of peak velocity from the two horizontal components. SP, from Sabetta and Pugliese (1987) for Italian data at soil sites; JB, from Joyner and Boore (1982) for western North American data at soil sites. Distance is as defined for Figure 12.
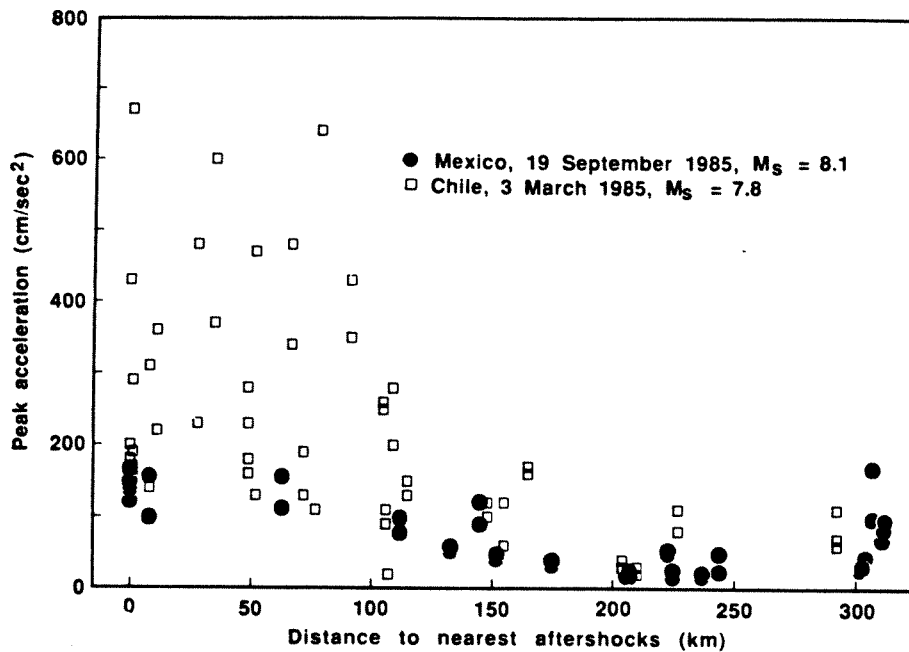
FIGURE 16. Peak horizontal acceleration in the 19 September 1985 Mexican earthquake and the 3 March 1985 Chilean earthquake plotted against distance outside the boundary of the aftershock zone (from Anderson *et al.*, 1986). Copyright 1986 by the AAAS.

TABLE 11. PARAMETERS IN THE PREDICTIVE EQUATIONS OF CROUSE *ET AL.* (1988) FOR THE RANDOMLY ORIENTED HORIZONTAL COMPONENT OF PSEUDOVELOCITY RESPONSE (CM/S) AT 5 PERCENT DAMPING

| Period (s) | $a$ | $b$ | $d$ | $q$ | $\sigma_{\ln y}$ |
|------------|------|------|-------|---------|-------------------|
| 0.1 | 1.86 | 0.48 | -1.02 | 0.0093 | 0.668 |
| 0.2 | 3.19 | 0.44 | -0.98 | .0053 | .672 |
| 0.4 | 1.29 | 0.68 | -0.84 | .0041 | .597 |
| 0.6 | 0.67 | 0.85 | -0.95 | .0030 | .674 |
| 0.8 | -0.38 | 0.96 | -0.87 | .0017 | .703 |
| 1.0 | -1.13 | 1.06 | -0.83 | .0 | .713 |
| 1.5 | -2.79 | 1.18 | -0.69 | - .0007 | .663 |
| 2.0 | -3.04 | 1.26 | -0.78 | - .0008 | .718 |
| 3.0 | -3.46 | 1.34 | -0.85 | - .0046 | .730 |
| 4.0 | -4.09 | 1.39 | -0.85 | -0.0053 | 0.720 |

## Theoretical Prediction

The usual method for calculating theoretical strong-motion seismograms is kinematic and requires specification of the distribution in space and time of slip on the fault and a means of calculating the Green's functions, which give the response to slip at a point. There are now available a number of methods for calculating complete Green's functions for earth models in which material properties vary only with depth (Spudich and Ascher, 1983; Ascher and Spudich, 1986; Olson *et al.*, 1984). If lateral heterogeneity is a significant factor, ray methods (Spudich and Frazer, 1984) can be used to compute high-frequency (> 1$Hz$) ground motions at near-source distances. The methods for calculating complete Green's functions have been used to infer the distribution of slip

Joyner and Boore

TABLE 12. PARAMETERS IN THE PREDICTIVE EQUATIONS
OF KAWASHIMA *ET AL.* (1984) FOR HORIZONTAL ACCELERATION
RESPONSE (GAL) AT 5 PERCENT DAMPING AND FOR PEAK HORIZONTAL
ACCELERATION (GAL), VELOCITY (CM/S), AND DISPLACEMENT (CM)

| Period (s) | $d$ | Ground group 1 | | | Ground group 2 | | | Ground group 3 | | |
|---|---|---|---|---|---|---|---|---|---|---|
| | | $a$ | $b$ | $\sigma_{\log y}$ | $a$ | $b$ | $\sigma_{\log y}$ | $a$ | $b$ | $\sigma_{\log y}$ |
| Acceleration response | | | | | | | | | | |
| 0.1 | -1.178 | 2420 | 0.211 | 0.262 | 848.0 | 0.262 | 0.256 | 1307 | 0.208 | 0.219 |
| 0.15 | -1.178 | 2407 | .216 | .229 | 629.1 | .288 | .244 | 948.2 | .238 | .218 |
| 0.2 | -1.178 | 1269 | .247 | .226 | 466.0 | .315 | .273 | 1128 | .228 | .211 |
| 0.3 | -1.178 | 574.8 | .273 | .241 | 266.8 | .345 | .270 | 1263 | .224 | .217 |
| 0.5 | -1.178 | 211.8 | .299 | .278 | 102.2 | .388 | .249 | 580.6 | .281 | .240 |
| 0.7 | -1.178 | 102.5 | .317 | .239 | 34.34 | .440 | .245 | 65.67 | .421 | .243 |
| 1.0 | -1.178 | 40.10 | .344 | .273 | 5.04 | .548 | .305 | 7.41 | .541 | .307 |
| 1.5 | -1.178 | 7.12 | .432 | .254 | 0.719 | .630 | .288 | 0.803 | .647 | .305 |
| 2.0 | -1.178 | 5.78 | .417 | .267 | 0.347 | .644 | .264 | 0.351 | .666 | .276 |
| 3.0 | -1.178 | 1.67 | 0.462 | 0.249 | 0.361 | 0.586 | 0.248 | 0.262 | 0.635 | 0.263 |
| Peak acceleration | | | | | | | | | | |
| | -1.218 | 987.4 | 0.216 | 0.216 | 232.5 | 0.313 | 0.224 | 403.8 | 0.265 | 0.197 |
| Peak velocity | | | | | | | | | | |
| | -1.222 | 20.8 | 0.263 | 0.236 | 2.81 | 0.430 | 0.239 | 5.11 | 0.404 | 0.243 |
| Peak displacement | | | | | | | | | | |
| | -1.254 | 0.626 | 0.372 | 0.262 | 0.062 | 0.567 | 0.258 | 0.070 | 0.584 | 0.262 |

TABLE 13. CLASSIFICATION OF SITE CONDITIONS FOR THE PREDICTIVE
EQUATIONS OF KAWASHIMA *ET AL.* (1984)

| | Geological Definition | Definition by Natural Period |
|---|---|---|
| Group 1 | Tertiary or older rock or diluvium less than 10m thick | Period less than 0.2 s |
| Group 2 | Diluvium with thickness 10m or more or alluvium less than 25 m thick including soft layer less than 5 m thick | Period between 0.2 and 0.6 s |
| Group 3 | Other than the above, usually soft alluvium or reclaimed land | Period more than 0.6 s |

in past earthquakes by direct inversion (Olson and Apsel, 1982; Hartzell and Heaton, 1983) and by trial-and-error forward modeling (Archuleta, 1984). Such studies are important in advancing our understanding of earthquake source processes. The calculation of theoretical seismograms for future earthquakes, however, requires a means of specifying the distribution of slip in future earthquakes. Assuming uniform slip would not give realistic seismograms. We have done computations indicating that the amplitude of ground motions at all frequencies of engineering interest is controlled by the heterogeneities in the fault rupture (Boore and Joyner, 1986). Because there is no way to predict the heterogeneities of future ruptures, we turn to stochastic source models as the basis for theoretical ground-motion prediction.

**Stochastic Source Models.** Stochastic source models make possible what we consider to be the first realistic theoretical predictions of strong ground motion. We describe two stochastic source

Joyner and Boore

models, the barrier model of Papageorgiou and Aki (1983a, b) and the stochastic $\omega$-square model of Hanks and McGuire (1981). In the barrier model a rectangular fault plane is covered by circular cracks of equal diameter separated by unbroken barriers. Individual cracks rupture independently and randomly, and their radiation is described by Sato and Hirasawa's (1973) equations. The Fourier spectrum of the resulting ground motion has random phase, which is the reason we classify the barrier model as a stochastic source model. The barrier model is specified by five basic parameters, fault length, fault width, maximum slip, rupture velocity, and barrier interval. A sixth parameter, the cohesive zone size, is introduced to explain the cutoff of high frequencies in the spectrum. The cutoff frequency $f_m$ (Hanks, 1982) is considered by Papageorgiou and Aki (1983a) to be a source parameter that may vary with other source parameters. This contrasts with the view of advocates of the Hanks-McGuire model who, while admitting the possibility of source-controlled cutoff, generally consider the cutoff of high frequencies to be an effect of near-surface attenuation at the recording site. Papageorgiou and Aki (1983b) applied the barrier model to the analysis of six California earthquakes and showed that the barrier interval is strongly related to the maximum slip.

According to the Hanks-McGuire (1981) model earthquake accelerations are band-limited white noise in the band between the corner frequency $f_0$ and $f_m$, and the spectral shape is given by the Brune (1970, 1971) spectrum. In addition to moment $M_0$, the model is specified by two parameters, the stress parameter $\Delta\sigma$ and $f_m$. Hanks and McGuire used this model with the aid of random vibration theory to predict horizontal peak acceleration and rms acceleration and obtained excellent agreement with empirical data over the magnitude range from 4.0 to 7.7. Boore (1983) made use of both stochastic simulations and random vibration theory to test the predictions of the Hanks-McGuire model for peak horizontal velocity and response spectra as well as peak acceleration. He showed agreement between model predictions and data covering a magnitude range from less than 1.0 to more than 7.0. Hanks and Boore (1984) showed that the model predictions reproduce the correlation between log moment and local magnitude $M_L$ for California earthquakes in the $M_L$ range from 0 to 7. Boore (1986) compared model predictions with peak teleseismic $P$-wave amplitudes given by Houston and Kanamori (1986) for earthquakes with moment magnitude up to 9.5 and showed good agreement.

A question with the Hanks-McGuire model arises in extending the model to magnitudes greater than the critical magnitude corresponding to rupture of the full width of the seismogenic zone. For larger earthquakes similarity must break down because rupture width can no longer increase as the moment increases. Joyner (1984) proposed a scaling law that accomplishes the extension of the Hanks-McGuire model to magnitudes for which similarity no longer applies.

**Ground-Motion Prediction with Stochastic Source Models.** Two methods are available for making ground-motion predictions with stochastic source models. One uses Monte Carlo simulations in the time domain and the other uses random-vibration theory. The two methods complement each other. Calculations with random-vibration theory require less computer time, whereas Monte Carlo simulations are useful in applications that require time series and serve as a check on the assumptions underlying the random-vibration approach. Both methods are summarized below; more detailed descriptions are given by Boore (1983, 1986, 1987; Boore and Joyner, 1984a; Boore and Atkinson, 1987).

For both methods the spectrum of ground motion is given as a function of frequency $f$ by

$$R(f) = CS(f)A(f)D(f)I(f) \tag{19}$$

Where the factors $C, S, A, D,$ and $I$ represent, respectively, a scaling factor, the source spectrum, an amplification factor, a diminution factor, and an instrument-response factor. Only $S(f)$ depends on seismic moment. $C$ is given by

$$C = \frac{R_{\Theta\Phi}FV}{4\pi\rho_0\beta_0^3\mathcal{R}} \tag{20}$$

where $R_{\Theta\Phi}$ is the radiation pattern averaged over an appropriate range of azimuth and takeoff angle (e.g., Boore and Boatwright, 1984), $F$ accounts for the free-surface effect, $V$ represents the

partition of energy from a vector into horizontal components (if needed), $\rho_0$ and $\beta_0$ are the density and shear velocity in the source region, and $\mathcal{R}$ is the geometric spreading factor. $F$ and $V$ are usually given values of 2 and $1/\sqrt{2}$, respectively. For body waves within about 100 km $\mathcal{R} = r$, where $r$ is hypocentral distance. For distances beyond 100 km, where the $L_g$ phase dominates, $\mathcal{R}$ will be proportional to $\sqrt{r}$. For teleseismic body waves a different treatment of geometric spreading is required (Boore, 1986).

For the barrier model the source factor $S(f)$ is given by Papageorgiou (1988). For the Hanks-McGuire model $S(f)$ is

$$S(f) = M_0/[1 + (f/f_0)^2] \tag{21}$$

where $M_0$ is the seismic moment and $f_0$ the corner frequency, given by

$$f_0 = 4.9 \times 10^6 \beta_0 (\Delta\sigma/M_0)^{1/3} \tag{22}$$

$\Delta\sigma$ is a parameter with the dimensions of stress, $f_0$ is in Hz, $\beta_0$ in km/s, $\Delta\sigma$ in bars, and $M_0$ in dyne-cm (Brune, 1970, 1971).

A modified version of $S(f)$ was given by Joyner (1984) to accommodate the breakdown of similarity which must occur when the moment exceeds the critical moment $M_{0c}$ corresponding to rupture of the entire width of the seismogenic zone.

$$
\begin{aligned}
S(f) &= M_0/(1 + if/f_B)^{1/2} &\qquad f \leq f_A \\
&= M_0 \left(\frac{f_A}{f}\right)^{3/2} / (1 + if/f_B)^{1/2} &\qquad f \geq f_A
\end{aligned}
\tag{23}
$$

where

$$
\begin{aligned}
f_A &= 4.9 \times 10^6 \beta_0 \lambda^{-1/4} (\Delta\sigma/M_0)^{1/3} \\
f_B &= 4.9 \times 10^6 \beta_0 \lambda^{3/4} (\Delta\sigma/M_0)^{1/3} &\qquad M_0 \leq M_{0c} \\[1em]
f_A &= 4.9 \times 10^6 \beta_0 \lambda^{-1/4} \Delta\sigma^{1/3} M_{0c}^{1/6} M_0^{-1/2} \\
f_B &= 4.9 \times 10^6 \beta_0 \lambda^{3/4} (\Delta\sigma/M_{0c})^{1/3} &\qquad M_0 \geq M_{0c}
\end{aligned}
\tag{24}
$$

$\lambda$ is the ratio between the length and the width of the fault [assigned a typical value of 4 by Joyner (1984)], and the other symbols are as defined for equation (22).

The amplification factor can be given in different ways. Perhaps the most familiar is the frequency-dependent transfer function that results from wave propagation in a stack of layers (e.g. Boore and Joyner, 1984b). Amplification can also be represented in terms of site impedance, as discussed previously. Conservation of energy requires that amplitude increase as impedance decreases in going from the source region to the recording site. The amplification factor can be approximated by $\sqrt{\rho_0\beta_0/\rho_r\beta_r}$, where the subscripts $r$ refers to material near the recorder and the subscript 0 refers to material near the source. Table 14 gives the logarithm of the correction factor as a function of frequency for a typical western North American strong-motion recording site on rock, as estimated by Boore (1986). The variations in density are expected to be minor for rock and were ignored in Table 14. The frequency dependence of the correction arises from the assumption that $\rho_r$ and $\beta_r$ are effective properties averaged over a depth equal to a quarter-wavelength (Joyner and Fumal, 1984). Note that the correction can be greater than a factor of two even at rock sites.

The diminution factor may be written

$$D(f) = \exp[-\pi f r/Q(f)\beta]P(f) \tag{25}$$

where $Q$ is a frequency-dependent attenuation function, $\beta$ is the propagation velocity averaged over the path, and $P$ is a high-cut filter. In western North America we use for $Q$ the following function that fits a number of observations collected by Aki (see Figure 2 in Boore, 1984):

$$Q = 29.4\frac{1 + (f/0.3)^{2.9}}{(f/0.3)^2} \tag{26}$$

### TABLE 14. AMPLIFICATION FACTORS FOR ROCK SITES IN WESTERN NORTH AMERICA

| $\log f$ | $\log \sqrt{\beta_0/\beta_r}$ |
|----------|-------------------------------|
| -1       | 0.01                          |
| -0.5     | 0.04                          |
| 0.0      | 0.13                          |
| 0.5      | 0.34                          |
| 1.0      | 0.37                          |

The high-frequency behavior of this function is consistent with our analysis of response spectral attenuation (Joyner and Boore, 1982), but, as referred to previously, we do not know to what extent the agreement indicates that the $Q$ function represents the true frequency dependence of $Q$ and to what extent the agreement is influenced by error in the assumed geometric spreading of $1/r$. The high-cut filter $P$ is needed to account for the observation that acceleration spectra generally show an abrupt depletion of high-frequency energy above some frequency $f_m$ (Hanks, 1982). This filter can be represented by a Butterworth filter [Boore, 1983, equation (4)] with a steep rolloff (approximately 24 db/octave) above the corner frequency $f_m$. Another form of the $P$ filter is

$$P(f) = \exp(-\pi\kappa_0 f) \tag{27}$$

The form and notion is from Anderson and Hough (1984). For small distances or large $Q$, the $P(f)$ factor contributes most of the attenuation, and the filter $D(f)$ is then roughly equivalent to a step high-cut filter with a cutoff frequency $f_m$ equal to $1/\pi\kappa_0$ (a relation pointed out to us by J. Boatwright). A possible physical mechanism for the $P(f)$ factor would be near-site attenuation in the upper kilometer or so of the ray path.

Finally, the filter $I(f)$ is used to shape the spectrum so that the output time series corresponds to the particular ground-motion parameter of interest. For example, if pseudo-velocity response spectra are to be computed, $I$ is the response to ground displacement of an oscillator of frequency $f_r$ and damping $\zeta$

$$I(f) = \frac{Vf^2}{(f^2 - f_r^2) - i(2\zeta f f_r)}, \tag{28}$$

with the magnification $V$ given by $2\pi f_r$. If Richter local magnitude $M_L$ is to be computed, $I$ is given by equation (28) with $f_r = 1.25$, $\zeta = 0.8$, and $V = 2800$, the values for the Wood-Anderson seismograph used in defining the $M_L$ scale. If peak velocity or peak acceleration are the quantities of interest, then

$$I(f) = (2\pi f i)^n \tag{29}$$

where $n = 1$ or 2, respectively, for velocity or acceleration. The uncorrected response of an accelerometer can be simulated by using equation (28) with appropriate $f_r$ and $\zeta$ (typically, $f_r = 25$ Hz and $\zeta = 0.6$) and $V = (2\pi f_r)^2$. The response equations for other instruments, such as the World Wide Standardized Seismograph Network short-period instrument, can be used as desired.

Once the spectrum $R(f)$ is determined, application of the time-domain method of ground-motion prediction is very simple. Gaussian white noise is generated with a random-number generator. The noise is windowed by either a shaping function or a box car whose duration $T_w$ is given by $1/f_0 + 0.05r$ for the Hanks-McGuire model and by $1/f_A + 0.05r$ for Joyner's (1984) modification, where $r$ is the source distance (km). The distance-dependent term is included to account for the spreading out of the source energy due to scattering and wave-propagation effects (Herrmann, 1985). The amplitude of the window is chosen so that the mean level of the white spectrum is unity. The noise sample is then filtered by the filter $R(f)$ from equation (19). [This method differs from the conventional engineering method for stochastic simulation in which white noise is filtered before being windowed rather than after. Şafak and Boore (1988) show that windowing filtered noise alters

the spectrum, so windowing should be done first.] Fourier transformation back to the time domain gives the simulated time series from which the peak value is obtained. The process is then repeated with different seeds for the random-number generator. Between 20 and 100 simulations are generally sufficient to give a good estimate of the peak motion. A spectrum of a single realization of the process will not match the target spectrum, but the average of a number of realizations will match, as shown in Figure 17. The time series for one realization for each of two different magnitudes are shown in Figure 18; the only parameter that was changed between the simulations for the two earthquakes was the magnitude.

The method of random-vibration theory can be used to obtain peak values without doing simulations. The method is based on the work of Cartwright and Longuet-Higgins (1956). To estimate the peak value $y_{max}$ of the ground-motion parameter $y$, we obtain the spectrum $R(f)$ of $y$ from equation (19) as in the simulation method. The zeroth, second, and fourth moments, $m_0$, $m_2$, and $m_4$, of the energy density spectrum are calculated from the equation

$$m_k = \frac{1}{\pi} \int_0^\infty \omega^k |R(f)|^2 d\omega \qquad (30)$$

where $\omega = 2\pi f$. The rms value of the ground-motion parameter is given by

$$y_{rms} = (m_0/T_r)^{1/2} \qquad (31)$$

For predicting peak acceleration or velocity $T_r$ is the same as $T_w$, the time duration of the motion determined as described for the simulation method. The determination of $T_r$ for predicting response spectral values is described later. The expected value of the peak $[E(y_{max})]$ is calculated either by an exact or an asymptotic formula depending on the values of the bandwidth parameter $\xi$ and the number of extrema $N$, where

$$\xi = m_2/(m_0 m_4)^{1/2} \qquad (32)$$

and $N$ is the largest integer contained in the number $2\tilde{f}T_w$, where

$$\tilde{f} = \frac{1}{2\pi}(m_4/m_2)^{1/2} \qquad (33)$$

If $N$ is less than $14.7/\xi - 8$ then the expected value of the peak is given by the exact formula

$$E(y_{max}) = y_{rms}\sqrt{\frac{\pi}{2}} \sum_{l=1}^N (-1)^{l+1} \frac{C_l^N}{\sqrt{l}} \xi^l \qquad (34)$$

where $C_l^N$ are the binomial coefficients $(= N!/l!(N-l)!)$. For larger values of $N$ there may be numerical problems with the exact formula and the asymptotic solution

$$E(y_{max}) = y_{rms}\{[2\ln(N)]^{1/2} + \gamma/[2\ln(N)]^{1/2}\} \qquad (35)$$

where $\gamma = 0.557216$ (Euler's constant), is recommended. For the asymptotic approximation, the quantities $\tilde{f}$ and $N$ are recalculated as follows

$$\tilde{f} = \frac{1}{2\pi}(m_2/m_0)^{1/2} \qquad (36)$$
$$N = 2\tilde{f}T_w$$

The cutoff between the exact and asymptotic solutions was determined from numerical experiments, with the criteria being that at the transition the difference between $\log E(y_{max})$ from the two equations was less than 0.01 units.

When estimating response spectra a further refinement is required to the basic random-vibration theory described above. The random-vibration approach assumes a stationary time series. For small
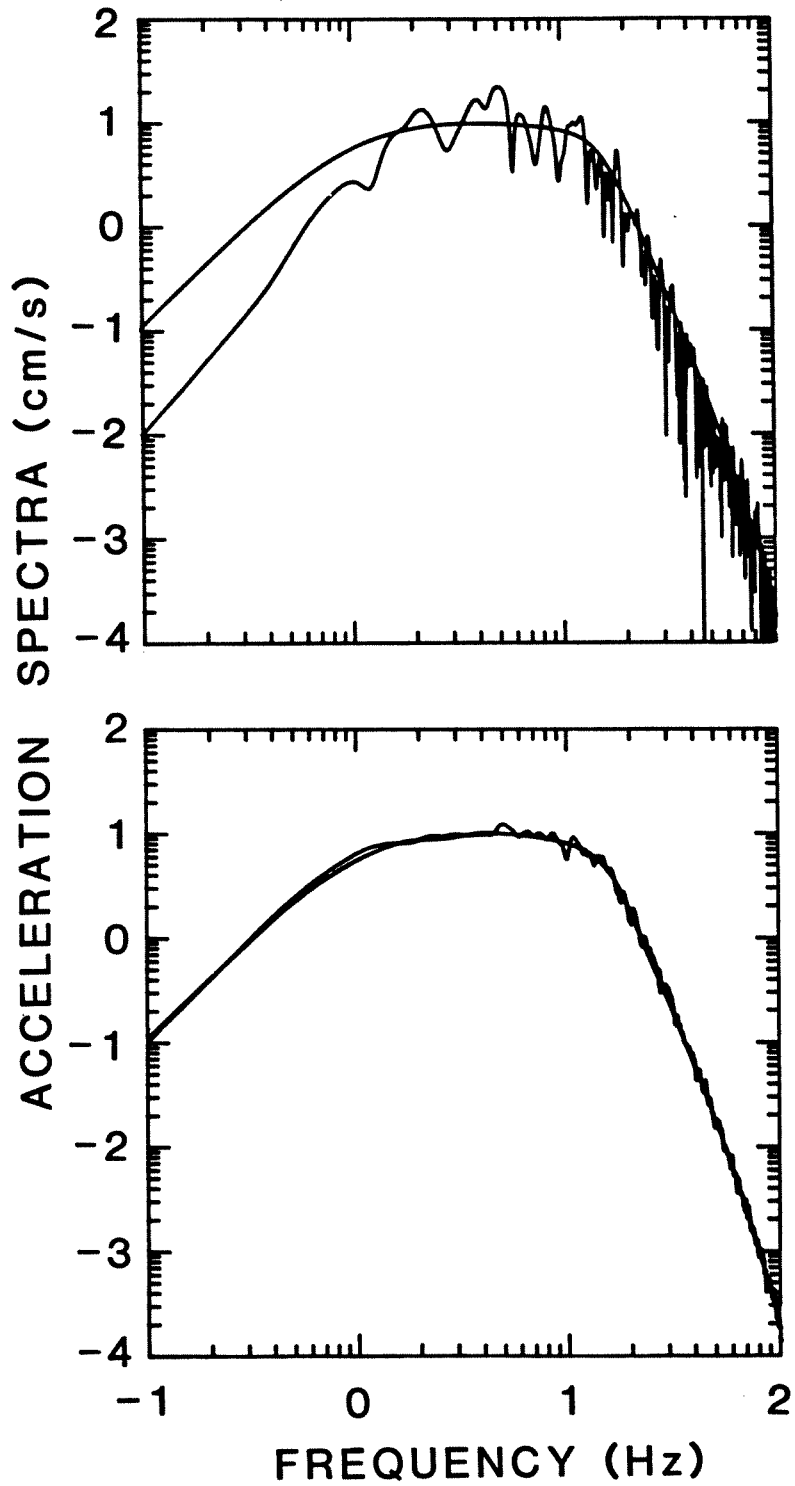
FIGURE 17. Fourier amplitude spectrum of acceleration at 10 km for magnitude 5.0. (Top) Smooth curve, given spectrum; jagged curve, spectrum for one realization of the simulation process. (Bottom) as above but averaged over 20 realizations (the average is the square root of the arithmetic mean of the squared moduli of the individual spectra).
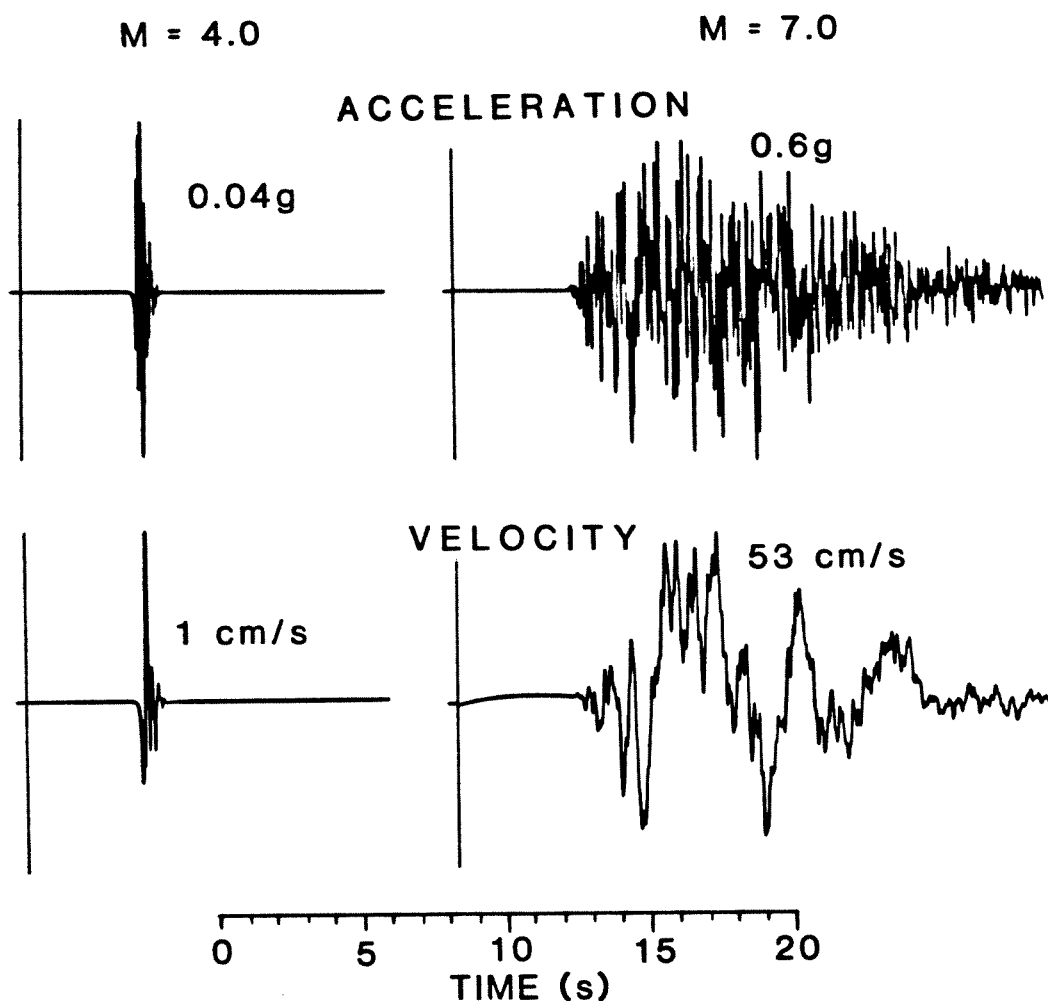
Joyner and Boore

FIGURE 18. Simulated time series for magnitude 4 and 7 earthquakes at a distance of 10 km. Values given for peak motions are the average of peaks from 20 such time series. A low-cut filter with a cutoff frequency of 0.10 Hz has been applied to the velocity time series.

to moderate earthquakes, or low oscillator frequencies, or light damping the duration of motion may not be long enough to generate a pseudo-stationary response. We have developed an empirical correction to the duration of motion $T_w$ to be applied in equation (31) [but not in the estimates of $N$] to account for the distribution of energy content beyond the ground-motion duration (Boore and Joyner, 1984a). We define the ground-motion duration $T_w$, as before, as $1/f_0 + 0.05r$ for the Hanks-McGuire model and as $1/f_A + 0.05r$ for Joyner's (1984) modification. The duration $T_r$ to be used in equation (31) for computing $y_{rms}$ is given by

$$T_r = T_w + \frac{T_0}{2\pi\zeta}\left(\frac{\gamma^3}{\gamma^3 + 1/3}\right) \tag{37}$$

where $T_0$ is the period of the oscillator in sec, $\zeta$ is the damping of the oscillator as a fraction of critical, and $\gamma = T_w/T_0$. Equation (37) was developed and verified by comparing the results of random-vibration theory with the results of Monte Carlo simulations.

As previously noted, the Hanks-McGuire model gives predictions in good agreement with the strong-motion data set collected in western North America. Encouraged by this agreement, Boore
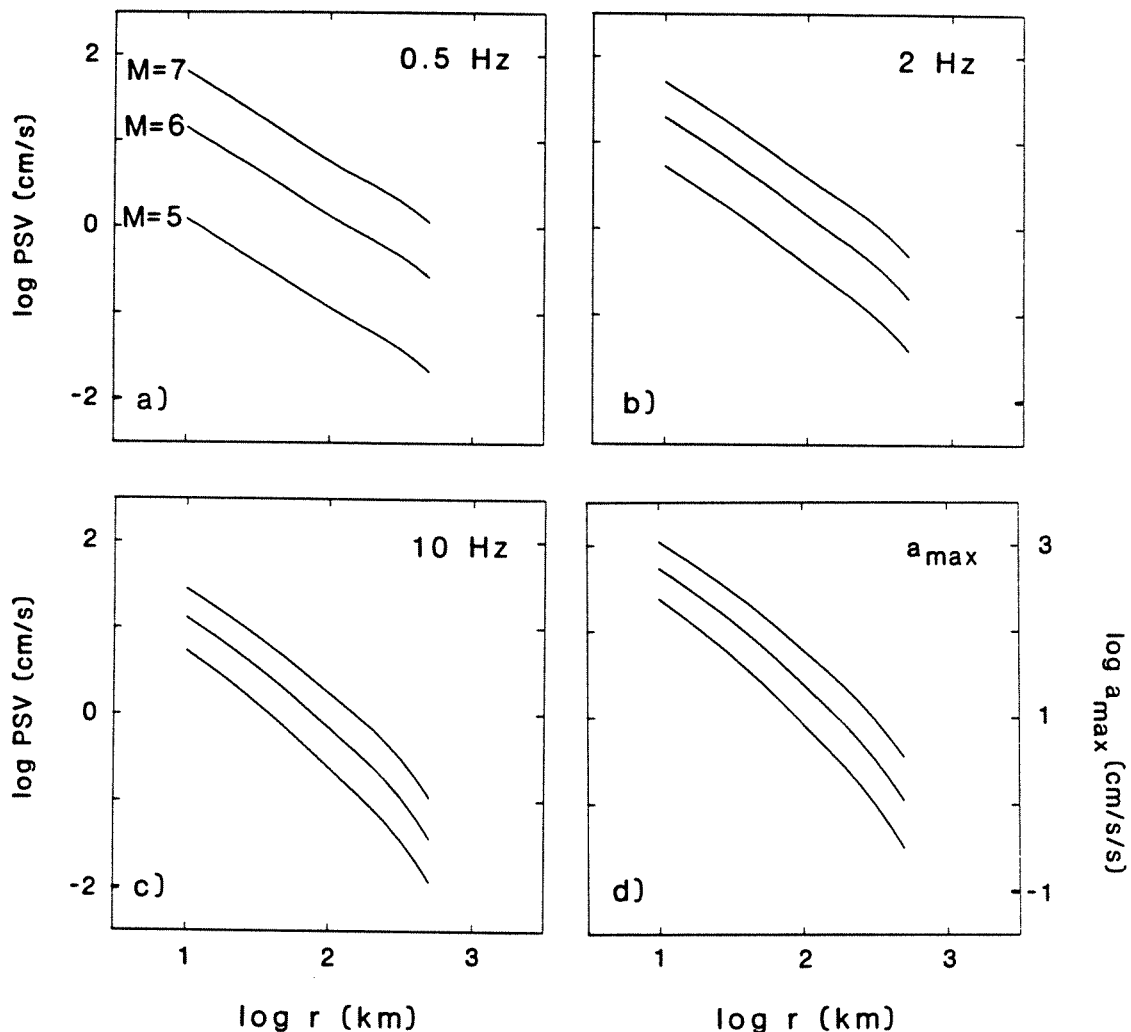
Joyner and Boore

FIGURE 19. Predictive relationships for hard-rock sites in eastern North America giving peak horizontal acceleration and pseudovelocity response at three periods for 5 percent damping (from Boore and Atkinson, 1987).

and Atkinson (1987) used the model to predict ground motion at rock sites in eastern North America, a region where there are few ground-motion recordings within 100 km of damaging earthquakes. They chose a $Q$ function and a value for $f_m$ appropriate for eastern North America. They ignored the amplification factor $A(f)$ on the grounds that near-surface shear velocity in rock in eastern North America is large enough to make the factor negligible. For a stress parameter $\Delta\sigma$ of 100 bars the model agrees with the limited available data. Figure 19 shows the predictions they made for peak horizontal acceleration and spectral response at 0.5, 2, and 10 Hz. Toro and McGuire (1987) also made a study applying the Hanks-McGuire model to the prediction of ground motion in eastern North America.

A limitation of the use of stochastic models for ground-motion predictions as described above is that the approach can be rigorously justified only for sites at distances large compared to the source dimensions. Joyner et al. (1988) have developed a method of stochastic simulation that is applicable at smaller distances. They start by generating functions over the rupture surface representing the total slip at each point. They do so by using Monte Carlo methods to obtain random-phase spectra in two-dimensional wave-number space. The spectra have constant amplitude (determined by the

Joyner and Boore

moment $M_0$) for wave-number vectors with modulus $p$ less than a critical value and amplitudes proportional to $p^{-1.5}$ for $p$ greater than the critical value. The critical value is controlled by the stress parameter $\Delta\sigma$ and is equal to $f_A/v$, where $f_A$ is given by equation (24) and $v$ is the rupture velocity. The function representing total slip is obtained by inverse Fourier transformation and multiplication by a window smoothly tapered to zero at the boundary of the rupture zone. Ground motion corresponding to a delta-function slip velocity at each point is calculated by assuming rupture propagation at uniform velocity from the hypocenter. The ground motion is Fourier transformed from the time to the frequency domain and multiplied by the filter $1/(1 + if/f_B)^{1/2}$ to obtain the spectrum $S(f)$ of ground motion corresponding to a slip-velocity function of the Kostrov (1964) type. The spectrum $S(f)$ is then multiplied by the factors $C$, $A$, $D$, and $I$ in equation (19) and transformed back to the time domain so that the peak value can be obtained. In the actual computations the rupture surface is broken up into zones based on distance to the recording site so that the $Q$ filter can be applied for the appropriate site distance. The process is repeated as many times as needed with different seeds for the Monte Carlo random-number generator. The ground motions resulting from this method have $\omega$-square spectra at distant sites. Simulations of the 1979 Imperial Valley, California, earthquake agree reasonably well with observed data at sites near the source for a rupture velocity of 0.8 $\beta_0$. The results, however, are highly sensitive to the assumed rupture velocity, with amplitudes at the fault lower by about a factor of two for a rupture velocity of 0.7 $\beta_0$.

**Comparison of the Hanks-McGuire Model and the Barrier Model.** The differences between the Hanks-McGuire model and the barrier model represent essentially philosophical differences about how best to describe the seismic source and do not necessarily imply large differences in predicted ground motion. With the methods described in the preceding section it is possible to show just what the differences are. Fourier spectra of horizontal acceleration for the two models are shown in Figure 20. The solid lines in Figure 20 represent Joyner's (1984) modification of the Hanks-McGuire model for a critical magnitude $M_{0c}$ larger than 8.0. The amplification factor is that in Table 14, corresponding to western North American rock sites, the $Q$ function is given by equation (26), $P(f) = \exp(-\pi\kappa_0 f)$ with $\kappa_0$ chosen as 0.02 to correspond to rock sites, and $\Delta\sigma = 50$ bars. The dashed lines represent the spectra appropriate for the barrier model as specified by Papageorgiou (1988) with no amplification factor applied. The data used by Papageorgiou to obtain the spectral shapes were recorded at the surface of the earth and therefore implicitly contain the amplification factors. Using the random-vibration method described in the previous section, we computed peak acceleration and response spectral values for both models. The values for peak acceleration are compared in Figure 21 for both models with the results of regression analysis of strong-motion data from western North America (Joyner and Boore, 1982). For magnitudes above 6 the results from the two models agree well with each other and with the data. The values for the response spectrum at 5 Hz and 5 percent damping are shown in Figure 22. The agreement is not quite so good in this case but still reasonably good above magnitude 6 with the barrier model a little closer to the observed data. The values for the response spectrum at 1 Hz and 5 percent damping are shown in Figure 23, which shows two curves for data, the upper one for soil sites and the lower one for rock sites. The curve representing Joyner's modification of the Hanks-McGuire model agrees with data for rock sites, which it should, given that the values of the amplification factor and $\kappa_0$ correspond to rock sites. The curve representing the barrier model agrees reasonably well above magnitude 6 with data from soil sites. Papageorgiou (1988) makes no distinction between spectra for rock sites and soil sites, but most of the strong-motion data available for guiding the choices that control the shape of the spectrum were recorded at soil sites. It is therefore not surprising that the predictions of the barrier model agree better with data recorded at soil sites.

## Hybrid Prediction

A method for predicting ground motion recently popular among seismologists is the summation of recordings of small earthquakes, considered as Green's functions, in an attempt to simulate the ground motion from larger events (Hartzell, 1978, 1982; Wu, 1978; Kanamori, 1979; Hadley and Helmberger, 1980; Mikumo et al., 1981; Irikura and Muramatu, 1982; Hadley et al., 1982;
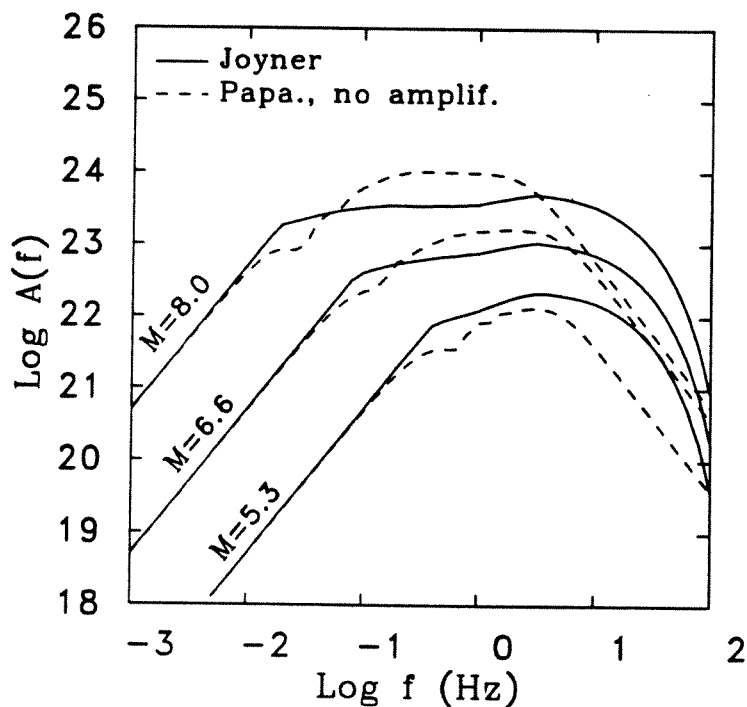
FIGURE 20. Spectra of horizontal acceleration at a distance of 20 km for the indicated magnitudes. Solid line, Joyner's (1984) modification of the Hanks-McGuire model with the amplification factor in Table 14, $Q$ given by equation (26), $P(f)=\exp(-\pi\kappa_0 f)$, $\kappa_0=0.02$, and $\Delta\sigma=50$ bars; dashed line, the barrier model as specified by Papageorgiou (1988) with no amplification factor applied.

Irikura, 1983; Coats et al., 1984; Houston and Kanamori, 1984; Imagawa et al., 1984; Munguiá and Brune, 1984; Hutchings, 1985; Heaton and Hartzell, 1986). The small earthquakes (henceforth called subevents) ideally are located near the hypothetical source and recorded at the site for which the large-event simulation is desired. If these ideal conditions are met, then the method incorporates wave-propagation effects over the whole path from source to recording site as well as local site effects. Generally, however, these conditions are not met. Users of the method generally postulate some distribution of subevents over a fault plane and sum them in accordance with an assumed geometry of rupture propagation. Most users include randomness of some sort in their methods for summing subevents. This randomness may be thought of as representing a degree of random heterogeneity characteristic of large earthquakes. It also performs an important function in preventing spurious periodicities in the simulated motion resulting from summing over uniform grids in space or over points equally spaced in time. Irikura (1983), who did not use any randomness in his summation, relied on a special smoothing technique to eliminate spurious periodicities.

In the spirit of the original concept of the subevent as a Green's function, the corner frequency of the subevent should be higher than any frequency of interest in the simulated motion. In that case the subevent record will be a true impulse response, and the spectrum of the simulated event will depend on how the subevents are distributed over the fault and in time. The quality of the simulation will depend, accordingly on how well the distribution of slip is represented over the fault and in time, in particular, how well the degree and kind of heterogeneity of faulting is represented. In the general case, however, because of limited dynamic range in the subevent records, it may not be possible to use subevents so small that their corner frequencies are higher than any frequency of engineering interest and still maintain the desired bandwidth in the simulated motion. For example, if we wanted to keep the subevent corner frequencies above 3 Hz, we could use subevents no larger than a moment magnitude of about 4; if we wanted to keep the subevent corner frequencies above
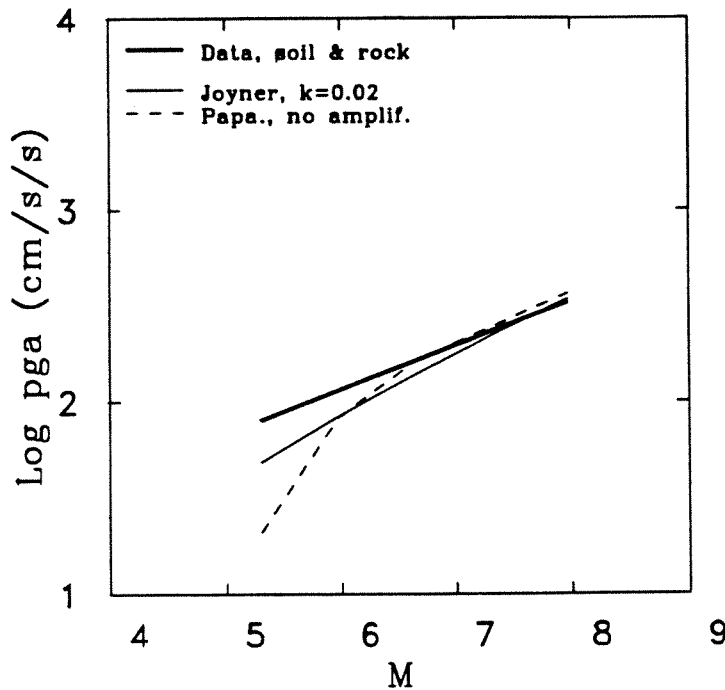
Joyner and Boore

FIGURE 21. Peak horizontal acceleration at 20 km for the randomly oriented horizontal component as a function of magnitude. Heavy line, data from shallow earthquakes in western North America (Joyner and Boore, (1982); light line, predictions for Joyner's modification of the Hanks-McGuire model; dashed line, predictions for the barrier model (see caption of Figure 20 for details).

10 Hz, we could use subevents no larger than a moment magnitude of about 3. Those who have done simulations by the method of summing subevents have generally used much larger subevents, a practice which suggests that it is generally necessary to consider frequencies above the subevent corner.

It is important to note that the effect of directivity will not be correctly modeled at frequencies above the subevent corner frequency unless the angle between the rupture direction and the source-to-recording-site vector is the same for the simulated event as the subevent.

The necessity to consider frequencies above the subevent corner frequency introduces a strong constraint on methods for random summation of subevents (Joyner and Boore, 1986). At very low frequency the subevent spectra will add coherently and the spectral values of the simulated event will be equal to the sum of the subevent values. At sufficiently high frequency the subevent spectra will add incoherently and the spectral values of the simulated event will be equal to the square root of the sum of squares of the subevent values. These rules in combination with seismic scaling relations form the constraint on methods of random summation. We describe a very simple method of random summation, and use it to illustrate the constraint.

In the method, $\eta$ subevents are added together with their start times distributed randomly with uniform probability over the source duration $T$ and their waveforms scaled by a factor $\nu$. Although randomly distributed in time the subevents can be considered to be distributed on a fault with later start times at progressively greater distances from the focus, simulating the irregular propagation of a coherent rupture front. At low frequencies the subevents add coherently, and the low-frequency level of the simulated-event spectrum is proportonal to $\nu\eta$. At high frequency the subevents add incoherently, and the high-frequency level of the simulated event will be proportional to $\nu\sqrt{\eta}$. Scaling laws of earthquake spectra can be used to determine $\eta$ and $\nu$. We are particularly interested in the
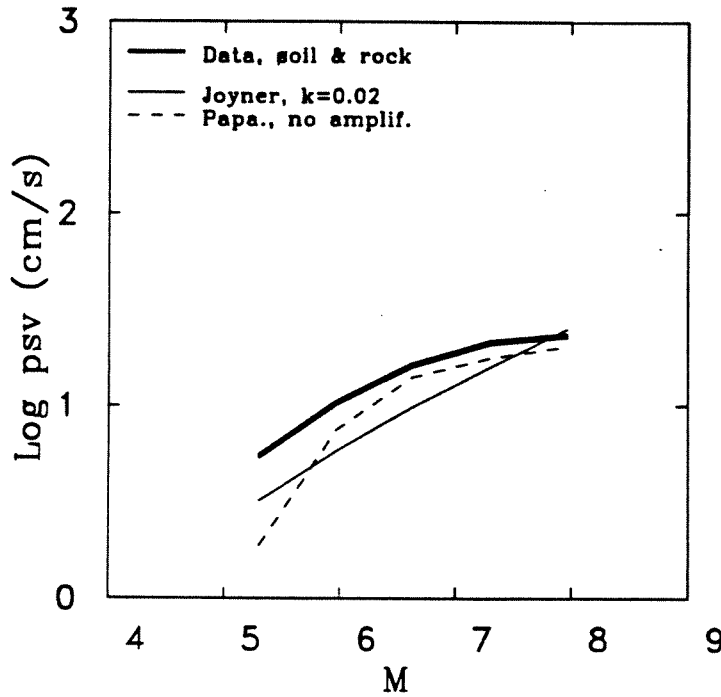
Joyner and Boore

FIGURE 22. Pseudovelocity response at 5 Hz and 5 percent damping for the randomly oriented horizontal component as a function of magnitude for a distance of 20 km. Heavy line, data from shallow earthquakes in western North America (Joyner and Boore, 1982); light line, predictions for Joyner's modification of the Hanks-McGuire model; dashed line, predictions for the barrier model (see caption of Figure 20 for details).

Hanks-McGuire model, which has a self-similar $\omega$-square spectrum (Aki, 1967; Brune, 1970). The equations for $\eta$ and $\nu$, however, can be derived for arbitrary scaling laws. If the displacement spectrum at high frequency falls off as $f^{-\alpha}$, and if the scaling conforms to constant $M_0 f_0^\delta$, then

$$\eta = \left(\frac{M_0}{M_{0e}}\right)^{2\alpha/\delta}$$
$$\nu = \left(\frac{M_0}{M_{0e}}\right)^{1-2\alpha/\delta} \tag{38}$$

where $M_0$ is the moment of the simulated event and $M_{0e}$ is the moment of the subevent (Joyner and Boore, 1986). For the $\omega$-square model $\alpha = 2$. If similarity holds, $M_0 f_0^3$ is constant for all earthquakes, and $\delta = 3$. So, for the $\omega$-square model with similarity

$$\eta = \left(\frac{M_0}{M_{0e}}\right)^{4/3}$$
$$\nu = \left(\frac{M_0}{M_{0e}}\right)^{-1/3} \tag{39}$$

Note that the exponent in the equation for $\nu$ is negative. The subevent records must be reduced in amplitude, and correspondingly larger numbers of them must be added together in order that the low-frequency and high-frequency spectral levels of the simulated event scale in accord with the $\omega$-square model with simularity.

Proper choice of $\eta$ and $\nu$ ensures that the low-frequency and high-frequency spectral levels of the simulated event obey desired scaling laws, but intermediate frequencies may be a problem
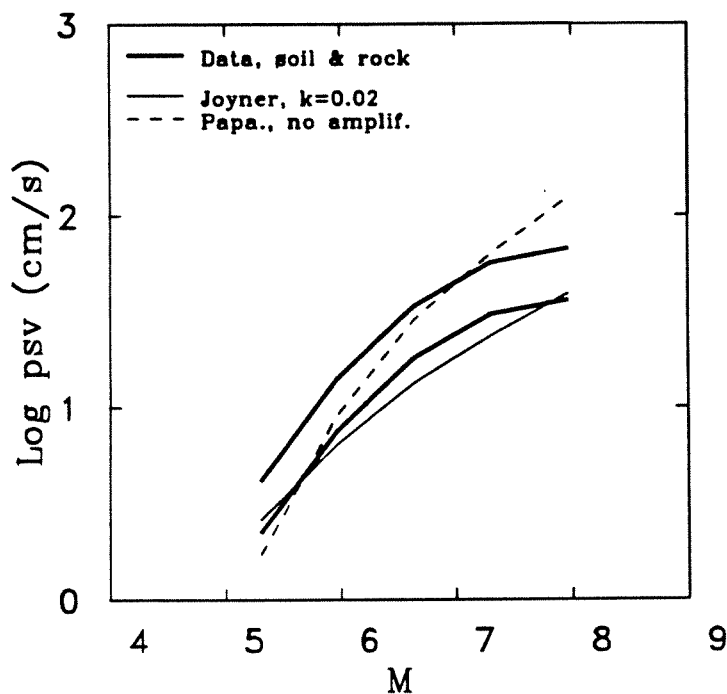
Joyner and Boore

FIGURE 23. Pseudovelocity response at 1 Hz and 5 percent damping for the randomly oriented horizontal component as a function of magnitude for a distance of 20 km. Heavy lines, data from shallow earthquakes in western North America (Joyner and Boore, 1982) at soil sites (upper heavy line) and rock sites (lower heavy line); light line, predictions for Joyner's modification of the Hanks-McGuire model; dashed line, predictions for the barrier model (see caption of Figure 20 for details).

for the method of simulating large events by summing recordings of small ones. The problem is illustrated in Figure 24, where the light line represents the expected value of the spectrum obtained by summing identical subevents according to equation (39) and the heavy line represents the $\omega$-square spectrum corresponding to the moment of the simulated event. The spectrum obtained by summing subevents falls significantly below the $\omega$-square spectrum in the vicinity of the corner frequency of the simulated event. In our earlier paper, from which Figure 24 is taken, we did not treat this difference as a significant problem (Joyner and Boore, 1986). We now believe that it is significant and that it is inherent in any method of summing subevents distributed randomly with uniform probability.
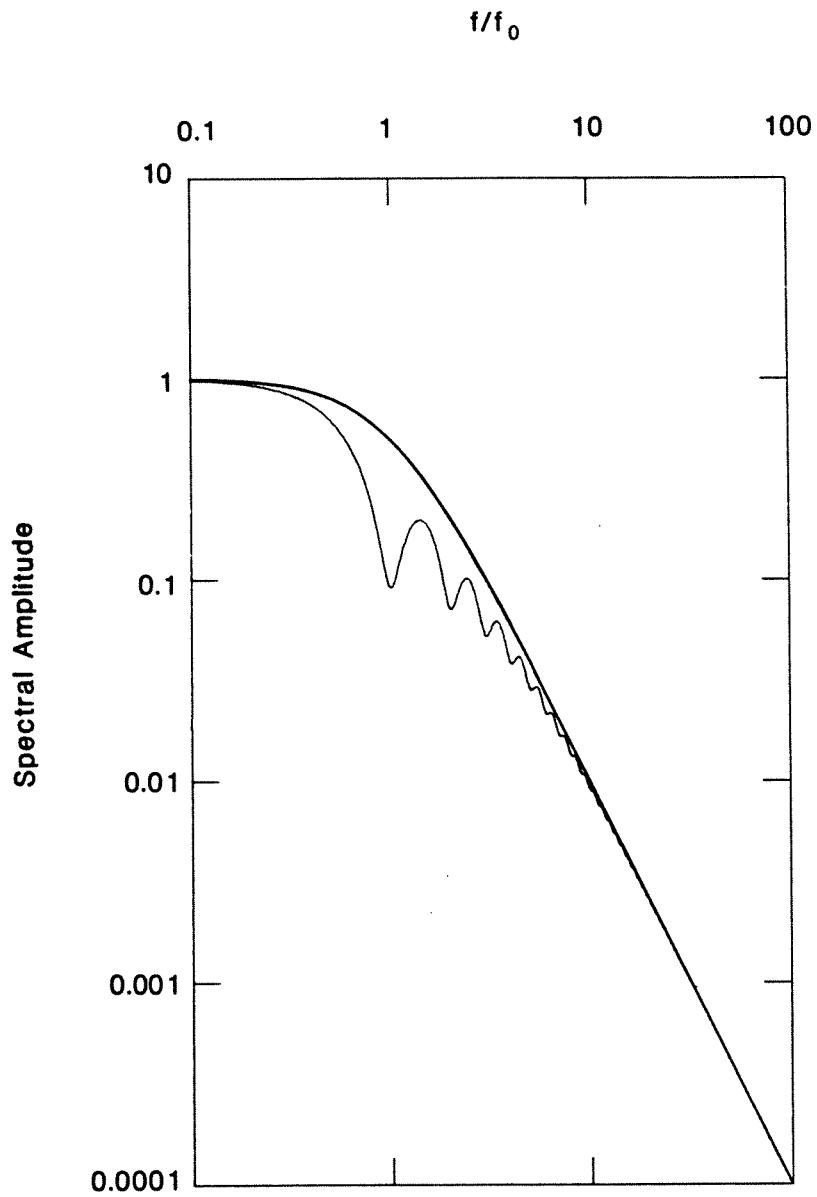
Joyner and Boore

FIGURE 24. Spectrum (light line) of the simulated event obtained by random summation of identical subevents according to equation (39) for a difference of one unit in moment magnitude between simulated event and subevent compared to the $\omega$-square spectrum (heavy line) corresponding to the moment of the simulated event. The axes have been normalized by the long-period level and corner frequency ($f_0$) of the simulated event.

Joyner and Boore

REFERENCES

Abrahamson, N. A. (1985). Estimation of seismic wave coherency and rupture velocity using the SMART 1 strong-motion array recordings, *Rep. UCB/EERC-85/02*, 134 p., Earthquake Engin. Res. Cen., Univ. of Calif., Berkeley.

Aki, K. (1967). Scaling law of seismic spectrum, *J. Geophys. Res.* **72**, 1217–1231.

Aki, K. and P. G. Richards (1980). *Quantitative Seismology Theory and Methods* **1**, 557 p., W. H. Freeman and Company.

Algermissen, S. T., and D. M. Perkins (1976). A probabilistic estimate of maximum acceleration in rock in the contiguous United States, *U.S. Geol. Surv. Open-File Rept. 76-416*, 45 p.

Algermissen, S. T., D. M. Perkins, P. C. Thenhaus, S. L. Hanson, and B. L. Bender (1982). Probabilistic estimates of maximum acceleration and velocity in rock in the contiguous United States, *U.S. Geol. Surv. Open-File Rept. 82-1033*, 99 p.

Anderson, J. G., J. N. Brune, J. Prince, and F. L. Vernon, III (1983). Preliminary report on the use of digital strong motion recorders in the Mexicali Valley, Baha California, *Bull. Seism. Soc. Am.* **73**, 1451–1467.

Anderson, J. G. and S. E. Hough (1984). A model for the shape of the Fourier amplitude spectrum of acceleration at high frequencies, *Bull. Seism. Soc. Am.* **74**, 1969–1993.

Anderson, J. G., P. Bodin, J. N. Brune, J. Prince, S. K. Singh, R. Quass, and M. Onate (1986). Strong ground motion from the Michaocan, Mexico, earthquake, *Science* **233**, 1043–1049, 5 September.

Andrews, M. C., C. Dietel, T. Noce, E. Sembera, and J. Bicknell (1988). Preliminary analyses of digital recordings of the Superstition Hills, California aftershock sequence (abs.), submitted to *Earthquake Notes*.

Applied Technology Council (1978). *Tentative Provisions for the Development of Seismic Regulations for Buildings*, Applied Technology Council Publication ATC 3-06, 505 p.

Araya, R. and A. Der Kiureghian (1986). Seismic hazard analysis including source directivity effect, *Proc. of 3rd. U.S. Nat. Conf. on Earthquake Engin.* **1**, convened Charleston, South Carolina, August 24–28, 1986, 269–280.

Archuleta, R. J. (1984). A faulting model for the 1979 Imperial Valley earthquake, *J. Geophys. Res.* **89**, 4459–4585.

Ascher, U. and P. Spudich (1986). A hybrid collocation method for calculating complete theoretical seismograms in vertically varying media, *Geophys. J. R. Astron. Soc.* **86**, 19–40.

Bakun, W. H. and W. B. Joyner (1984). The $M_L$ scale in central California, *Bull. Seism. Soc. Am.* **74**, 1827–1843

Bard, P.-Y. and B. E. Tucker (1985). Underground and ridge site effects: a comparison of observation and theory, *Bull. Seism. Soc. Am.* **75**, 905–922.

Barker, J. S., P. G. Somerville, and J. P. McLaren (1988). Modeling ground-motion attenuation in eastern North America, in *Proc. Symp. on Seismic Hazards, Ground Motions, Soil-Liquifaction and Engineering Practice in Eastern North America*, K. H. Jacob, ed., National Center for

Earthquake Engineering Research Tech. Report NCEER-87-0025, 339-352.

Ben-Menahem, A. (1961). Radiation of seismic surface-waves from finite moving sources, *Bull. Seism. Soc. Am.* **51**, 401-435.

Berger, J., L. M. Baker, J. N. Brune, J. B. Fletcher, T. C. Hanks, and F. L. Vernon, III, (1984). The Anza array: a high-dynamic-range, broadband, digitally radiotelemetered, seismic array, *Bull. Seism. Soc. Am.* **74**, 1469-1481.

Bevington, P. R. (1969). *Data Reduction and Error Analysis for the Physical Sciences*, 336 p., McGraw-Hill.

Boatwright, J. and D. M. Boore (1982). Analysis of the ground accelerations radiated by the 1980 Livermore Valley earthquakes for directivity and dynamic source characteristics, *Bull. Seism. Soc. Am.* **72**, 1843-1865.

Boatwright, J. (1985). Characteristics of the aftershock sequence of the Borah Peak, Idaho, earthquake determined from digital recordings of the events, Bull. Seism. Soc. Am. **75**, 1265-1284.

Bolt, B. A., N. Abrahamson, and Y. T. Yeh (1984). The variation of strong ground motion over short distances, in *Proc. of 8th World Conf. on Earthquake Engin. (San Francisco)* **2**, 183-189.

Boore, D. M. (1972). A note on the effect of simple topography on seismic $SH$ waves, *Bull. Seism. Soc. Am.* **62**, 275-284.

Boore, D. M. (1973). The effect of simple topography on seismic waves: implications for the accelerations recorded at Pacoima Dam, San Fernando Valley, California, *Bull. Seism. Soc. Am.* **63**, 1603-1609.

Boore, D. M. and W. B. Joyner (1978). The influence of rupture incoherence on seismic directivity, *Bull. Seism. Soc. Am.* **68**, 283-300.

Boore, D. M. and W. B. Joyner (1982). The empirical prediction of ground motion, *Bull. Seism. Soc. Am.* **72**, S43-S60.

Boore, D. M. (1983). Stochastic simulation of high-frequency ground motions based on seismological models of the radiated spectra, *Bull. Seism. Soc. Am.* **73**, 1865-1894.

Boore, D. M. (1984). Use of seismoscope records to determine $M_L$ and peak velocities, *Bull. Seism. Soc. Am.* **74**, 315-324.

Boore, D. M. and J. Boatwright (1984). Average body-wave radiation coefficients, *Bull. Seism. Soc. Am.* **74**, 1615-1621.

Boore, D. M. and W. B. Joyner (1984a). A note on the use of random vibration theory to predict peak amplitudes of transient signals, *Bull. Seism. Soc. Am.* **74**, 2035-2039.

Boore, D. M. and W. B. Joyner (1984b). Ground motions and response spectra at soil sites from seismological models of radiated spectra, in *Proc. of Eighth World Conf. on Earthquake Engin. (San Francisco)* **2**, 457-464.

Boore, D. M. (1986). Short-period $P$- and $S$-wave radiation from large earthquakes: implications for spectral scaling relations, *Bull. Seism. Soc. Am.* **76**, 43-64.

Boore, D. M. and W. B. Joyner (1986). Prediction of earthquake ground motion at periods of interest for base-isolated structures, in Proc. Seminar and Workshop on Base Isolation and Passive Energy Dissipation, March 12–14, 1986, San Francisco, Calif., 355–370, Applied Technology Council.

Boore, D. M. (1987). The prediction of strong ground motion, in *Strong Ground Motion Seismology*, M. Erdik and M. N. Toksöz, Editors, NATO Advanced Studies Institute series, D. Reidel Publishing Company, Dordrecht, The Netherlands, 109–141.

Boore, D. M. and G. M. Atkinson (1987). Stochastic prediction of ground motion and spectral response parameters at hard-rock sites in eastern North America, *Bull. Seism. Soc. Am.* **77**, 440–467.

Boore, D. M. (1988). The Richter scale—its development and use for determining earthquake source parameters, submitted to *Physics of the Earth and Planetary Interiors*, in press.

Borcherdt, R. D. (1970). Effects of local geology on ground motion near San Francisco Bay, *Bull. Seism. Soc. Am.* **60**, 29–61.

Borcherdt, R. D., G. L. Maxwell, C. S. Mueller, R. McClearn, G. Sembera, and L. Wennerberg (1983). Digital strong-motion data recorded by U.S. Geological Survey near Coalinga, California, in *The Coalinga Earthquake Sequence Commencing May 2, 1983*, 61–76, U.S. Geol. Surv. Open-File Rep. 83-511.

Borcherdt, R. D., J. G. Anderson, C. B. Crouse, N. C. Donovan, T. V. McEvilly, and A. F. Shakal (1984). *National Planning Considerations for the Acquisition of Strong-Ground-Motion Data, Pub. 84-08 Earthquake Engin. Res. Inst.*, 57 p.

Borcherdt, R. D., J. B. Fletcher, E. G. Jensen, G. L. Maxwell, J. R. Van Schaak, R. E. Warrick, E. Cranswick, M. J. S. Johnston, and R. McClearn (1985). A general earthquake-observation system, *Bull. Seism. Soc. Am.* **75**, 1783–1825.

Bouchon, M. (1973). Effect of topography on surface motion, *Bull. Seism. Soc. Am.* **63**, 615–632.

Bouchon, M. (1982). The complete synthesis of seismic crustal phases at regional distances, *J. Geophys. Res.* **87**, 1735–1741.

Brady, A. G., R. L. Porcella, G. N. Bycroft, E. C. Etheredge, P. N. Mork, B. Silverstein, and A. F. Shakal (1984a). Strong-motion results from the main shock of April 24, 1984, in *The Morgan Hill, California Earthquake of April 24, 1984 (A Preliminary Report)* 1, 18–26, *U.S. Geol. Surv. Open-File Rep. 84-498A.*

Brady, A. G., R. L. Porcella, G. N. Bycroft, E. C. Etheredge, P. N. Mork, B. Silverstein, and A. F. Shakal (1984b). Strong-motion results from the main shock of April 24, 1984—computer plots, *The Morgan Hill, California earthquake of April 24, 1984 (A Preliminary Report)* 2, *U.S. Geol. Surv. Open-File Rep.84-498B*, 118 p.

Brillinger, D. R. and H. K. Preisler (1984). An exploratory analysis of the Joyner-Boore attenuation data, *Bull. Seism. Soc. Am.* **74**, 1441–1450.

Brillinger, D. R. and H. K. Preisler (1985). Further analysis of the Joyner-Boore attenuation data, *Bull. Seism. Soc. Am.* **75**, 611–614.

Brune, J. N. (1970). Tectonic stress and the spectra of seismic shear waves from earthquakes, *J. Geophys. Res.* 75, 4997–5009.

Brune, J. N. (1971). Correction, *J. Geophys. Res.* 76, 5002.

Brune, J. N., R. Lovberg, R. Anooshehpoor, and L. Wang (1984). Measurements of topographic amplification on foam rubber models using newly designed quadrant position detectors (abs.), *Earthquake Notes* 55, 22.

Burger, R. W., P. G. Somerville, J. S. Barker, R. B. Herrmann, and D. V. Helmberger (1987). The effect of crustal structure on strong ground motion attenuation relations in eastern North America, *Bull. Seism. Soc. Am.* 77, 420–439.

Bycroft, G. N. (1978). The effect of soil-structure interaction on seismometer readings, *Bull. Seism. Soc. Am.* 68, 823–843.

Campbell, K. W. (1981). Near-source attenuation of peak horizontal acceleration, *Bull. Seism. Soc. Am.* 71, 2039–2070.

Campbell, K. W. (1985). Strong motion attenuation relations: a ten-year perspective, *Earthquake Spectra* 1, 759–804.

Campbell, K. W. (1988). Predicting strong ground motion in Utah, in *Evaluation of Regional and Urban Earthquake Hazards and Risk in Utah*, W. W. Hays and P. L. Gori, Editors, *U.S. Geol. Surv. Profess. Paper*, in preparation.

Cartwright, D. E. and M. S. Longuet-Higgins (1956). The statistical distribution of the maxima of a random function, *Proc. R. Soc. London* 237, 212–232.

Coats, D. A., H. Kanamori, and H. Houston (1984). Simulation of strong motion from the 1964 Alaskan earthquake (abs.), *Earthquake Notes* 55, 18.

Converse, A. M. (1984). AGRAM: a series of computer programs for processing digitized strong-motion accelerograms, *U.S. Geol. Surv. Open-File Rep. 84-525*.

Converse, A. M., A. G. Brady, and W. B. Joyner (1984). Improvements in strong-motion data processing procedures, in *Proc. of 8th World Conf. on Earthquake Engin. (San Francisco)*, 2, 143–148.

Cornell, C. A. and R. T. Sewell (1987). Non-linear-behavior intensity measures in seismic hazard analysis, *Proc. Internat. Seminar on Seismic Zonation*, December, 1987, Guangzhou, China.

Crouse, C. B., G. C. Liang, and G. R. Martin (1984). Experimental study of soil-structure interaction at an accelerograph station, *Bull. Seism. Soc. Am.* 74, 1995–2013.

Crouse, C. B. and B. Hushmand (1987). Experimental investigations of soil-structure interaction at CDMG and USGS accelerograph statons (abs.), *Earthquake Notes* 58, 10.

Crouse, C. B., Y. K. Vyas, and B. A. Schell (1988). Ground motions from subduction-zone earthquakes, *Bull. Seism. Soc. Am.* 78, 1–25.

Donovan, N. C. and A. E. Bornstein (1978). Uncertainties in seismic risk procedures, *Proc. Am. Soc. Civil Eng., J. Geotech. Eng. Div.* 104, 869–887.

Ekström, G. and A. M. Dziewonski (1985). Centroid-moment tensor solutions for 35 earthquakes in Western North America (1977–1983), *Bull. Seism. Soc. Am.* 75, 23–29.

Etheredge, E. C. and R. L. Porcella (1987). Strong-motion data from the October 1, 1987 Whittier

Narrows earthquake, *U.S. Geol. Surv. Open-File Rep. 87-616*, 64 p.

Ewing, W. M., W. S. Jardetzky, and F. Press (1957). *Elastic Waves in Layered Media*, 380 p., McGraw-Hill.

Frankel, F. and L. Wennerberg (1987). On the frequency dependence of shear-wave $Q$ in the crust from 1 to 15 Hz (abs.), *EOS, Trans. Am. Geophys. Union* 68, 1362.

Fletcher, J. B., A. G. Brady, and T. C. Hanks (1980). Strong-motion accelerograms of the Oroville, California, aftershocks: data processing and the aftershock of 0350 August 6, 1975, *Bull. Seism. Soc. Am.* 70, 243–367.

Geli, L., P.-Y. Bard, and B. Jullien (1988). The effect of topography on earthquake ground motion: a review and new results, *Bull. Seism. Soc. Am.* 78, 42–63.

Gutenberg, B. (1957). Effects of ground on earthquake motion, *Bull. Seism. Soc. Am.* 47, 221–250.

Guzman, R. A. and P. C. Jennings (1976). Design spectra for nuclear power plants, *Proc. Am. Soc. Civil Engin., J. Power Div.* 102, 165–178.

Hadley, D. M. and D. V. Helmberger (1980). Simulation of strong ground motions, *Bull. Seism. Soc. Am.* 70, 617–610.

Hadley, D. M., D. V. Helmberger, and J. A. Orcutt (1982). Peak acceleration scaling studies, *Bull. Seism. Soc. Am.* 72, 959–979.

Hanks, T. C. (1975). Strong ground motion of the San Fernando, California, earthquake: ground displacements, *Bull. Seism. Soc. Am.* 65, 193–225.

Hanks, T. C. and H. Kanamori (1979). A moment magnitude scale, *J. Geophys. Res.* 84, 2348–2350.

Hanks, T. C. and R. K. McGuire (1981). The character of high-frequency strong ground motion, *Bull. Seism. Soc. Am.* 71, 2071–2095.

Hanks, T. C. (1982). $f_{max}$, *Bull. Seism.Soc. Am.* 72, 1867–1879.

Hanks, T. C. and D. M. Boore (1984). Moment-magnitude relations in theory and practice, *J. Geophys. Res.* 89, 6229–6235.

Hartzell, S. H. (1978). Earthquake aftershocks as Green's functions, *Geophys. Res. Lett.* 5, 1–4.

Hartzell, S. H. (1982). Simulation of ground accelerations for the May 1980 Mammoth Lakes, California, earthquakes, *Bull. Seism. Soc. Am.* 72, 2381–2387.

Hartzell, S. H. and T. H. Heaton (1983). Inversion of strong ground motion and teleseismic waveform data for the fault rupture history of the 1979 Imperial Valley, California, earthquake, *Bull. Seism. Soc. Am.* 73, 1553–1583.

Heaton, T. H., and S. H. Hartzell (1986). Estimation of strong ground motions from hypothetical earthquakes on the Cascadia subduction zone, Pacific Northwest, *U.S. Geol. Surv. Open-File Rep. 86-328*, 40 p.

Heaton, T. H., F. Tajima, and A. W. Mori (1986). Estimating ground motions using recorded accelerograms, *Surveys in Geophys.* 8, 25–83.

Herrmann, R. B. (1985). An extension of random vibration theory estimates of strong ground motion to large distances, *Bull. Seism. Soc. Am.* **75**, 1447–1453.

Houston, H. and H. Kanamori (1984). The effect of asperities on short-period seismic radiation with application to the 1964 Alaskan earthquake (abs.), *Earthqukae Notes* **55**, 18.

Houston, H. and H. Kanamori (1986). Source spectra of great earthquakes: teleseismic constraints on rupture processes and strong motion, *Bull. Seism. Soc. Am.* **76**, 19–42.

Huang, M. J., A. F. Shakal, D. L. Parke, R. W. Sherburne, and R. V. Nutt (1985). Processed data from the strong-motion records of the Morgan Hill earthquake of 24 April 1984. Part II. Structural-response records, *Rep. OSMS 85-05*, 320 p., Office of Strong Motion Studies, Calif. Div. Mines and Geol.

Huang, M. J., R. W. Sherburne, D. L. Parke, and A. F. Shakal (1986). CSMIP strong-motion records from the Palm Springs, California earthquake of 8 July 1986, *Rep. OSMS 86-05*, 74 p., Office of Strong Motion Studies, Calif. Div. Mines and Geol.

Huang, M. J., T. Q. Cao, C. E. Ventura, D. L. Parke, and A. F. Shakal (1987). CSMIP strong-motion records from the Superstition Hills, Imperial County, California earthquakes of 23 and 24 November 1987, *Rep. OSMS 87-06*, 42 p., Office of Strong Motion Studies, Calif. Div. Mines and Geol.

Hutchings, L. (1985). Modeling earthquakes with empirical Green's functions (abs.), *Earthquake Notes* **56**, 14.

Hutton, L. K. and D. M. Boore (1987). The $M_L$ scale in southern California, *Bull. Seism. Soc. Am.* **77**, 2074–2094.

Idriss, I. M. and H. B. Seed (1968). Seismic response of horizontal soil layers, *Proc. Am. Soc. Civil Engin., J. Soil Mech. and Found. Div* **94**, 1003–1031.

Idriss, I. M. (1979). Characteristics of earthquake ground motions, in *Earthquake Engineering and Soil Dynamics, Proc. Am. Soc. Civil Eng. Geotech. Eng. Div. Specialty Conf.*, June 19–21, 1978, Pasadena, California, **3**, 1151–1265.

Idriss, I. M. (1985). Evaluating seismic risk in engineering practice, *Proc. Eleventh Internat. Conf. on Soil Mech. and Foundation Eng.*, August 12–16, 1985, San Francisco, California, **1**, 255–320, A. A. Balkema, Rotterdam.

Idriss, I. M. (1987). Earthquake ground motions, Lecture notes, Course on Strong Ground Motion, Earthquake Engin. Res. Inst., Pasadena, Calif., April 10–11, 1987.

Imagawa, K., N. Mikami, and T. Mikumo (1984). Analytical and semi-empirical synthesis of near-field seismic waveforms for investigating the rupture mechanism of major earthquakes, *J. Phys. Earth* **32**, 317–338.

International Conference of Building Officials (1988). *Uniform Building Code*, 1988 edition, in preparation.

Irikura, K. and I. Muramatu (1982). Synthesis of strong ground motions from large earthquakes using observed seismograms of small events, *Proc. of 3rd Internat. Microzonation Conf.* **1**, Seattle, 447–458.

Irikura, K. (1983). Semi-empirical estimation of strong ground motions during large earthquakes,

*Bull. Disaster Prevention Res. Inst. (Kyoto Univ.)* **33**, 63–104.

Iwan, W. D., M. A. Moser, and C.-Y. Peng (1985). Some observations on strong-motion earthquake measurement using a digital accelerograph, *Bull. Seism. Soc. Am.* **75**, 1225–1246.

Jackson, S. M. and J. Boatwright (1985). The Borah Peak, Idaho earthquake of October 28, 1983—strong ground motion, *Earthquake Spectra* **2**, 51–69.

Jacob, K. H. and J. Mori (1984). Strong motions in Alaska-type subduction zone environments, *Proc. Eighth World Conf. on Earthquake Engin. (San Francisco)* **2**, 311–317.

Johnson, L. R. and W. Silva (1981). The effects of unconsolidated sediments upon the ground motion during local earthquakes, *Bull. Seism. Soc. Am.* **71**, 127–142.

Joyner, W. B. and A. T. F. Chen (1975). Calculation of nonlinear ground response in earthquakes, *Bull. Seism. Soc. Am.* **65**, 1315–1336.

Joyner, W. B., R. E. Warrick, and A. A. Oliver, III, (1976). Analysis of seismograms from a downhole array in sediments near San Francisco Bay, *Bull. Seism. Soc. Am.* **66**, 937–958.

Joyner, W. B. and D. M. Boore (1981). Peak horizontal acceleration and velocity from strong-motion records including records from the 1979 Imperial Valley, California, earthquake, *Bull. Seism. Soc. Am.* **71**, 2011–2038.

Joyner, W. B. and D. M. Boore (1982). Prediction of earthquake response spectra, *Proc. 51st Ann. Convention Structural Eng. Assoc. of Cal.*, also *U. S. Geol. Surv. Open-File Rept. 82-977*, 16 p.

Joyner, W. B. (1984). A scaling law for the spectra of large earthquakes, *Bull. Seism. Soc. Am.* **74**, 1167–1188.

Joyner, W. B. and T. E. Fumal (1984). Use of measured shear-wave velocity for predicting geologic site effects on strong ground motion, *Proc. Eighth World Conf. on Earthquake Eng. (San Francisco)* **2**, 777–783.

Joyner, W. B. and D. M. Boore (1986). On simulating large earthquakes by Green's-function addition of smaller earthquakes, in *Earthquake Source Mechanics, Maurice Ewing Ser.* **6**, edited by S. Das *et al.*, 269–274, Am. Geophys. Union.

Joyner, W. B., K. W. Campbell, and S. C. Harmsen (1988). Near-source simulation of earthquake ground motion based on the stochastic omega-square model (abs.), submitted to *Earthquake Notes*.

Kanai, K. (1952). Relation between the nature of surface layer and the amplitudes of earthquake motions, *Bull. Earthquake Res. Inst., Tokyo Univ.* **30**, 31–37.

Kanamori, H. (1979). A semi-empirical approach to prediction of long-period ground motions from great earthquakes, *Bull. Seism. Soc. Am.* **69**, 1645–1670.

Kanamori, H. and C. R. Allen (1986). Earthquake repeat time and average stress drop, in *Earthquake Source Mechanics, Maurice Ewing Ser.* **6**, edited by S. Das *et al.*, 227–235, Am. Geophys. Union.

Kawashima, K., K. Aizawa, and K. Takahashi (1984). Attenuation of peak ground motion and absolute acceleration response spectra, *Proc. Eighth World Conf. on Earthquake Engin. (San Francisco)* **2**, 257–264.

Kennett, B. L. N. (1985). On regional S, *Bull. Seism. Soc. Am.* **75**, 1077–1086.

Kostrov, B. V. (1964). Self-similar problems of propagation of shear cracks (translation), *J. Appl. Math. Mech.* **28**, 1077–1078.

Khemici, O. and W.-L. Chiang (1984). Frequency domain corrections of earthquake accelerograms with experimental verifications, *Proc. Eighth World Conf. on Earthquake Engin. (San Francisco)* **2**, 103–110.

King, J. L. and B. E. Tucker (1984). Observed variations of earthquake motion across a sediment-filled valley, *Bull. Seism. Soc. Am.* **74**, 137–151.

Lee, V. W. and M. D. Trifunac (1984). Current developments in data processing of strong motion accelerograms, *Rep. 84-01*, 99 p., Dept. Civil Engin., Univ. So. Calif., Los Angeles.

Maley, R. P., A. G. Brady, E. C. Etheredge, D. A. Johnson, P. N. Mork, and J. C. Switzer (1983). Analog strong-motion data and processed main event records obtained by U.S. Geological Survey near Coalinga, California, in *The Coalinga Earthquake Sequence Commencing May 2, 1983*, 38–60, *U.S. Geol. Surv. Open-File Rep. 83-511*.

Maley, R. P., E. C. Etheredge, and A. Acosta (1986). U. S. Geological Survey strong-motion records from the Chalfant Valley, California, earthquake of July 21, 1986, *U. S. Geol. Surv. Open-File Rep. 86-568*, 19 p.

McGarr, A. (1984). Scaling of ground motion parameters, state of stress, and focal depth, *J. Geophys. Res.* **89**, 6969–6979.

McGarr, A. (1986). Some observations indicating complications in the nature of earthquake scaling, in *Earthquake Source Mechanics, Maurice Ewing Ser. 6*, edited by S. Das *et al.*, 217–225, Am. Geophys. Union.

McGuire, R. K. (1974). Seismic structural response risk analysis, incorporating peak response regressions on earthquake magnitude and distance, *Research Report R74-51*, Dept. Civil Eng., Mass. Inst. of Tech., Cambridge, Mass., 371 p.

McGuire, R. K. (1978). Seismic ground motion parameter relations, *Proc. Am. Soc. Civil Eng., J. Geotech. Eng. Div.* **104**, 481–490.

McJunkin, R. D. and A. F. Shakal (1983). The Parkfield strong-motion array, *Calif. Geol.* **36**, 27–34.

Mikumo, T., K. Irikura, and K. Imagawa (1981). Near-field strong-motion synthesis from foreshock and aftershock records and the rupture process of the main shock fault (abs.), *IASPEI 21st General Assembly*, London, Canada, July 20–30, 1981.

Mohraz, B. (1976). A study of earthquake response spectra for different geological conditions, *Bull. Seism. Soc. Am.* **66**, 915–935.

Munguiá, L. and J. N. Brune (1984). Simulations of strong ground motions for earthquakes in the Mexicali-Imperial valley, *Proc. of Workshop on Strong Ground Motion Simulation and Earthquake Engineering Applications, Pub. 85-02 Earthquake Engin. Res. Inst.*, April 30–May 3, 1984, Los Altos, California, 21-1–21-19.

Newmark, N. M. and W. J. Hall (1969). Seismic design criteria for nuclear reactor facilities, *Proc. Fourth World Conf. on Earthquake Eng. (Santiago)* **2**, B4-37–B4-50.

New Zealand Geological Survey (1987). The March 2, 1987, earthquake near Edgecumbe, North Island, New Zealand, *EOS, Trans. Am. Geophys. Union* 68, 1162–1171.

Olson, A. H. and R. J. Apsel (1982). Finite faults and inverse theory with applications to the 1979 Imperial Valley earthquake, *Bull. Seism. Soc. Am.* 72, 1969–2001.

Olson, A. H., J. A. Orcutt, and G. A. Frazier (1984). The discrete wavenumber/finite element method for synthetic seismograms, *Geophys. J. R. Astron. Soc.* 77, 421–460.

Papageorgiou, A. S. and K. Aki (1983a). A specific barrier model for the quantitative description of inhomogeneous faulting and the prediction of strong ground motion. I. Description of the model, *Bull. Seism. Soc. Am.* 73, 693–722.

Papageorgiou, A. S. and K. Aki (1983b). A specific barrier model for the quantitative description of inhomogeneous faulting and the prediction of strong ground motion. Part II. Applications of the model, *Bull. Seism. Soc. Am.* 73, 953–978.

Papageorgiou, A. S. (1988). On two characteristic frequencies of acceleration spectra: patch corner frequency and $f_{max}$, *Bull. Seism. Soc. Am.*, scheduled for the April issue.

Porcella, R. L., E. C. Etheredge, R. P. Maley, and J. C. Switzer (1987a). Strong-motion data from the July 8, 1986 North Palm Springs earthquake and aftershocks, *U.S. Geol. Surv. Open-File Rep. 87-155*, 37 p.

Porcella, R. L., E. C. Etheredge, R. P. Maley, and J. C. Switzer (1987b). Strong-motion data from the Superstition Hills earthquakes of 0154 and 1315 (GMT), November 24, 1987, *U.S. Geol. Surv. Open-File Rep. 87-672*, 56 p.

Raugh, M. R. (1981). Procedures for analysis of strong-motion records (abs.), *Earthquake Notes* 52, 17.

Rogers, A. M., R. D. Borcherdt, P. A. Covington, and D. M. Perkins (1984). A comparative ground response study near Los Angeles using recordings of Nevada nuclear tests and the 1971 San Fernando earthquake, *Bull. Seism. Soc. Am.* 74, 1925–1949.

Rogers, A. M., S. C. Harmsen, R. B. Herrmann, and M. E. Meremonte (1987). A study of ground motion attenuation in the southern Great Basin, Nevada-California, using several techniques for estimates of $Q_S$, $\log A_0$, and coda $Q$, *J. Geophys. Res.* 92, 3527–3540.

Sabetta, F. and A. Pugliese (1987). Attenuation of peak horizontal acceleration and velocity from Italian strong-motion records, *Bull. Seism. Soc. Am.* 77, 1491–1513.

Sadigh, K., J. Egan, and R. Youngs (1986). Specification of ground motion for seismic design of long period structures (abs.), *Earthquake Notes* 57, 13.

Şafak, E. and D. M. Boore (1988). On low-frequency errors of uniformly modulated filtered white-noise models for ground motions, *Earthquake Engineering and Structural Dynamics* 16, in press.

Saragoni, R. H., M. B. Fresard, and S. Gonzales (1985). Analisis de los acelerogramas del terremoto del 3 de Marzo de 1985, I Parte, in Publicacion SES I 4/1985 (199), University of Chile.

Sato, T. and T. Hirasawa (1973). Body wave spectra from propagating shear cracks, *J. Phys. Earth* 21, 415–431.

Schnabel, P., H. B. Seed, and J. Lysmer (1972). Modification of seismograph records for effects of

local soil conditions, *Bull. Seism. Soc. Am.* **62**, 1649–1664.

Schnabel, P. B. and H. B. Seed (1973). Accelerations in rock for earthquakes in the western United States, *Bull. Seism. Soc. Am.* **63**, 501–516.

Shakal, A. F. and D. L. Bernreuter (1981). *Empirical analyses of near-source ground motion, U.S. Nuclear Regulatory Commission Report NUREG/CR-2095.*

Shakal, A. F. and R. D. McJunkin (1983). Preliminary summary of CDMG strong-motion records from the 2 May 1983 Coalinga, California, earthquake, *Rep. OSMS 83-5.2*, 49 p., Office of Strong Motion Studies, Calif. Div. Mines and Geol.

Shakal, A. F. and J. T. Ragsdale (1984). Acceleration, velocity and displacement noise analysis for the CSMIP acceleration digitization system, *Proc. Eighth World Conf. on Earthquake Eng. (San Francisco)* **2**, 111–118.

Shakal, A. F., M. J. Huang, D. L. Parke, and R. W. Sherburne (1986a). Processed data from the strong-motion records of the Morgan Hill earthquake of 24 April 1984. Part I ground-response records, *Rep. OSMS 84-04*, 249 p., Office of Strong Motion Studies, Calif. Div. Mines and Geol.

Shakal, A. F., R. Linares, M. J. Huang, and D. L. Parke (1986b). Processed strong motion data from the San Salvador earthquake of October 10, 1986, *Rep. OSMS 86-07*, 113 p., Office of Strong Motion Studies, Calif. Div. Mines and Geol.

Shakal, A. F., M. J. Huang, C. E. Ventura, D. L. Parke, T. Q. Cao, R. W. Sherburne, and R. Blazquez (1987). CSMIP strong-motion records from the Whittier, California earthquake of 1 October 1987, *Rep. OSMS 87-05*, 198 p., Office of Strong Motion Studies, Calif. Div. Mines and Geol.

Shyam Sunder, S. and J. J. Connor (1982). A new procedure for processing strong-motion earthquake signals, *Bull. Seism. Soc. Am.* **72**, 643–661.

Silva, W. (1976). Body waves in a layered anelastic solid, *Bull. Seism. Soc. Am.* **66**, 1539–1554.

Singh, S. K., E. Mena, and R. Castro (1988). Some aspects of source characteristics of the September 19, 1985, Michaocan earthquake and ground motion amplification in and near Mexico City from strong motion data, *Bull. Seis. Soc. Am.*, scheduled for the April issue.

Spudich, P. and U. Ascher (1983). Calculation of complete theoretical seismograms in vertically varying media using collocation methods, *Geophys. J. R. Astron. Soc.* **75**, 101–124.

Spudich, P. and L. N. Frazer (1984). Use of ray theory to calculate high-frequency radiation from earthquake sources having spatially variable rupture velocity and stress drop, *Bull. Seism. Soc. Am.* **74**, 2061–2082.

Spudich, P. and E. Cranswick (1984). Direct observation of rupture propagation during the 1979 Imperial Valley earthquake using a short baseline accelerometer array, *Bull. Seism. Soc. Am.* **74**, 2083–2114.

Structural Engineers Association of California (1980). *Recommended Lateral Force Requirements and Commentary*, Fourth Edition Revised.

Structural Engineers Association of California (1988). *Recommended Lateral Force Requirements and Commentary*, Fifth Edition, in preparation.

Toro, G. R. and R. K. McGuire (1987). An investigation into earthquake ground motion characteristics in eastern North America, *Bull. Seism. Soc. Am.* **77**, 468–489.

Trifunac, M. D. (1971). Zero baseline correction of strong-motion accelerograms, *Bull. Seism. Soc Am.* **61**, 1201–1211.

Trifunac, M. D. (1972). A note on correction of strong-motion accelerograms for instrument response, *Bull. Seism. Soc Am.* **62**, 401–409.

Trifunac, M. D. and V. W. Lee (1973). Routine processing of strong motion accelerograms, *Rep. EERL 73-03*, 360 p., Earthquake Engin. Res. Lab., Calif. Inst. Tech., Pasadena.

Trifunac, M. D. and J. G. Anderson (1978). Preliminary empirical models for scaling pseudo relative velocity spectra, appendix A in *Methods for Prediction of Strong Earthquake Ground Motion*, *U.S. Nuclear Regulatory Commission Report NUREG/CR-0689*, A1–A90.

Trifunac, M. D. and V. W. Lee (1979). Dependence of pseudo relative velocity spectra of strong motion acceleration on the depth of sedimentary deposits, *Report No. CE 79-02*, Dept. Civil Eng., Univ. of Southern Cal., Los Angeles, Cal., 67 p.

Tucker, B. E., J. L. King, D. Hatzfeld, and I. L. Nersesov (1984). Observations of hard-rock site effects, *Bull. Seis. Soc. Am.* **74**, 121–136.

U.S. Atomic Energy Commission (1973). Design response spectra for seismic design of nuclear power plants, *Regulatory Guide 1.60*, 4 p.

Vidale, J. E. and D. V. Helmberger (1988). Elastic finite-difference modeling of the 1971 San Fernando, California earthquake, *Bull. Seism. Soc. Am.* **78**, 122–141.

Vyas, Y. K., C. B. Crouse, and B. A. Schell (1988). Regional design ground motion criteria for the southern Bering Sea, *Conf. Offshore Mech. and Arctic Engin.*, Houston, Texas, February 7–12, 1988.

Weichert, D. H., R. J. Wetmiller, R. B. Horner, P. S. Munro, and P. N. Mork (1986). Strong motion records from the 23 December 1985, $M_S$ 6.9 Nahanni, NWT, and some associated earthquakes, *Geological Survey of Canada Open File Rept. 86-1-PGC*, 9 p.

Westaway, R. and R. B. Smith (1987). Strong ground motion parameters for normal-faulting earthquakes (abs.), *EOS, Trans. Am. Geophys. Union* **68**, 1348.

Wu, F. T. (1978). Prediction of strong ground motion using small earthquakes, *Proc. of 2nd Internat. Microzonation Conf.* **2**, San Francisco, 701–704.